Molecular interactions of the human PEX1/PEX6 AAA+ ATPase complex and *in vivo* mRNA editing of the *PEX1-G843D* mutation

Dissertation

der Mathematisch-Naturwissenschaftlichen Fakultät
der Eberhard Karls Universität Tübingen
zur Erlangung des Grades eines
Doktors der Naturwissenschaften
(Dr. rer. nat.)

vorgelegt von
Saroj Pandey
aus Nuwakot, Nepal

Tübingen
2024

Gedruckt mit Genehmigung der Mathematisch-Naturwissenschaftlichen Fakultät der Eberhard Karls Universität Tübingen.

Tag der mündlichen Qualifikation:	16.05.2024
Dekan:	Prof. Dr. Thilo Stehle
1. Berichterstatterin:	Prof. Dr. Gabriele Dodt
2. Berichterstatter:	Prof. Dr. Thorsten Stafforst

Abstract

Peroxisomes, ubiquitous and highly dynamic organelles in eukaryotic cells, are crucial for human health and development. They are needed for oxidative metabolic processes, including the breakdown of fatty acids and the regulation of the cellular redox balance. These functions are conserved across species and rely on proteins encoded by nuclear DNA, which are subsequently targeted into the peroxisomal matrix after translation. Specialized proteins, known as peroxins or PEX proteins are involved in peroxisome biogenesis, ensuring a continuous influx of peroxisomal proteins. Among these, PEX1 and PEX6, members of the type II AAA+ ATPase family, are core components of the receptor export module (REM) and essential for peroxisomal matrix protein import. Together, PEX1 and PEX6 form a heterohexameric ATPase complex whose activity facilitates the release of the receptor PEX5, ensuring a steady supply of receptors for subsequent protein import.

Mutations in either of the mammalian PEX1 and PEX6 proteins disrupt peroxisome biogenesis, leading to severe peroxisomal disorders and early death. A missense mutation *PEX1-G843D* is one of the most common causes of a milder variant of peroxisomal disorders. Some chemical and pharmacological chaperones such as betaine and diosmetin have been found to improve peroxisomal matrix protein import by restoring the PEX1-G843D function. The task of this thesis was to study the interactions of these drugs with the human PEX1/PEX6 complex and the correction of the *PEX1-G843D* mutation at the mRNA level.

Recombinant human PEX1 and PEX6 were expressed in HEK293TT cells for protein production and the complex was purified in sequential steps. The purification is based on the knowledge that a heterohexameric AAA+ ATPase complex is formed by three subunits of PEX1 and three subunits of PEX6 proteins. A two-step purification of the complex using a C-terminal His_6 tag in PEX1 and an N-terminal 2xFLAG or Strep-tag II in PEX6 was performed to get a pure complex. The purified protein complex was analyzed by microscale thermophoresis (MST) to examine binding affinity of PEX1 with the pharmacological compounds, betaine and diosmetin. The K_D values for betaine were in the millimolar range while that for diosmetin fall in the micromolar range indicating stronger interaction of diosmetin with the PEX1/PEX6 complex.

In collaboration with the lab of Prof. Dr. Thorsten Stafforst, the *in-vivo* correction of the *PEX1-G843D* (c.2528G>A) mRNA was studied. One approach for this was the use of ectopically expressed SNAP-ADAR proteins and transfected guide RNAs. In another approach, endogenous ADAR proteins were utilized in combination with transfected antisense nucleotides (ASOs). In both methods, the guide RNAs/ASOs specific to the point mutation site were able to partially correct the mutation, thus forming the wildtype PEX1 protein. The level of mRNA correction was calculated after Sanger sequencing and the restoration of matrix protein import was confirmed by fluorescence microscopy.

Zusammenfassung

Peroxisomen, allgegenwärtige und hochdynamische Organellen in eukaryotischen Zellen, sind für die menschliche Gesundheit und Entwicklung von entscheidender Bedeutung. Sie werden für oxidative Stoffwechselprozesse benötigt, darunter den Abbau von Fettsäuren und die Regulierung des zellulären Redoxgleichgewichts. Diese Funktionen sind artenübergreifend konserviert und basieren auf Proteinen, die von der Kern-DNA kodiert werden und posttranslational in die peroxisomale Matrix gelangen. Spezialisierte Proteine, sogenannte Peroxine oder PEX-Proteine, sind an der Peroxisomen-Biogenese beteiligt und sorgen für einen kontinuierlichen Zustrom peroxisomaler Proteine. Unter diesen sind PEX1 und PEX6, Mitglieder der AAA+ ATPase-Familie vom Typ II, Kernkomponenten des Rezeptorexportmoduls (REM) und essenziell für den Import peroxisomaler Matrixproteine. Zusammen bilden PEX1 und PEX6 einen heterohexameren ATPase-Komplex, dessen Aktivität die Freisetzung des Rezeptors PEX5 erleichtert und so eine stetige Versorgung mit Rezeptoren für nachfolgende Proteinimporte gewährleistet.

Mutationen in einem der Säugetierproteine PEX1 und PEX6 stören die Peroxisomenbiogenese, was zu schweren peroxisomalen Störungen und frühem Tod führt. Eine Missense-Mutation PEX1-G843D ist eine der häufigsten Ursachen für eine mildere Variante dieser peroxisomalen Erkrankungen. Es wurde festgestellt, dass einige chemische und pharmakologische Chaperone wie Betain und Diosmetin den Import peroxisomaler Matrixproteine verbessern, indem sie die PEX1-G843D-Funktion wiederherstellen. Diese Dissertation beschäftigte sich mit der Untersuchung der Wechselwirkungen dieser Substanzen mit dem humanen PEX1/PEX6-Komplexes und der Korrektur der PEX1-G843D-Mutation auf mRNA-Ebene.

Rekombinantes menschliches PEX1 und PEX6 wurden in HEK293TT-Zellen zur Proteinproduktion exprimiert und der Komplex wurde in aufeinanderfolgenden Schritten gereinigt. Die Reinigung basiert auf der Erkenntnis, dass ein heterohexamerer AAA+ ATPase-Komplex aus drei Untereinheiten von PEX1- und drei Untereinheiten von PEX6-Proteinen gebildet wird. Um einen reinen Komplex zu erhalten, wurde eine zweistufige Reinigung des Komplexes unter Verwendung des C-terminalen His6-Tags in PEX1 und des N-terminalen 2xFLAG- oder Strep-Tag II in PEX6 durchgeführt. Der

gereinigte Proteinkomplex wurde durch Thermophorese im Mikromaßstab (MST) analysiert, um die Bindungsaffinität von PEX1 mit den pharmakologischen Verbindungen Betain und Diosmetin zu untersuchen. Die K_D-Werte für Betain lagen im millimolaren Bereich, während die für Diosmetin im mikromolaren Bereich lagen, was auf eine stärkere Wechselwirkung von Diosmetin mit dem PEX1/PEX6-Komplex hinweist.

In Zusammenarbeit mit dem Labor von Prof. Dr. Thorsten Stafforst wurde die In-vivo-Korrektur der *PEX1-G843D* (c.2528G>A) mRNA untersucht. Ein Ansatz hierfür war die Verwendung ektopisch exprimierte SNAP-ADAR-Proteine und transfizierter Guide-RNAs. In einem anderen Ansatz wurden endogene ADAR-Proteine in Kombination mit transfizierten Antisense-Nukleotiden (ASOs) verwendet. Bei beiden Methoden konnten die für die Punktmutationsstelle spezifischen Guide-RNAs/ASOs die Mutation teilweise korrigieren und so das Wildtyp-PEX1-Protein bilden. Der Grad der mRNA-Korrektur wurde nach der Sanger-Sequenzierung berechnet und die Wiederherstellung des Matrixproteinimports wurde durch Fluoreszenzmikroskopie bestätigt.

Table of Contents

List of abbreviations

A-to-I	adenosine to inosine
AAA+	ATPases associated with diverse cellular activities
ABC	ATP-binding cassette
ADAR	adenosine deaminase that acts on RNA
ADAT	adenosine deaminase that acts on tRNA
AGT	alanine glyoxylate aminotransferase
AH	amphipathic helix
AMACR	2-Methylacyl-CoA racemace
APOBEC	apolipoprotein B mRNA-editing enzyme, catalytic polypeptide
ASO	antisense nucleotide
BCA	bicinchoninic acid
BG	O^6-benzylguanine
BSA	bovine serum albumin
C-to-U	cytidine to uridine
Cas	CRISPR-associated proteins
DD	deaminase domain
DHA	docosahexaenoic acid
DMEM	Dulbecco's Modified Eagle Medium
DOX	doxycycline
DPB-S	Dulbecco's phosphate-buffered saline
dsRBDs	double stranded RNA binding domains
DTM	docking/translocation Module
E. coli	*Escherichia coli*
EF1α	elongation factor 1 alpha
EM	electron microscopy
ER	endoplasmic reticulum
FCS	fetal calf serum
FSC	forward scatter
gRNA	guide RNA
GSNO	S-nitrosoglutathione
hAGT	O^6-alkylguanine-DNA alkyltransferase
HBSS	Hank's Balanced Salt Solution
HRP	horseradish peroxidase
HS	Heimler syndrome
IF	immunofluorescence
IHF	integration host factor
Int	integrase
IR	infrared
IRD	infantile Refsum disease

K_D	dissociation constant
LB	Luria Bertani
MCSs	membrane contact sites
MST	microscale thermophoresis
MW	molecular weight
NC	nitrocellulose
NES	nuclear export signal
NLS	nuclear localization signal
NSF	N-ethylmaleimide-sensitive fusion protein
NTA	nitrilotriacetic acid
ORF	open reading frame
PBDs	Peroxisome biogenesis disorders
PCR	polymerase chain reaction
PEDs	peroxisomal single enzyme and transporter deficiencies
PEI	polyethyleneimine
PEX	peroxisomal protein or peroxin
Pi	inorganic phosphate
PNS	post nuclear supernatant
PTSs	peroxisomal targeting sequences
REM	receptor export module
RESTORE	Recruiting endogenous ADAR to specific transcripts for oligonucleotide-mediated RNA editing
RING	Really Interesting New Gene
RNP	ribonucleoprotein
ROS	reactive oxygen species
SA	SNAP-ADAR
SDRE	site-directed RNA-editing
SDS	sodium dodecyl sulfate
SDS-PAGE	sodium dodecyl sulphate–polyacrylamide gel electrophoresis
SNAREs	soluble NSF attachment protein receptors
SSC	side scatter
TM	transmembrane helix
TPR	tetratricopeptide repeat
tris	tris(hydroxymethyl)aminomethane
Ub-PEX5	ubiquitinated PEX5
VLFCA	very long-chain fatty acids
WB	Walker B
X-ALD	X-linked adrenoleukodystrophy
Xis	excisionase
ZSDs	Zellweger spectrum disorders

Notes

- Nomenclature: Unless specified, all yeast genes have been written in all small letters and italics (as in *pex1*) and the proteins are written with first letter in capital (as in Pex1). Human genes are written in all capital and italics (as in *PEX1*) and protein in all capital letters (as in PEX1).
- Figure permission: Permission to use and modify all figures used in this thesis have been received from the corresponding publishers/authors. Acquired figures have been cited in the caption.

1 Introduction

1.1 Peroxisomes

Peroxisomes are single membrane bound and ubiquitously found organelles in most eukaryotic cells. They are versatile organelles that can adapt to various environmental conditions and perform specialized roles in different organisms [1]. Initially discovered as microbodies in 1954 [2], these organelles earned the name "peroxisomes" about ten years later due to their ability to neutralize hydrogen peroxide [3]. They are globular to ovoid shaped with a diameter of 0.1 to 1 μm and have a granular matrix containing a tissue-specific dense protein core [3–5]. The understanding of morphology, organization and interactions of peroxisomes are still advancing and techniques like electron microscopy (EM) and super-resolution microscopy have significantly helped in the process [6,7]. Peroxisomes play crucial roles in various metabolic processes, including the detoxification of reactive oxygen species (ROS), β-oxidation of very long-chain fatty acids (VLCFA), α-oxidation of branched fatty acids, and the synthesis of plasmalogens [8–10].

1.1.1 Functions of peroxisomes

Peroxisomes are involved in a wide range of catabolic and anabolic functions required for health and overall development. Numbering up to several hundred per mammalian cells, each of these organelles contain about 115 different proteins and are involved in more than 50 different metabolic reactions [11,12]. The size, number, content, and characteristics of peroxisomes vary according to the organisms they originate from and their homeostatic state. Therefore, peroxisomes execute specialized biological roles to maintain cellular physiology developing organism-specific metabolic processes [13]. Within cells, peroxisomes are integrated into the complex network of subcellular organelles. Peroxisomes are known to have physical and metabolic contacts with several other organelles like mitochondria, endoplasmic reticulum (ER), lysosomes and lipid droplets (reviewed in [1]) and such cooperation is carried out by the formation of membrane contact sites (MCSs) via tether proteins to allow the transfer of metabolites [14]. In order to carry out an array of metabolic roles, peroxisomes need to import metabolites from the cytosol and export metabolic products. Although still disputed, a growing consensus says that the peroxisomal membrane is selectively permeable where

low molecular weight (MW) metabolites are transported freely whereas larger metabolites require a carrier-mediated transport [15]. An overview of main metabolic pathways and key enzymes occurring in peroxisomes is shown in Figure 1.

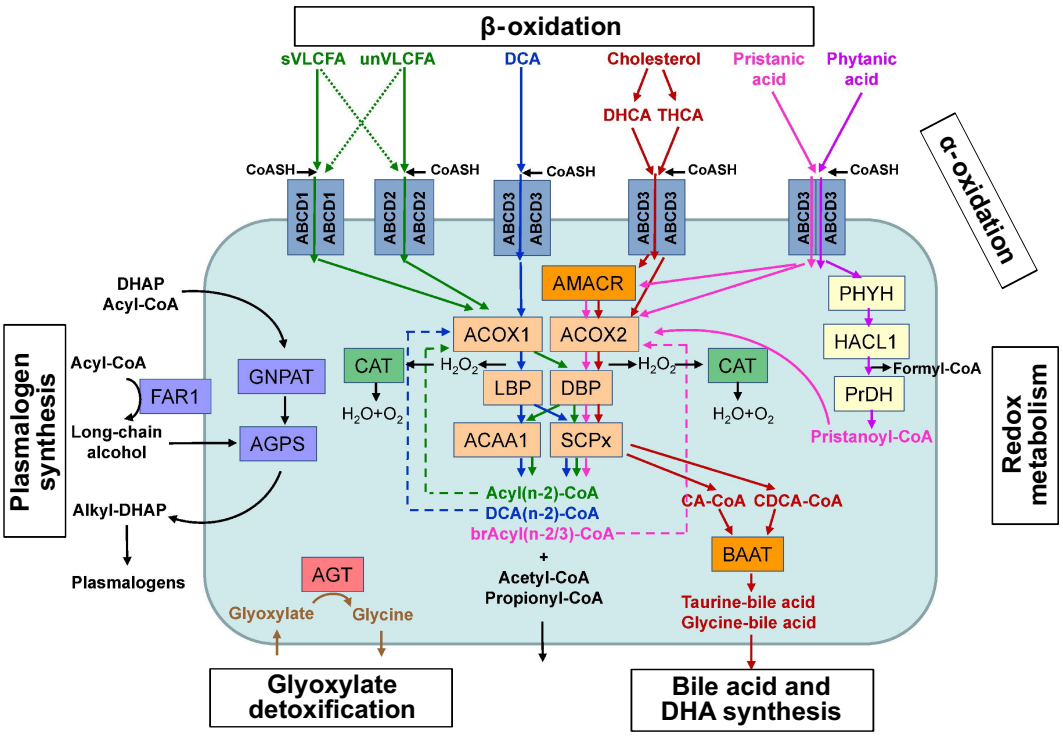

Figure 1: Main metabolic pathways in peroxisomes. Shown are the main metabolic pathways in which peroxisomes are involved. Peroxisomal proteins involved in the different pathways are indicated by their respective gene names and boxed. Substrates and products are unboxed. The main enzymes involved in the peroxisomal fatty acid beta-oxidation pathway are indicated in light orange, alpha-oxidation of phytanic acid in yellow, plasmalogen synthesis in purple, bile acid synthesis in bright and light orange, glyoxylate detoxification in red and catalase required for H_2O_2 degradation in green. The peroxisomal fatty acid beta-oxidation pathway can handle different substrates, including very long chain fatty acids (sVLCFA, unVLCFA), dicarboxylic acids (DCA), the bile intermediates DHCA and THCA, and pristanic acid, which are imported into peroxisomes by the different ABCD transporters. ACAA1: 3-ketoacyl-CoA thiolase, ACOX1: Acyl-CoA oxidase 1, ACOX2: acyl-CoA oxidase 2, ABCD1: ABC transporter D1, ABCD2: ABC transporter D2, ABCD3: ABC transporter D3, AGPS: alkyl-dihydroxyacetonephosphate synthase, AGT: alanine-glyoxylate aminotransferase, AMACR: 2-methylacyl-CoA racemace, BAAT: bile acid–CoA amino acid N-acyltransferase, brAcyl: branched-acyl, CA: cholic acid, CAT: catalase, CDCA: chenodeoxycholic acid, DBP: D-bifunctional protein, DCA: dicarboxylic acids, DHAP: dihydroxyacetone phosphate, DHCA: dihydroxycholestanoic acid, FAR1: fatty acyl reductase 1, GNPAT: dihydroxyacetonephosphate acyltransferase, HACL1: 2-hydroxyphytanoyl-CoA lyase, LBP: L-bifunctional protein, PHYH: phytanoyl-CoA 2-hydoxylase, PrDH: pristanal dehydrogenase, SCPx: Sterol carrier protein X, sVLCFA: saturated very long chain fatty acids, THCA: trihydroxycholestanoic acid, unVLCFA: unsaturated very long chain fatty acids. Adopted from Waterham et al., 2016 **[16]**.

In mammalian cells, both mitochondria and peroxisomes are involved in the β-oxidation of lipids [17]. While mitochondria can only metabolize fatty acids containing 18 or less carbons, peroxisomes are involved in the catabolism of VLCFAs via β-oxidation, as well as branched-chain fatty acids through α-oxidation [16,18,19]. However β-oxidation of fatty acids in plants and fungi takes place exclusively in the peroxisomes [17,20].

Peroxisomes are also involved in anabolic functions such as the maturation of bile metabolites and synthesis of docosahexaenoic acid (DHA) [21,22]. Peroxisomes also have an important role in the integral components of cardiac and neuronal tissues [23]. Similarly, they are also involved in the first steps of ether phospholipid anabolism [24].

The role of peroxisomes in cellular redox metabolism and signaling is significant [25,26]. Anti-oxidant enzymes present in the peroxisomes like catalase and peroxiredoxin V are important in the degradation of hydrogen peroxide and other ROS generated in the peroxisomal lumen [10,27]. Similarly, the peroxisomal enzyme alanine glyoxylate aminotransferase (AGT) helps in the detoxification of glyoxylate converting it to glycine which otherwise turns into glycolate or oxalate [28]. Peroxisomes are also involved in the degradation of several D-amino acids [29] as well as in purine metabolism.

1.1.2 Peroxisomal matrix protein import

Enzymes and proteins needed for proper functioning of peroxisomes are synthesized in the cytosol by polyribosomes and transported into the organellar matrix within minutes [5]. Either of the two types of peroxisomal targeting sequences (PTSs), PTS1 or PTS2, present in these proteins define their sorting and shuttling into the peroxisomes by the receptor proteins [30–33]. Proteins with C-terminal tripeptide targeting signal, a tripeptide PTS1 (S/A/C-K/R/L-L/M), are transported by the receptor protein PEX5 [33], whereas those with the N-terminal nonapeptide PTS2 signal (R-L/V/I/Q-X-X-L/V/I/H-L/S/G/A-X-H/Q-L/A) are delivered to the organelle by PEX7, a 40-kDa WD-repeat protein, with the help of a coreceptor like PEX5L (a long splice isoform of PEX5) in mammals [34–36] or Pex18 or Pex21 in yeast [37,38].

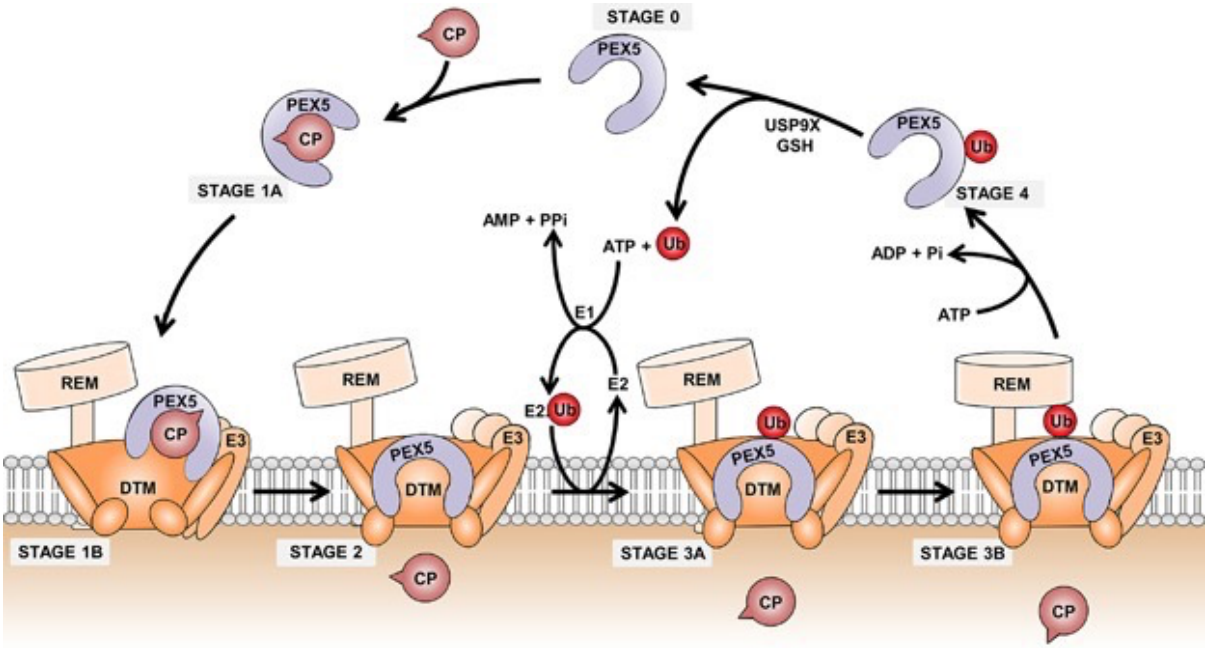

Figure 2: The peroxisomal matrix protein import mechanism. Peroxisomal matrix proteins are synthesized on cytosolic ribosomes and bound by the shuttling receptor PEX5 (stage 1A). The PEX5-cargo complex then docks at (stage 1B) and becomes inserted into the DTM (stage 2) resulting in cargo translocation across the peroxisomal membrane and its release into the organelle matrix. PEX5 is then monoubiquitinated at a conserved cysteine residue (cysteine 11 in mammals) (stage 3A), a mandatory modification for the subsequent interaction with the receptor export module (REM; stage 3B). Finally, after the ATP-dependent extraction of monoubiquitinated PEX5 into the cytosol (stage 4), PEX5 is deubiquitinated probably by a combination of non-enzymatic (e.g. glutathione (GSH)) and enzymatic mechanisms (e.g. USP9X in mammals). Free PEX5 (stage 0) can then start a new protein transport cycle. Import of PTS2-containing proteins involves the receptor $PEX5^{PEX7}$. PEX7 remains bound to PEX5 during most of the steps of this pathway. For simplicity PEX7 is not shown in the figure. E1: ubiquitin-activating enzyme, E2: ubiquitin-conjugating enzyme (i.e. E2D1/2/3), E3: ubiquitin RING ligases (i.e. PEX2, PEX10, and PEX12), PPi: pyrophosphate; Ub: ubiquitin. Adopted from Francisco et al., 2017 **[39]**.

The mechanism of peroxisomal matrix protein import is depicted in Figure 2 where PEX5 plays the central role. Consisting of a long unstructured N-terminal region, PEX5 also has a globular tetratricopeptide repeat (TPR) domain at the C-terminus which ensures direct binding to the PTS1 peptide of cargo proteins [40,41] (see Figure 3B). The N-terminal domain has a holdase-like activity [42] that surrounds the cargo protein preventing its interaction with other proteins [43,44]. Cargo-loaded PEX5 is transported into the docking/translocation module (DTM), a peroxisomal transmembrane complex made up of 5 proteins: PEX13, PEX14; and the RING (Really Interesting New Gene) finger complex proteins PEX2, PEX10 and PEX12 [45,46]. The arrangement of these proteins in the DTM however is not yet fully understood. PEX13 and PEX14 both contain PEX5-binding

domains and are the main components of the translocation channel [47–49]. The processing of PEX5 and the loaded cargo by the DTM occurs in two sequential steps, a reversible docking step followed by an irreversible insertion step [50,51]. By the formation of a flexible and gated channel via DTM components, PEX5 attains a transmembrane topology where its N-terminal part is exposed towards the cytosol and the cargo-bound C-terminal part faces the matrix [52].

Another theory also suggests that a channel formed by PEX13 is responsible for the transfer of PEX5 into the peroxisomal membrane and PEX5 completely enters the matrix [41,53]. The YG domain of PEX13 forms a meshwork similar to the nuclear pore complex that is selective to certain proteins (Figure 3A). Due to the presence of an amphipathic helix (AH) and the transmembrane helix (TM), PEX13 is also able to have dual topology: either the N-terminus faces the cytosol, and the C-terminal faces the matrix, or vice versa. The AH segments of multiple PEX13 molecules pack together, forming a ring-like structure with the aqueous YG network in the middle [41]. According to a recent study, such a structure is formed only during protein translocation [54]. As the cargo-loaded PEX5 enters the PEX13 YG meshwork, an N-terminal domain of PEX14 exhibits strong affinity to the WxxxF/Y motifs of PEX5 driving it completely into the matrix [55–57]. The PTS2 receptor PEX7 has also been shown to enter the matrix [58–60]. The localization of the N-Terminus and the C-terminus of PEX13 had been inconclusive for quite a while [61–64].

In addition, a “transient pore model” of translocation of PEX5 had also been proposed because of its hydrophilic nature [65]. According to this model, one or several PEX5 proteins get inserted into the peroxisomal membrane forming a hydrophilic channel through which the cargo proteins get imported [65,66].

Translocation of cargo loaded PEX5 (or PEX5L-PEX7) into the peroxisomal matrix as well as the release of the cargo proteins occur via protein-protein interactions and do not require energy [50,51,67]. However, the extraction of these shuttling proteins from the DTM to the cytosol requires ATP hydrolysis [50] thus making them available for another round of import. Several proteins are involved in the extraction process. The ubiquitin ligase complex consisting of the RING peroxins PEX2, PEX10 and PEX12 carries out the monoubiquitination of the N-terminally located conserved cysteine residue (Cys11) in

PEX5 [68,69]. The REM, consisting of PEX1, PEX6 and PEX26 in mammals (or APEM9 in plants and PEX15 in yeasts) uses ATP hydrolysis to extract the ubiquitinated PEX5 (Ub-PEX5) from the DTM [52,70,71]. The export process additionally involves ubiquitin, a ubiquitin-activating enzyme, a ubiquitin-conjugating enzyme (such as E2D1/2/3 in mammals [72], or the PEX4/PEX22 in fungi and plants [73,74]), and AWP1, which is suggested to be a ubiquitin-binding adaptor associated with the mammalian PEX1/PEX6 complex [75]. Finally, the cytosolic Ub-PEX5 is deubiquitinated mediated by deubiquitinating enzymes such as UBP15 (in yeast) and USP9X (in mammals) [76,77].

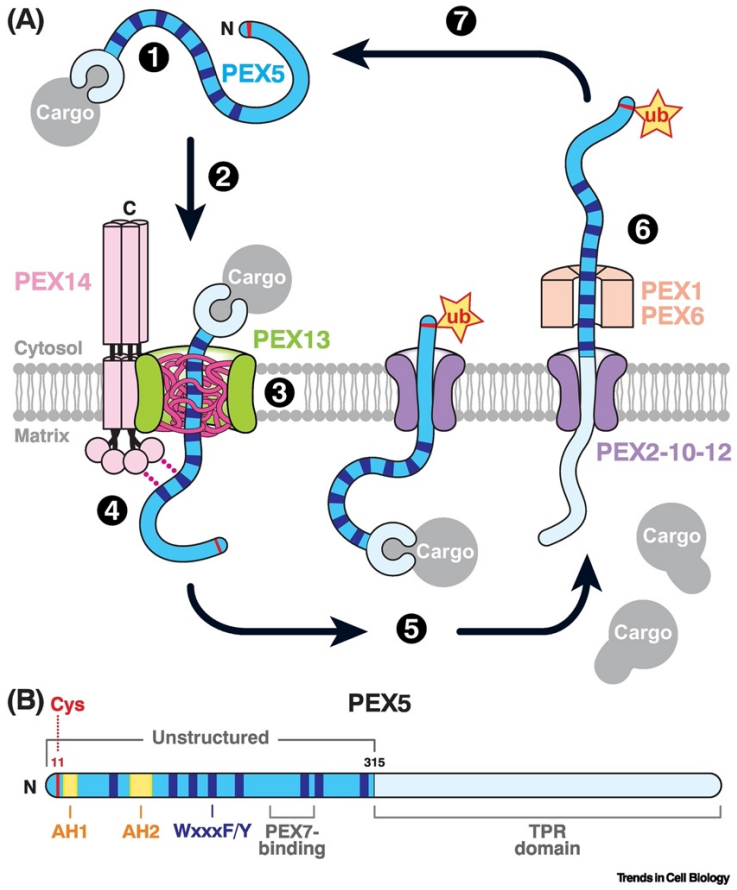

Figure 3: Import of peroxisomal matrix proteins by the receptor PEX5. (A) Model of peroxisomal matrix protein import in metazoans. (Step 1) PEX5 binds to cargo proteins in the cytosol. (Step 2) Cargo-bound PEX5 is recruited to peroxisomes by a complex containing the membrane proteins PEX13 and PEX14. (Step 3) Cargo-bound PEX5 traverses the membrane through a conduit formed by multiple copies of PEX13. The conduit contains a dense meshwork formed from the PEX13 Tyr/Gly-rich YG domain (pink), into which PEX5 partitions using its WxxxF/Y motifs (dark blue). (Step 4) PEX5 is drawn into the matrix by favorable lumenal interactions (represented by pink dotted lines) between the receptor WxxxF/Y motifs and PEX14 oligomers. (Step 5) PEX5 spools its flexible N terminus into the cytosol through a pore in the PEX2–PEX10–PEX12 ubiquitin ligase complex, which then monoubiquitinates the receptor on a conserved cysteine (red). (Step 6) Monoubiquitinated PEX5 is pulled out of the matrix through the ligase pore by the PEX1–PEX6 AAA ATPase

which unfolds the receptor and causes cargo to be stripped off inside the matrix. (Step 7) PEX5 refolds in the cytosol and ubiquitin is removed by deubiquitinases, resetting the receptor for another import cycle. (B) Diagram illustrating key features of metazoan PEX5, including the site of monoubiquitination (Cys), amphipathic helices (AHs) 1 and 2 that are required for recycling, the WxxxF/Y motifs (dark blue), the TPR domain that binds to PTS1 cargo, and the binding site for the adapter PEX7 that binds to PTS2 cargo. Residue coordinates in the human protein are labeled above. TPR: tetratricopeptide repeat; ub: ubiquitin. Adopted from Skowyra *et al.*, 2023 **[41].**

1.1.3 Peroxisomes and diseases

The role of peroxisomes in cell metabolism and normal functioning of human development is very crucial [30] as any defect in peroxisomal proteins results in various diseases and serious metabolic conditions. Progressive developmental and neurological abnormalities are associated with the loss of peroxisomal functions. Peroxisomal disorders encompass a diverse range of genetic conditions, arising from either a malfunction in peroxisome biogenesis (Peroxisome biogenesis disorders (PBDs)) or a disruption in one of the metabolic functions (peroxisomal single enzyme and transporter deficiencies (PEDs)) [16] (Figure 4). Large varieties of peroxisomal diseases have been identified till date and together, they have a prevalence rate of 1:5000 individuals [16]. Some age-related as well as inflammation-related diseases have also been linked to the role of peroxisomes [78,79].

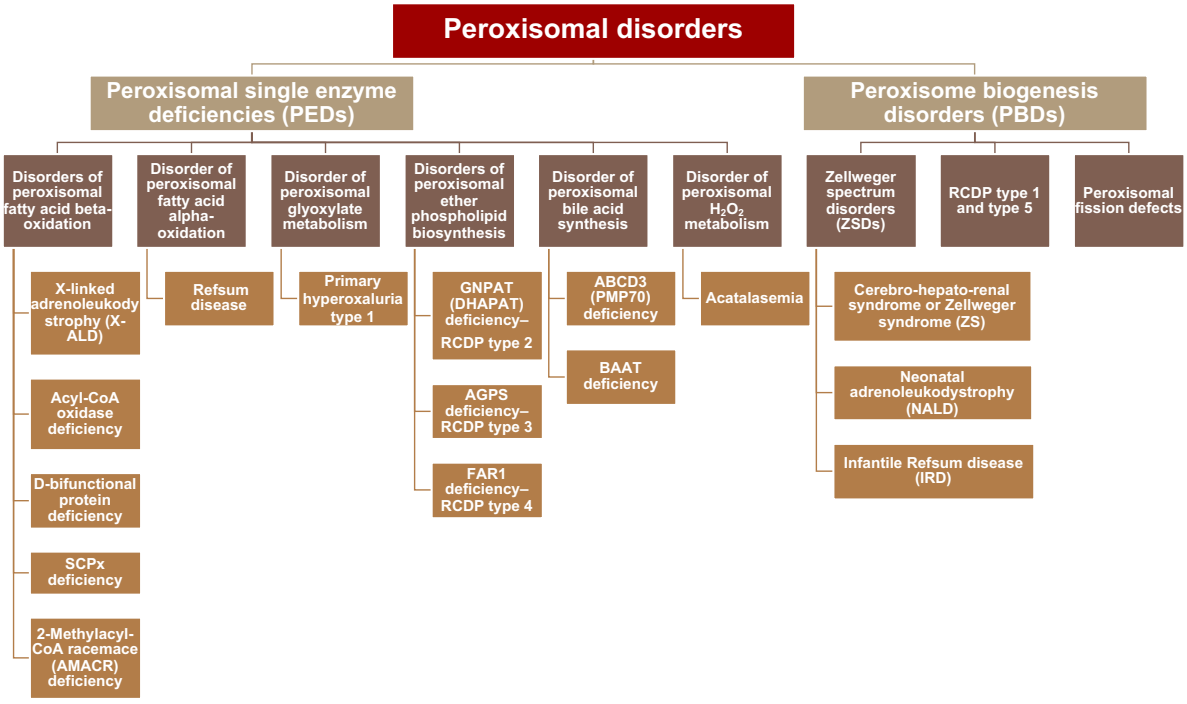

Figure 4: Peroxisomal disorders. Peroxisomal single enzyme/transporter deficiencies (PEDs) are grouped according to the major affected pathway and the diseases are named as the deficiency of affected enzymes. Peroxisomal biogenesis disorders (PBDs) are categorized based on clinical presentations. SCPx: sterol carrier protein X. GNPAT: dihydroxyacetonephosphate acyltransferase, DHAPAT: dihydroxyacetone phosphate acyltransferase, AGPS: alkyl-dihydroxyacetonephosphate synthase, FAR1: fatty acyl reductase 1, ABCD3: ABC transporter D3, PMP70: 70 kDa peroxisomal membrane protein, BAAT: Bile acidCoA:amino acid N-acyltransferase, RCDP: rhizomelic chondriodysplasia punctata. Classification based on Waterham *et al.*, 2016 **[16]**.

1.1.3.1 Peroxisomal single enzyme and transporter deficiencies (PEDs)

PEDs arise from the defect in specific peroxisomal matrix enzymes or membrane transporters and are mostly attributed to the affected biochemical pathway. Deficiencies in peroxisomal function lead to abnormal accumulation or degradation of biomolecules reliant on peroxisomal activity, resulting in symptoms attributed to either metabolic intoxications or deficiencies in crucial biomolecules [80]. Most of the peroxisomal functions of PED patients remain intact apart from the role of the defected protein [81]. However, the size and number of peroxisomes may vary [82].

Mutations have been discovered in the genes responsible for 11 peroxisomal enzymes and transporter proteins, leading to inherited human disorders [80]. The majority of these enzymes are involved in fatty acid degradation and bile acid metabolism. Diseases occurring from defects in these proteins are categorized in Figure 4.

X-linked adrenoleukodystrophy (X-ALD) is the most common disorder associated with the peroxisomes, with an approximate occurrence rate of 1 in every 17000 individuals [83]. X-ALD is caused due to mutations in the *ABCD1* gene encoding a transporter protein involved in the ATP-driven fatty acid transport across the peroxisomal membrane [84,85]. It is one of the few peroxisomal diseases for which effective therapy is available to prevent disease progression [86].

Acyl-CoA oxidase deficiency results from mutations in the ACOX1 gene encoding the ACOX1 protein that is involved in beta-oxidation of straight chain fatty acids [87,88]. Similarly, D-bifunctional protein deficiency, SCPx deficiency and 2-Methylacyl-CoA racemace (AMACR) deficiency are other diseases affecting the beta-oxidation pathway in peroxisomes. Other PEDs occur due to the defect in proteins required in bile acid

maturation, plasmalogen biosynthesis; or the glyoxylate as well as hydrogen peroxide detoxification [80].

1.1.3.2 Peroxisome biogenesis disorders (PBDs)

Biogenesis of peroxisomes includes processes required in the formation and maintenance of functional peroxisomes. These processes are carried out by different peroxisomal proteins (peroxins or PEX proteins) and the consequence of losing these functions give rise to the peroxisomal biogenesis disorders (PBDs). PBDs occur due to biallelic mutations in one or more of the 14 *PEX* genes that encode the peroxins involved in peroxisomal biogenesis and inheritance [11,16,89–91].

Patients with PBDs exhibit a spectrum of clinical manifestations, including mild isolated visual/hearing impairments, late-onset progressive neurological conditions to severe, often fatal multisystemic disorders. These disorders are categorized into three distinct subtypes based on clinical features: Zellweger spectrum disorders (ZSDs), RCDP type 1 and type 5, and peroxisomal fission defects [16]. Defects in PEX1, PEX2, PEX3, PEX5, PEX6, PEX10, PEX11β, PEX12, PEX13, PEX14, PEX16, PEX19 and PEX26 genes result in ZSDs. Mutations in PEX7 result in the specific characteristics observed in RCDP type 1 [92]. No human disease has been linked to abnormalities in PEX11α and PEX11γ thus far [11].

ZSDs are again classified into subcategories as the most severe Zellweger Syndrome (or cerebro-hepato-renal syndrome), less severe neonatal adrenoleukodystrophy (NALD), relatively mild infantile Refsum disease (IRD) and Heimler syndrome (HS) [93–96]. ZSDs causes peroxisomes to enlarge and reduce in numbers in the cells where the import of matrix proteins is also diminished and the resulting structures are termed as “peroxisomal ghosts” [97]. ZSS presents with hepatic/renal dysfunction, hypotonia, developmental delay, neurological abnormalities, craniofacial malformations, seizures, eye diseases (cataracts, glaucoma, retinal dystrophy, optic atrophy), and sensorineural deafness. Liver enlargement and elevated transaminases, cholestasis, and coagulopathy are also common [11]. Patients afflicted with ZS typically do not survive beyond the first year of life. Patients diagnosed with NALD may survive into their teenage years, while those with IRD might potentially reach adulthood [98].

As only the import of PTS2 proteins is affected in RCDP1, peroxisome number and structure remain normal, with a deficiency limited to a subset of matrix enzymes. Enzymes with PTS2 targeting sequences, like 3-ketoacyl-CoA thiolase, AGPS, and phytanoyl-CoA hydroxylase, fail to enter peroxisomes, leading to a deficiency in plasmalogen synthesis and alpha-oxidation [16]. RCDP type 5 is caused due to the loss of the PEX5L isoform. Since PEX5L is also involved in the PTS2 matrix protein import, RCDP type 5 also manifests biochemical and clinical phenotype comparable to RCDP type 1 [99]. Patients are characterized by the presence of shortened limbs, punctate calcifications in epiphyseal cartilage, and congenital cataracts [100–102]. Patients also display severe postnatal growth and intellectual deficiency [103].

Peroxisomal fission defects represent patients with mutations in proteins involved in the division of peroxisomes such as DLP1 [104], MFF [105], GDAP1 [106], and PEX11β [107]. Since these proteins are also involved in the division of mitochondria, deficiency of these proteins often results in elongated peroxisomes and mitochondria. Although very few patients are detected with peroxisomal fission defects, most of them exhibit combined peroxisomal and mitochondrial dysfunctions.

1.1.4 The AAA+ ATPase proteins PEX1 and PEX6

ATPases associated with diverse cellular activities (AAA+ proteins) belong to a large family of ATPases that participate in various biological pathways such as membrane fusion, protein unfolding, proteolysis, vesicle trafficking, organelle biogenesis and DNA replication [108–113]. AAA+ proteins have a conserved ATPase domain that transforms hydrolysis of ATP into mechanical force [114]. Common structural features of the AAA+ ATPases are the presence of Walker A motifs (ATP binding), Walker B motifs (ATP hydrolysis), arginine fingers, and sensor 1 motifs [115,116]. Type I AAA+ ATPases contain each of these motifs collectively known as the D1 domain whereas the type II AAA+ ATPases have two such domains (D1 and D2) [117,118]. Proteins containing either one or two AAA+ domains tend to assemble into either homo- or hetero-oligomers, often leading to the formation of hexameric rings. [109,115]. This arrangement positions the ATP-binding/hydrolysis site at the junction of two subunits, with one subunit contributing the Walker A/B and sensor 1 residues whereas the other providing the

arginine finger, thus generating a central pore which often plays a crucial functional role [115,116].

PEX1 and PEX6 are members of a family of type II AAA+ ATPase proteins and make up a complex that is attached to the peroxisomal membrane via PEX26, a tail anchored protein in mammals [70,119]. Both of these proteins are conserved in all eukaryotes [120]. The most common cause of PBDs such as Zellweger syndrome in humans are mutations associated with PEX1 and PEX6 [121,122]. Total loss of their functionality leads to the formation of "empty" peroxisomes, referred to as peroxisomal ghosts. These peroxisomes retain certain membrane proteins but lack matrix proteins, rendering them incapable of executing their typical functions. This deficiency results in severe illness and, ultimately, mortality. The PEX1/PEX6 complex shares close similarities with extensively studied AAA-ATPases such as N-ethylmaleimide-sensitive fusion protein (NSF) and *Sc*Cdc48 (known as valosin-containing protein or p97 in humans) [123]. NSF functions in breaking down postfusion oligomers of soluble NSF attachment protein receptors (SNAREs) formed in the process of vesicle fusion [124]. Cdc48 serves as a versatile unfoldase, collaborating with various partners to unfold ubiquitinated substrates. It disassembles complexes, unfolds proteins for proteasomal degradation, and removes proteins from membranes [125,126].

Multiple sequence alignments reveal that PEX1 and PEX6 consist of two consecutive nucleotide-binding domains (D1 and D2), surrounded by less conserved sections at both the N- and C-termini [127,128]. Along with the two AAA+ domains, PEX1 and PEX6 also have two N-terminal domains (N1 and N2), each with sequence similar to single N-domain of p97/CDC48 and NSF (Figure 5). The second AAA+ domain (D2) found in both PEX1 and PEX6 contains all the standard residues essential for binding and hydrolysis of ATP. However, the first AAA+ domain (D1) is somewhat degenerated, as it lacks several of the residues necessary for ATP hydrolysis. [120,121,129–132].

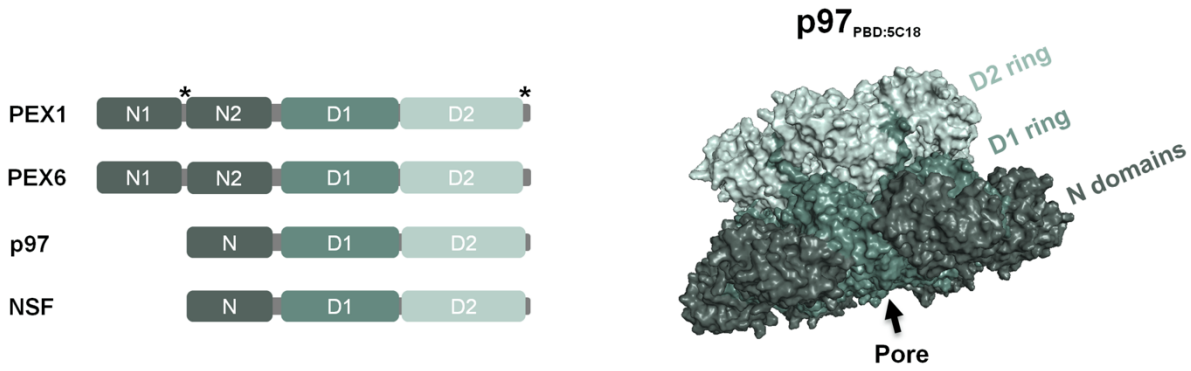

Figure 5: Domain architecture of the type II AAA+ proteins PEX1, PEX6, p97 and NSF. The two N-domains of PEX1 and PEX6 (N1 and N2) homologous to the N-domain of p97 and NSF (N-domain), and the two AAA+ domains (D1 and D2) are shown (left). Note that mammalian PEX1 is longer than the yeast protein, possessing a different spacing between its N-domains, it also has an extended C-terminal tail after the D2 domain (marked with asterisks). Atomic model of a p97 hexamer (right; PDB code 5C18, **[133]**) showing the common type II AAA+ structure consisting of one ring of D1 domains on top of another ring of D2 domains, and the six N-domains located on the side of the D1 ring. Note that this p97 structure was obtained in the presence of a non-hydrolysable ATP analogue and in the absence of substrate **[133]**. Adopted from Pedrosa *et al.*, 2019 **[134]**.

Negative-stain and cryo-electron microscopy studies have shed some light on the structure of the yeast Pex1/Pex6 complex [120,130,131,135,136] which reveal that alternating Pex1 and Pex6 subunits from a heterohexameric ring with and a large pore at the center. A distinct triangular shape is formed due to such alternate arrangement (Figure 6). The ATPase domains (D1 and D2) from each of the six subunits come together to form two concentric rings around a central pore. Positioned above the D1 ring are the N2 domains of Pex1 and Pex6, while the N1 domain of Pex6 sits at the same level as the D1 ring [120]. In a recent study by Ali *et al.*, the X-ray crystallography structure of the isolated Pex6 N1 domain was integrated with a cryo-EM reconstruction of Pex1/Pex6, alongside predictions from AlphaFold2 and biochemical analyses. The findings revealed that Pex6 N1 plays a crucial role in binding to the peroxisomal membrane anchor Pex15 as well as to the extended loop originating from the Pex1 D2 ATPase domain. This interaction significantly impacts the stability of the Pex1/Pex6 heterohexamer [136].

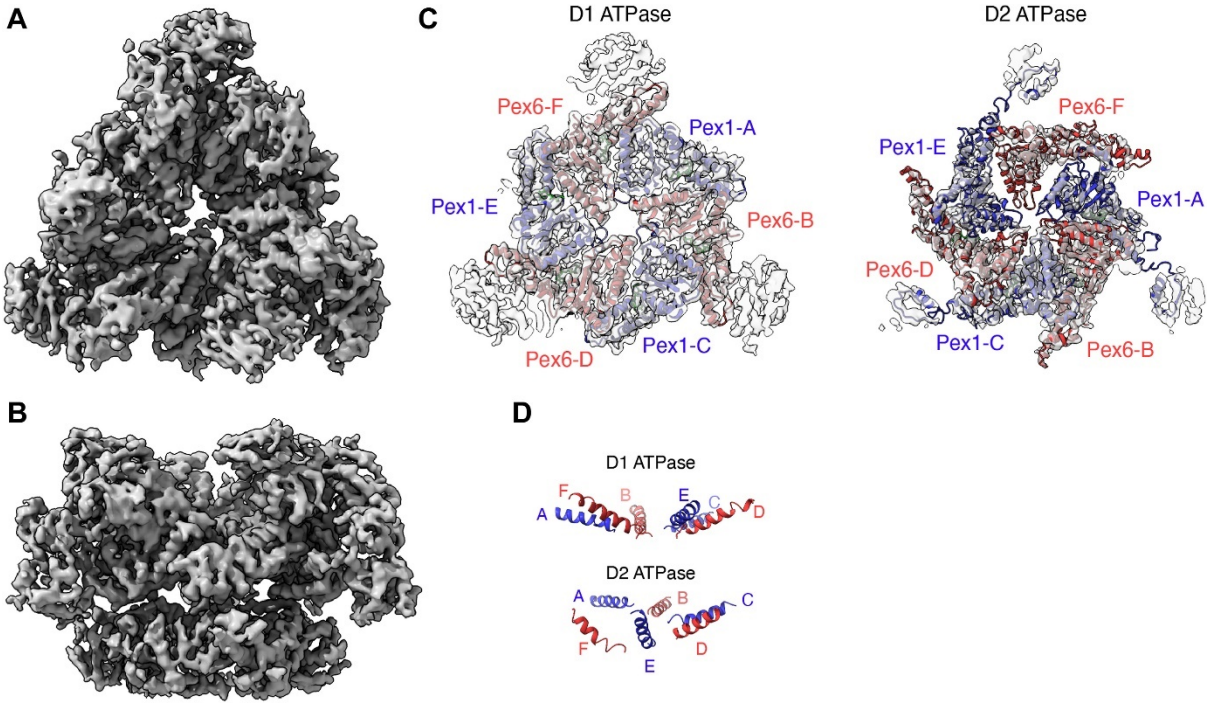

Figure 6: Cryo-EM structure of the *S. cerevisiae* Pex1/Pex6 complex. (A) top view of cryo-EM structure of Pex1/Pex6 in ATP. (B) sideview of cryo-EM structure of Pex1/Pex6 in ATP. (C) top views of slices showing the D1 ATPase ring and D2 ATPase ring, with atomic models for Pex1 (blue) and Pex6 (red). (D) side view of the relative positions of Pex1 and Pex6 pore loop α-helices for the D1 ATPase domains (Pex1 499-517, Pex6 518-539) and D2 ATPase domains (Pex1 772-789; Pex6 807-822) showing a planar arrangement for the D1 ring and a “spiral staircase” for the D2 ring. Adopted from Ali *et al.*, 2024 **[136]**.

Pex1/Pex6 ATPase activity is crucial for accumulating the proteins in the peroxisomes by helping in the extraction process of the receptor protein Pex5 back into the cytosol. Pex1 and Pex6 employ a threading mechanism to process substrates, wherein "pore loops" containing conserved aromatic residues within the ATPase channel physically interact with the substrate protein. This interaction, coupled with hydrolysis-powered vertical motions of the ATPase components, facilitates the pulling of the substrate through the hexamer’s central pore [137]. The mechanism of substrate recognition by Pex1/Pex6 complex is still unknown. However, as the ATPase domain of the AAA+ ATPases are highly conserved, it can be speculated that the substrate selection is done by the N-terminal domains [136].

1.1.5 The PEX1-G843D mutation

Out of all the patients with Zellweger Spectrum disorder, about 60% are associated with mutation in the *PEX1* gene in which 90 distinct mutations have been detected, comprising 23 missense, 15 nonsense, 30 deletion, 11 insertion, 7 splice site, 2 indel mutations and 2 disruptions of the start codon [89]. Out of all these, the most abundant mutation in *PEX1* is a missense mutation, the *PEX1*-c.[2528G>A] allele, encoding p.[Gly843Asp] or p.G843D, where a glycine at amino acid position 843 located in the second ATP-binding domain is changed into aspartic acid. As a result, PEX1-G843D has reduced assembly with PEX6 [138,139]. However, the overproduction of PEX6 has been shown to improve the association [122].

Patients with a homozygous PEX1-G843D mutation exhibit less severe manifestations of PBDs. The G843D missense mutation in PEX1 weakens PEX1 stability and function [121]. Later C. Walter *et al.* described that the PEX1-G843D missense mutation causes misfolding of the protein and that the protein is more stable at lower temperatures [140]. Imamura *et al.* described that the temperature sensitive PEX1 phenotype could be responsible for the deficiency of peroxisome in the cells of patients suffering from infantile Refsum disease (IRD) [138].

Studies conducted on PEX1-G843D fibroblasts indicate that this protein is misfolded and the folding and functionality can be improved by either culturing cells at 30°C or administering chaperone drugs [140,141]. PEX1-G843D results in a partial impairment in matrix protein import in comparison to the patients with truncated PEX1 variants, suggesting that PEX1-G843D is a hypomorphic allele [140]. About 50% reduction in the level of *PEX1* mRNA and 3-20% reduction in the amount of PEX1 protein has been associated with PEX1-G843D [139,140]. Clinical presentations with PEX1-G843D are similar to those with peroxisome dysfunctions, such as altered metabolism and visual impairment. This phenotype also occurs in a mouse model, even when there is no reduction of the protein level in mice carrying the mutation (PEX1-G844D) [142].

Sequence alignment studies involving PEX1 as well as related AAA-ATPases reveal that PEX1 Gly843 is conserved in other organisms and the glycine residue is situated within the loop of the D2 large subdomain and contacts the adjacent small subdomain (Figure 7). The presence of aspartate, instead of glycine, due to its side chain could disrupt the

protein folding. The fact that the Gly843 equivalent in other ATPases contacts ATP [120,143] may also indicate that the PEX1-G843D mutation could at least disrupt the ATP binding even if the PEX1 folding is preserved. Although ATP binding at the PEX1 D2 ATPase site is recognized as crucial for complex formation [144], ATPase activity within the PEX1 D2 ATPase is not essential for *in vivo* Pex1 function [130,137]. Therefore, it has yet to be established whether PEX1-G843D affects the activity of the ATPase complex formed by PEX1 and PEX6.

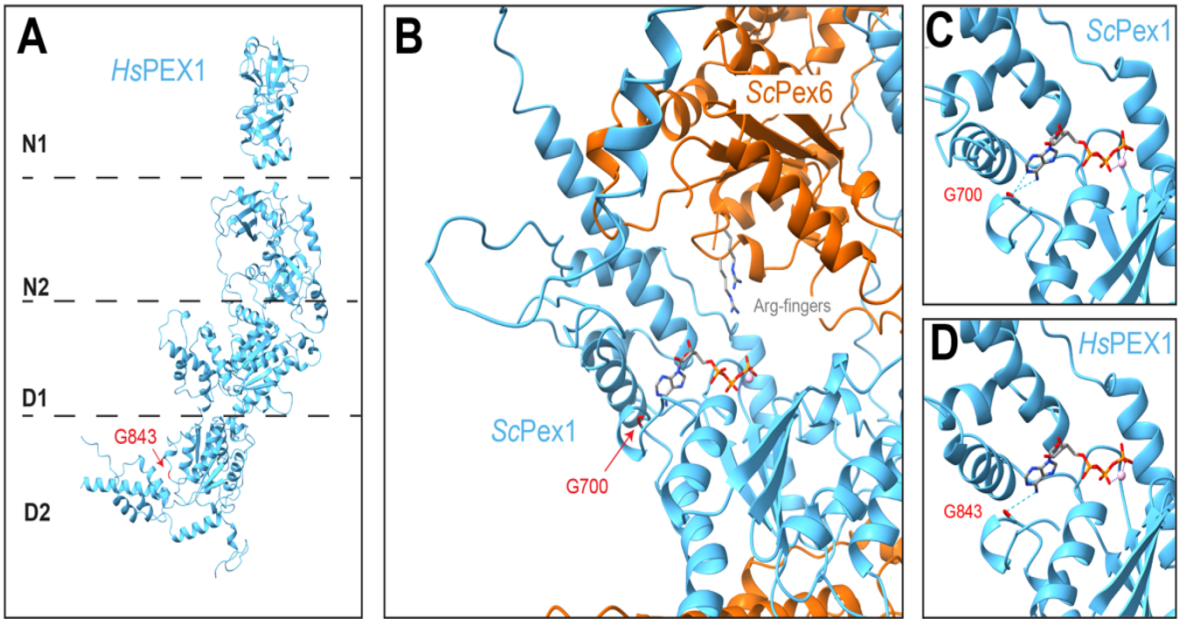

Figure 7: PEX1-G843D is expected to disrupt ATP binding and/or protomer folding. (A) HsPEX1, based on AlphaFold2 and X-ray crystallography. G843 is in the PEX1 D2 ring. (B) ScPex1 D2 ATPase in the Pex1/Pex6 hexamer at the Pex1 site most likely to be nucleotide-bound (AlphaFold2, EMDB-6359, **[120]**). Note that nucleotides are not discernible in experimental structures of Pex1/Pex6; an ATP is modeled based on alignment with a high-resolution structure of Hsp97 (PDB 7LN5, **[139]**). (C) The glycine G843 in HsPEX1 is conserved. The homologous residue in ScPex1 (G700) is colored in red and the backbone is predicted to hydrogen bond with the adenosine of ATP (**[139]**, ChimeraX). (D) In the structurally similar ScPex1 and HsPEX1 ATPase sites, G700 or G843 hydrogen bond (dotted lines) with ATP. Adopted from Judy *et al.*, 2022 **[123]**.

1.1.6 Recovery of peroxisomal protein import by chaperones and small molecules

Chemical chaperones refer to small compounds that nonselectively stabilize abnormal proteins by changing their surroundings through weak thermodynamic interactions and often require high concentrations for efficacy [146]. Pharmacological chaperones on the other hand are designed to bind specifically to target proteins helping in the folding of abnormal protein intermediates into their native state and are effective at much lower

concentrations [147]. Chemical chaperones like glycerol, betaine and trimethylamine N-oxide as well as flavonoid-based molecules like acacetin and diosmetin have been identified as molecules that can improve the import of PTS1 proteins in PEX1-G843D patient fibroblasts [141,148]. The exact mode of action of these molecules is yet to be understood; whether they stabilize PEX1, increase binding affinity to PEX6 or keep the PEX1/PEX6 complex together via other mechanisms.

Since PEX1-G843D has been identified as the most common mutation in PBD, research efforts are being made to target this mutation and improve the complex assembly. The formation of PEX1/PEX6 complex requires the interaction of ATP-binding sites (D1 and D2 rings) of both proteins [120] which also depends on the cellular ATP concentration. Small molecules that bind to or at the vicinity of the ATP-binding pockets in the PEX1-G843D/PEX6 complex might improve its stability. Speculations have been made about the candidate flavonoid diosmetin, based on its structure similarity to ATP, that it dynamically interacts with the ATP-binding regions of PEX1-G843D alone or the PEX1-G843D/PEX6 complex thereby increasing peroxisomal import. A combination therapy involving betaine (a chemical chaperone) and flavonoids (pharmacological chaperones) has also been more effective at lower doses and could potentially reduce side effects [148]. Some of these compounds have already been approved for other conditions and optimization studies involving peroxisomal targets could pave the way for their use in ZSD.

A recent study revealed that the heterohexameric complex stability is also influenced by the N1 domain of Pex6 which mediates binding to the extended loop of the D2 ATPase domain of Pex1 in *Saccharomyces cerevisiae* [136]. Alphafold2 predicts that this loop in human PEX1 is extended [149,150] which is subject to phosphorylation and could be a place for possible regulation [151,152]. Therefore, obtaining a detailed structure of the human PEX1/PEX6 complex is crucial for characterizing the binding interfaces and help in designing small molecules to enhance PEX1/PEX6 assembly.

1.2 RNA editing

Single-nucleotide mutations are responsible for more than half of all disease causing genetic variations in humans [153] and several techniques have been designed and studied to reverse the effect of such pathogenic point mutations [154]. Gene replacement therapy has been employed through a single injection, yet it faces constraints due to the payload capacity of viral vectors and the potential for toxicity from prolonged overexpression of the therapeutic gene [155]. DNA editing techniques, using Zinc-finger nucleases and CRISPR-associated proteins (Cas), have been modified to target the genome [156,157]. However DNA editing might sometime result in undesired and permanent alterations [158] and genome editing is mostly unfeasible for postmitotic cells that lack reliable mechanisms for repairing DNA breaks [159,160].

As an alternative, the use of programmable RNA base editors represents a promising avenue for flexible and reversible therapeutics, as RNA degradation by cells allows for the removal of errors introduced by RNA-based therapy over time [161,162]. Alteration in RNA nucleotide bases is not permanent or inheritable but instead can be reversed and dose-adjusted, making them adaptable for a range of therapeutic uses [163–165]. The method is also regarded ethical as germline editing/manipulation is not of concern. Currently four major RNA-targeting systems are being used namely (i) CRISPR-based systems, (ii) CRISPR-free ribonucleoprotein (RNP)-based systems, (iii) protein-alone targeting systems, and (iv) RNA-alone targeting systems [166].

RNA base editing is an inherent biological phenomenon observed in eukaryotic organisms. Apart from methylation and isomerization, RNA base editing is another post-transcriptional modification that imparts various alterations in RNA functionality. A family of adenosine deaminases that act on RNA (ADARs) convert adenosines to inosines (A-to-I) (Figure 8) which is read as guanosine by the translation machinery [167,168]. A group of apolipoprotein B mRNA-editing enzyme, catalytic polypeptide (APOBEC), a cytidine deaminase converts cytidine to uridine (C-to-U) in single stranded RNA [169,170]. Similarly, the family of adenosine deaminases that act on tRNA (ADATs) are active in tRNAs for A-to-I deamination [171].

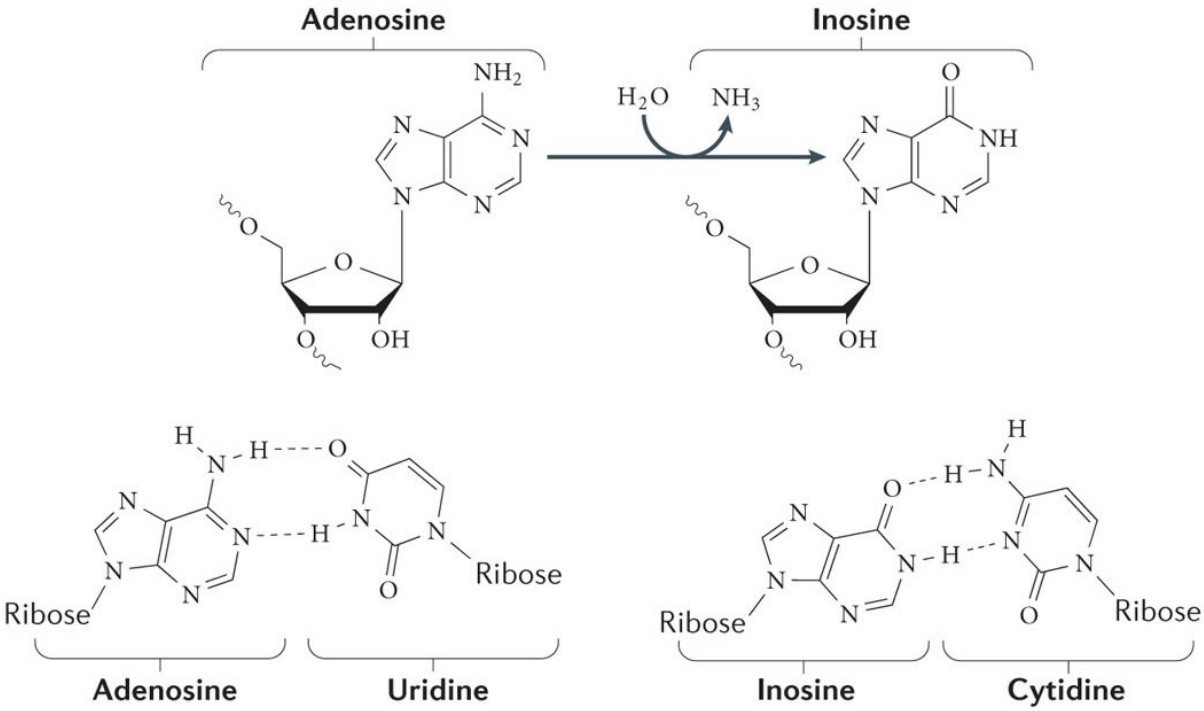

Figure 8: Deamination of adenosine to inosine by adenosine deaminases acting on RNA (ADAR) proteins. ADARs catalyze a hydrolytic deamination reaction that converts adenosine to inosine (top). Whereas adenosine base-pairs with uridine, inosine behaves like a guanosine, as it base-pairs with cytidine in a Watson–Crick-bonding configuration (bottom). Adopted from Nishikura, 2016 **[172]**.

Initially, it was documented that RNA duplexes introduced into *Xenopus laevis* eggs and embryos experienced a process of unwinding, a phenomenon later attributed to RNA editing [173–175]. Following this, mammalian ADAR genes were discovered and subsequently cloned [176–179] which gave rise to the field of RNA editing. Efforts to modify RNAs through site-directed RNA-editing (SDRE) techniques are relatively new and current practice of RNA base editing is mainly concentrated in A-to-I and C-to-U editing (reviewed in [172]).

1.2.1 The ADAR protein family

Three types of ADARs are found in most vertebrates: ADAR1, ADAR2 and ADAR3 [172,180]. All three types contain a C-terminally located deaminase binding domain, a nuclear localization signal (NLS) and two to three double stranded RNA binding domains (dsRBDs) (Figure 9). ADAR3 is catalytically inactive and additionally contains N-terminal arginine-rich single stranded RNA binding domain [179]. Two isoforms of ADAR1 are available due to alternative splicing: ADAR1 p150 and p110 [181]. Interferon-inducible ADAR1p150, a 150 kDa isoform, possesses a Zα and a Zβ Z-RNA binding domain [182]

along with a nuclear export signal (NES). Constitutively expressed ADAR1p110, a shorter 110 kDa isoform, lacks the Zα domain, as well as an N-terminal segment and the NES. ADAR1p110 and ADAR2 are localized to the nucleus [183,184]. ADAR1p150 is predominantly found in the cytoplasm but can also shuttle between cytoplasm and nucleus due to the presence of both, an NLS and an NES [168]. Expression of ADAR1 is found in all tissues whereas ADAR2 and ADAR3 are mainly found in the brain [185].

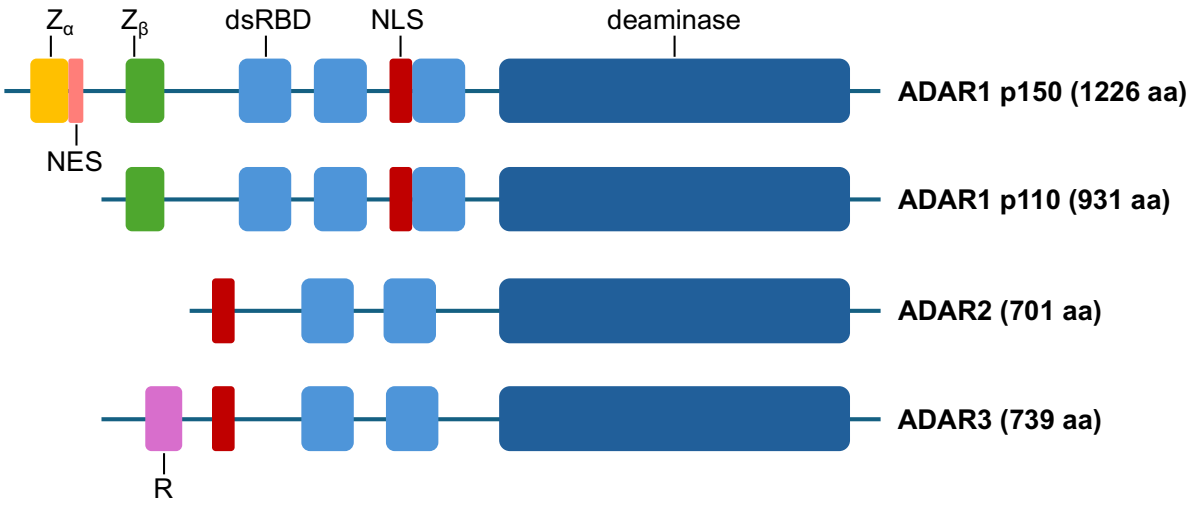

Figure 9: Domain organization of the ADAR protein family. Each type of ADAR protein exhibits comparable yet distinct functional domains, including a deaminase domain (dark blue), two to three double-stranded RNA binding domains (dsRBDs) (light blue), a nuclear localization signal (NLS) (red), a nuclear export signal (NES) (orange), a Zα (yellow) and/or a Zβ (green) Z-RNA binding domain, and an arginine-rich single-stranded RNA binding domain (R) (purple). Figure based on Datta *et al.*, 2024 **[186]**.

RNA A-to-I editing can take place in any dsRNAs of 20 base-pairs or more [187] for which the editing site needs to be recognized by ADARs. ADARs access the target adenosine in the RNA duplex using a base flipping mechanism [188] and convert it to inosine by an irreversible hydrolytic deamination reaction [189]. The selection of adenosines for editing seems to be dependent on the secondary structure of the RNA [190]. The editing efficiency of ADARs can range from 2-100% [189,191,192] which depends on the type of cells/tissues tested [193] and the developmental stages [194].

Due to the specific editing efficiency and specificity of ADAR enzymes, they have been employed in cells and mouse models to correct pathologies. Since ADARs require duplex RNA for activity, guide RNA strands complementary to the target region are designed that recruit ADARs to the disease-causing mutations. Methods using ectopically

overexpressed as well as the endogenous ADARs are being studied to correct disease specific point mutations [164,195–199].

1.2.2 SNAP-ADAR based RNA editing

SNAP-ADAR technology is a well adjustable SDRE strategy established by the Stafforst lab which has been employed in cells as well as in embryos [161,200]. In this method, a wildtype or hyperactive (E/Q mutant) deaminase domain (DD) of ADAR1 or ADAR2 is fused to an N-terminal SNAP enzyme where a nuclease-resistant guide RNA (gRNA) conjugated to O^6-benzylguanine (BG) is utilized for substrate recognition (Figure 10) [200,201].

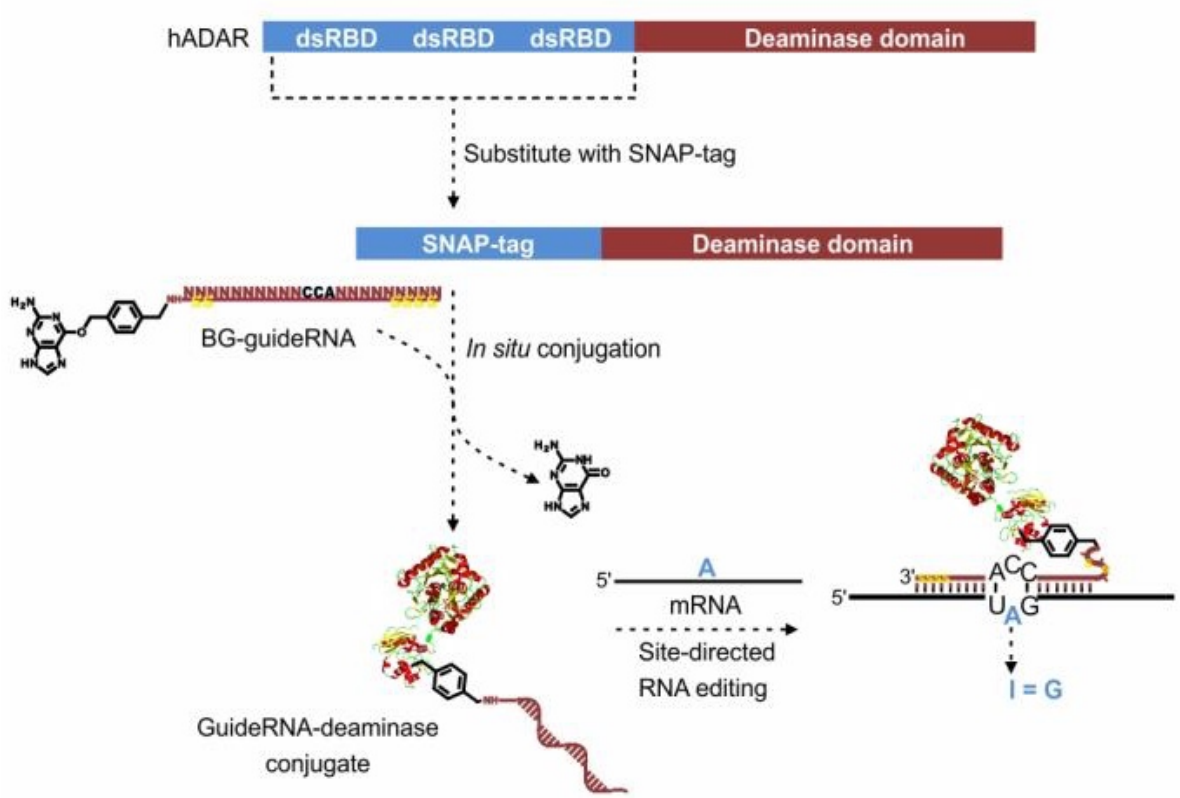

Figure 10: Site-directed RNA editing by SNAP-tagged ADARs driven by short, chemically modified guide RNAs. The double-stranded RNA-binding domains (dsRBDs) of hADAR have been substituted with the SNAP-tag. The latter can form a covalent bond to a guideRNA that is modified with benzylguanine (BG). When bound to the SNAP-ADAR, the guideRNA steers the attached SNAP-ADAR protein to the target RNA and forms the necessary secondary structure for A-to-I editing catalyzed by the deaminase domain. Adopted from Vogel *et al.*, 2018 **[163]**.

SNAP-ADAR is engineered to link with the BG gRNA in a 1:1 stoichiometry which is then guided to the target point for modification. To use this system, the cells are first modified

to stably express the SNAP-ADAR fusion under the induction of an antibiotic such as doxycycline. Specific BG gRNAs are then transfected to those cells which recruit the SNAP-ADAR enzyme to the target mutation for editing [163]. Chemical modification of the gRNAs can increase their stability and resistance to ribonucleases as well as reduce the number of off-target editing. This system can also be used to target multiple sites by co-transfecting a mixture of BG gRNAs into the cells.

As the BG moiety is an essential part of the editase, the SNAP-ADAR system cannot be genetically encoded. However, this system has the potential of chemical modifications and optimizations such as specificity, potency and stability that can be difficult in the endogenous system [163]. BisBG (BB) modified gRNAs have also been developed for this method by the Stafforst lab. BisBG is a dimeric linker that facilitates the attachment of two SNAP-ADAR fusion proteins to either 3'- or 5'- end of a single gRNA. When using the hyperactive variants of SNAP-ADAR enzyme, editing efficiency as high as 90% has been achieved [162].

By utilizing photocaged BG-gRNAs, light-triggered assembly of the SNAP-ADAR conjugates was successful. These conjugates could modify the localization of reporter proteins by incorporating localization signals [202] and even facilitated SDRE in living organisms [203]. Therefore, the SNAP-ADAR system is highly adaptable and serves as a valuable technique applicable in both in vitro and in vivo systems, demonstrating immense potential in clinical research.

1.2.3 RESTORE based RNA editing

SDRE techniques using exogenous editases, as in the SNAP-ADAR system, although having high editing efficiency, also come with hindrances. Such methods require the ectopic expression of the enzyme and are also prone to off-target editing in some cases [161]. Harnessing of the endogenous ADAR enzymes, that are expressed and active in most human tissues, is therefore a promising alternative for site directed editing [164].

Recruiting endogenous ADAR to specific transcripts for oligonucleotide-mediated RNA editing (RESTORE) is a technique that employs chemically stabilized antisense oligonucleotides (ASOs) to tether endogenous ADAR proteins for editing target mutations [164]. Chemically modified ASOs have improved pharmacological properties as

compared to the guide RNAs with the exact sequence lacking modification [204]. Such chemical modifications can regulate the drug delivery, enhance metabolic stability and efficiency, [205,206] and also prevent the ASOs from ribonuclease degradation [207]. The ASOs typically consist of a segment of 20-40 nucleotides that complement the target sequence (specificity domain) and a distinctive hairpin motif that enables ADAR dsRBD binding (ADAR-recruiting domain) (Figure 11). An ASO-mRNA complex is formed where the precise editing at the mRNA site is governed by the chemically altered ASO, leading to a specific adenosine-to-inosine alteration.

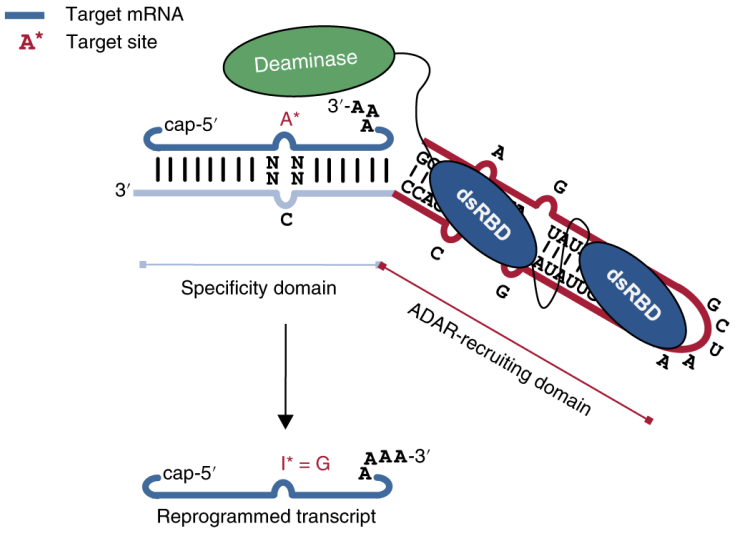

Figure 11: Design of ADAR-directing ASOs. ASOs comprise a programmable specificity domain that determines target mRNA binding and an invariant ADAR-recruiting domain to steer endogenous ADAR to the ASO:mRNA hybrid. Site-directed RNA editing at the mRNA is controlled by the chemically modified ASO and results in a specific adenosine-to-inosine change (functionally equivalent to an adenosine-to-guanosine change). dsRBD: double-stranded RNA-binding domain; A* or I*: adenosine or inosine base at target site, respectively. Adopted from Merkle *et al.*, 2019 **[164]**.

The RESTORE technique shows significant promise for translation into clinical research due to its precision in editing efficiency and no need of transgene expression.

1.3 Aims of this study

The AAA ATPases PEX1 and PEX6 play a crucial role during the matrix protein import in the peroxisomes and are essential for their proper functioning. Mutations in the genes encoding these proteins are major causes of several peroxisome biogenesis disorders (PBDs). One such mutation, PEX1-c.2528G>A (p.G843D), potentially leads to misfolded PEX1.

Studies of *S. cerevisiae* Pex1/Pex6 have revealed cryo-EM structures that allowed to analyze substrate processing methods of the complex. Although predictions have been made about the human PEX1/PEX6 complex, proper purification and structural data are still unavailable. Therefore, one of the main aims of this work was to establish a method to purify the recombinant human wildtype PEX1/PEX6 as well as the mutant PEX1-G843D/PEX6 complex. For this, the open reading frames (ORFs) of PEX1, PEX6 as well as PEX1-G843D with suitable tags should be cloned into separate vectors allowing the expression of the proteins in HEK293TT cells. Protein complexes were to be purified by sequential affinity chromatography methods and analyzed by western blotting and silver staining techniques to check the purity of the complexes.

Studies have shown that treatment with various chemical and pharmacological drugs, such as betaine and diosmetin, can restore the import function in patient cells expressing PEX1-G843D, however the exact mechanism remains unknown. Therefore, it was aimed to study possible interactions of these drugs with the PEX1/PEX6 complex using microscale thermophoresis (MST) by fluorescently labeling the PEX1 protein and measuring the binding events between proteins and ligands (drugs). The effect of the drugs in mutant cells should also be studied by immunofluorescence microscopy.

Furthermore, it was aimed to reverse the PEX1-G843D mutation in mutant fibroblast and HEK Flp-In cells at the mRNA level by utilizing two different methods of side directed RNA editing (SDRE). One method, the SNAP-ADAR system utilizes stably integrated deaminase to edit the target site with the help of BB-gRNA while the other RESTORE method uses chemically modified ASOs to harness endogenous ADARs to correct the point mutation. In both methods, the editing efficiency should be analyzed using Sanger sequencing and immunofluorescence microscopy.

2 Materials and methods

Unless otherwise stated, all chemicals and reagents used in this work used for preparing buffers and solutions were purchased from Carl Roth (Karlsruhe, Germany), Sigma Aldrich (München, Germany), Thermo Scientific (Karlsruhe, Germany) or Invitrogen (Karlsruhe, Germany). All enzymes and solutions used for cloning and PCR were purchased from Thermo Scientific (Karlsruhe, Germany), Qiagen (Hilden, Germany) or New England Biolabs (Frankfurt am Main, Germany). Oligonucleotides were purchased Biomers (Ulm, Germany). Sanger sequencing data were evaluated with ApE- A plasmid Editor v2.0.61. This thesis was written in Microsoft Word for Mac v16.75 (License: Microsoft 365) and all figures were prepared with Affinity designer v1.10.5.

2.1 Molecular biology

2.1.1 Oligonucleotides

Oligonucleotides used in this study for PCR and sequencing (listed in Table 2.1 and Table 2.2 respectively) were purchased from Biomers (Ulm, Germany). Oligonucleotides used in the RNA editing experiments (Table 2.3, Table 2.4 and Table 2.5) were kindly provided from the lab of Prof. Dr. Thorsten Stafforst, IFIB Tübingen.

Table 2.1: PCR primers to amplify PEX1 and PEX6 ORFs

Label	Name	Sequence (5' -> 3')
GD571	PEX6_F	CTCCTTCACCCTCCTCGTTG
GD572	PEX6_2xFLAG_R	TCAGCGAGCTCTAGCATTTAGG
GD573	PEX1_F	GCCACCATGTGGGGCAGCGATC
GD574	PEX1_Tev.His_6_R	TTAATGGTGATGGTGATGGTGTCCCTGAAAATACAGGTTTTCTGC TAAAGTTACTTTCTGTCCAGGTCGAAACATTGTTC
GD589	Kozak-StrepII-TEV-PEX6_F	GCCACCATGTGGAGTCATCCACAATTTGAAAAGGAAAACCTGTAT TTTCAGGGAGCGCTGGCTGTCTTGCGGGTCCT
GD590	PEX6_R	TTAGCAGGCAGCAAACTTGCGCTGG
GD591	PEX6_StrepII_R	TTACTTTTCGAACTGCGGGTGGCTCCAGCAGGCAGCAAACTTGCG
GD577	PEX1_G2528A_F	TGGGACAAGATTGATGGGTTACATGAA
GD578	PEX1_G2528A_R	TTCATGTAACCCATCAATCTTGTCCCA

Table 2.2: Primers for plasmid sequencing

Label	Name	Sequence (5' -> 3')
GD592	pGwf_PEX1_rv#1	TAGAGGAACAACCTTTGACTGC
GD593	pGwf_PEX1_fw#1	TGGCACTTGATGTAATTCTCC
GD594	pGwf_PEX1_fw#2	CTGTGGGAATCACTGAATCTAATG
GD595	pGwf_PEX1_fw#3	TTTCTGTTGAGTCCCAATTTGC
GD596	pGwf_PEX1_fw#4	TTTACAGTACTTGTGGATCGAGC
GD597	pGwf_PEX1_fw#5	AGTGGACTCCAGGATGGAAG
GD598	pGwf_PEX6_rv#1	GAGCCTTCCAAGTACCTCTG
GD599	pGwf_PEX6_fw#1	TTTCTTCCATTTCAGGTGTCG
GD600	pGwf_PEX6_fw#2	AGGCCAGAGAGTCATCGAAC
GD601	pGwf_PEX6_fw#3	TGGGCTCCACTTACTGAAGG
GD602	pGwf_PEX6_fw#4	TAGCCACTGAGTGCAGCCTTA
GD608	GW1(TOPO)	GTTGCAACAAATTGATGAGCAATGC
GD609	GW2(TOPO)	GTTGCAACAAATTGATGAGCAATTA

Table 2.3: gRNAs used in RNA editing

Name	Target	Length	Properties
BB283	PEX1-G843D	25 nt	Moderate modification
NH283	none	25 nt	unmodified and NH_2-terminal
BB180	STAT1 Y701C	25 nt	Moderate modification
NH180	none	25 nt	unmodified and NH_2-terminal

Table 2.4: Antisense oligonucleotides (ASOs) used for RNA editing

Name	Target	Length	Editing site / Modification
Control ASOs (Sequence 5'->3' ; Base opposite of editing site is bold and underlined)			
AI-0111	β-Actin 3'-UTR	45 nt	GCATTACATAATTTACACGAAAGCAATG C**C**A TCACCTCCCCTGTG
TMR84	GAPDH L157L	59 nt	UUGUCAUGGAUGACCUUGGCCAGGGGUG C**C**A AGCAGUUGGUGGUGCAGGAGGCAUUGCU
TMR469	STAT1 Y701C	59 nt	CAGACACAGAAAUCAACUCAGUCUUGAU A**C**A UC CAGUUCCUUUAGGGCCAUCAAGUUCC
TMR131	STAT1 Y701C	45 nt	very few chemical modifications, very instable
TMR141	STAT1 Y701C	59 nt	same chemical modifications as TMR131
TMR174	STAT1 Y701C	59 nt	same sequence and length as TMR141
PEX1 ASOs			
TMR177	PEX1-G843D	59 nt	same chemical modifications as TMR 141, PEX1 equivalent to STAT1 TMR141
TMR178	PEX1-G843D	45 nt	same chemical modifications as TMR131
TMR204	PEX1-G843D	59 nt	more chemical modifications, PEX1 equivalent to the STAT1 TMR174
TMR205	PEX1-G843D	59 nt	same number of chemical modifications as TMR204, but slightly different combination
TMR423	PEX1-G843D	59 nt	same modifications and length as TMR177

The targeted adenosine on the PEX1 transcript is in a 5'-GAU context. Opposite of the target site, the ASO sequence of TMR177 is 5'-ACC, meaning the targeted adenosine is put into mismatch with a C. For TMR423, the ASO sequence in that area is 5'-ACG, meaning besides the A:C mismatch that marks the target adenosine, there is a G:G mismatch right next to it. This effect has already been published [208].

Table 2.5: PCR and sequencing primers used in RNA editing

Name	Sequence (5' -> 3')	Target
Sense_BB283	GGGACAAGATTGCTGGGTTACAACC	PEX1-G843D
Sense_TMR177/ 204/205	ACCTAGAGACCTGGGTTGGGACAAGATTGCTGGGTTACAT GAAGTTAGGCAGATACTCAACC	PEX1-G843D
Sense_TMR178	GACAAGATTGCTGGGTTACATGAAGTTAGGCAGATACTCA TGGATTGA	PEX1-G843D
Sense_TMR131/ 141	TTCTGTGTTCACTTACACTTCAGACACAGAAATCAACTCA GTCTTGATAGATCCAGTTCCCTATAGTGAGTCGTATTA	PEX1-G843D
STAT1 fw	GCTTCATCAGCAAGGAGCGAGAGCG	STAT1 Y701C
STAT1 rev	CTTCAGACACAGAAATCAACTCAGTC	STAT1 Y701C
STAT1 seq #fw	GGCTGCTGAGAATATTCCTGAGAATC	STAT1 Y701C
ACTB_F	CGAGCATCCCCCAAAGTTCAC	β-Actin 3'-UTR
ACTB_R	CACTCCCAGGGAGACCAAAAGC	β-Actin 3'-UTR
Sense_ACTB	GGGAGGTGATGGCATTGCTTTCGTGTAAATTATGTAATGC AAAATAAA	β-Actin 3'-UTR
GAPDH_F	CTCAAGATCATCAGCAATGCCTCCTGC	GAPDH L157L
GAPDH_R	GAGCACAGGGTACTTTATTGATGGTACATGACAAGG	GAPDH L157L
GAPDH_seq	GCTGTTGAAGTCAGAGGAGACC	GAPDH L157L
Sense_GAPDH	CCAACUGCUUCGCACCCCUGGCCAAGGUCAUCCAUGACAA	GAPDH L157L
G843D_9_Fw	CGATCTTGACCTGCAGCAT	PEX1-G843D
G843D_10_Rv	CCCGAACAGCTTGTTCACTT	PEX1-G843D
G843D_43_Fw	ACTTGTGGATCGAGCCATACATTCT	PEX1-G843D
G843D_44_Rv	CAGCTTGTTCACTTGCTCCAATGTA	PEX1-G843D
G843D_53_Fw	CAGTCTCAGCAATCTCTACATC	PEX1-G843D
G843D_54_Rv	GAGTATCTGCCTAACTTCATGT	PEX1-G843D

2.1.2 Plasmids

All plasmids used during this work are listed in Table 2.6. Maps of the plasmids produced during this work as well as the respective amino acid sequences of the corresponding proteins (PEX1 or PEX6) are listed in Appendix 6.1. PiggyBac transposon and transposase plasmids used in this project were kindly provided by the group of Prof. Dr. Thorsten

Stafforst, IFIB Tübingen. The vector pGwf was purchased from addgene [209] and pCR8.GW.TOPO from Thermo Scientific.

Table 2.6: Plasmids generated and used

Label	Construct (cDNA and tags)	Bacterial Antibiotic Resistance	Source
pSE5.1	pcDNA3.1_PEX6.2xFLAG	Ampicillin	Patrick Schulte-Euler
pBM57	pcDNA3.1Zeo_PEX1	Ampicillin	Britta Möllers
TOPO	pCR8.GW.TOPO	Spectinomycin	Invitrogen
pGWf	pGwf	Chloramphenicol and Zeocin	Addgene: 22517 [209]
pSP01	pCR8.GW.TOPO_PEX6.2xFLAG	Spectinomycin	This study
pSP02	pCR8.GW.TOPO_PEX1.TEV.HIS_6	Spectinomycin	This study
pSP03	pGwf_PEX6.2xFLAG	Zeocin	This study
pSP05	pGwf_PEX1.TEV.HIS_6	Zeocin	This study
pSP07	pGwf_PEX1(G843D).TEV.HIS_6	Zeocin	This study
pSP09	pCR8.GW.TOPO_Strep.TEV.Pex6	Spectinomycin	This study
pSP10	pCR8.GW.TOPO_Pex6.Strep	Spectinomycin	This study
pSP11	pGwf_Strep.TEV.Pex6	Zeocin	This study
pSP12	pGwf_Pex6.Strep	Zeocin	This study
pTS990	SA1_Xlone_BSD	Ampicillin	Stafforst lab, IFIB
pTS1018	SA1EQ__Xlone_BSD	Ampicillin	Stafforst lab, IFIB
pTS1019	SA2__Xlone_BSD	Ampicillin	Stafforst lab, IFIB
pTS1020	SA2EQ_Xlone_BSD	Ampicillin	Stafforst lab, IFIB
pTS687	Transposase	Ampicillin	Stafforst lab, IFIB

2.1.3 Bacteria

Escherichia coli (*E. coli*) strains used for cloning are given in Table 2.7. Cells were grown in Luria Bertani (LB) liquid medium supplemented with appropriate antibiotics at 37 °C and shaking at 150 rpm for 16-18 hours. LB media was prepared using 0.5% (w/v) yeast extract, 1.0% (w/v) peptone and 0.5% (w/v) NaCl in ddH_20 and autoclaved. 1.5% (w/v) agar was added for making solid plates.

Table 2.7 *E. coli* strains used

***E. coli* strain**	**Genotype**	**Source**
One Shot™ TOP10	F-*mcrA* Δ(*mrr-hsd*RMS-*mcr*BC) Φ80*Lac*ZΔM15 Δ *Lac*X74 *rec*A1 *ara*D139 Δ(*araleu*) 7697 *gal*U *gal*K *rps*L (StrR) *end*A1 *nup*G	Invitrogen
DH5α	F-, ø80dlacZΔM15, Δ(lacZYA-argF)U169, deoR, recA1, endA1, hsdR17(rk^-, mk^+), phoA, supE44, λ-, thi-1, gyrA96, relA1	Invitrogen

2.1.4 Gateway Cloning

For functional analysis and protein expression, the Gateway® Technology offers a quick and highly effective method to transfer DNA fragments into various types of vectors [210]. The Gateway® Technology utilizes the bacteriophage lambda site-specific recombination system, which enables integration into the chromosome of *E. coli* and facilitates the transition between the lytic and lysogenic pathways, with modified components to enhance the specificity and efficiency of the system [211].

As opposed to the classical restriction cloning method, Gateway cloning does not require the use of restriction enzymes. Instead, it comprises a two-step recombination process in which a target gene is cloned twice to first form an entry clone in the first step and an expression clone in the latter step. During this study, the linear TOPO vector was used for entry clone preparation, whereas a pGwf vector was used as a destination vector in expression clone preparation. An overview of the steps applied in preparation of the expression vectors used in this work is depicted in Figure 13.

2.1.4.1 Polymerase chain reaction (PCR)

Primers used in the amplification of the PEX1 and PEX6 ORFs are listed in Table 2.1. Primers were designed and used to amplify target regions, the open reading frames of hsPEX1 and hsPEX6, from the plasmids pBM57 and pSE5.1 respectively. Some primers were designed with overhangs to introduce the desired tags at N- or C-terminal ends of the proteins. Components for the PCR are listed in Table 2.8 and the thermocycling conditions in Table 2.9. Target regions were first amplified using a temperature gradient. Then the best annealing temperature was selected after running the products on an agarose gel. The selected temperature for each plasmid-primer combination was then used to amplify the target region: 64 °C for (PEX6.2xFLAG), 64 °C for (StrepII.TEV.PEX6) and 69 °C for (PEX1.TEV.HIS6). PCR products were loaded on an agarose gel (0.8%), run until the bands separated which were then excised and purified (GenElute™ Gel Extraction Kit, Sigma Aldrich).

Table 2.8: PCR Components

Components	Volume (µL)
5X HF buffer	20
10mM dNTPs	2
Fwd Primer (10 µM)	5
Rev Primer (10 µM)	5
dimethyl sulfoxide (DMSO) (5%)	5
Template DNA (plasmid)	20 ng
Phusion polymerase	2U
H_2O	To 100

Table 2.9: Thermocycling conditions

Step	Cycles	Temperature (°C)	Time (s)
Initial denaturation	1	98	30
Denaturation	30	98	8
Annealing		PEX6: 56 - 70 PEX1: 64 - 72	25
Extension		72	25s/kb
Final Extension	1	72	600
Hold	1	4	0

2.1.4.2 3'A overhang extension PCR

As the entry clone preparation (TOPO TA cloning) relies on the presence of 3'A overhangs in the PCR products, a 3'A overhang extension PCR was carried out in presence of Taq polymerase. For this, the PCR mix was prepared according to the Table 2.10 and kept in a thermocycler at 72 °C for 20 minutes. The resulting product was once again run on an agarose (0.8%) gel and purified.

Table 2.10: Components for 3'A overhand extension PCR

Components	Final concentration	Quantity
Purified PCR product	0.15 to 1.5 pmol	4 µg
dATP (10mM)	0.2 mM	2 µL
PCR buffer with Mg (10X)	1X	10 µL
Taq DNA polymerase	1U	0.4 µL
H_2O	-	To 100 µL

2.1.4.3 TOPO TA cloning

DNA topoisomerase I is a vital component in TOPO TA cloning, serving dual roles as both a restriction enzyme and a ligase. Its natural function involves cleaving and rejoining DNA during replication. To leverage the DNA rejoining capability of topoisomerase I, TOPO™ vectors are designed with topoisomerase I covalently attached to the 3´ phosphates at each end which allows the vectors to easily ligate DNA sequences with compatible ends.

pCR8/GW/Topo TA cloning kit (Thermo Scientific) was used to prepare entry clones containing the respective constructs. Reaction mixtures were prepared as in Table 2.11 and incubated at room temperature for 1 hour, then overnight at 4°C. Using heat shock method, the cloned vectors were transformed into One Shot™ TOP10 *E. coli* cells. Positive colonies were selected in LB agar with an antibiotic (100µg/mL Spectinomycin) and stored (see Section 2.1.6). Purified plasmids from selected cells were sent for Sanger sequencing (with primers GW1 and GW2, from the kit) and correct constructs were stored frozen. These plasmids served as entry clones for the LR reaction.

Table 2.11: TOPO TA cloning components

Components	Volume (µL)
Fresh PCR product (100ng/ µL)	2-4
Salt solution (6X)	1
H_2O	0-2
TOPO vector	1

2.1.4.4 LR cloning

This is the final step in Gateway cloning in preparation of the destination clone for which the LR Clonase® II enzyme mix consisting of integrase (Int), integration host factor (IHF) and excisionase (Xis) was used. This exclusive blend of lambda recombination proteins facilitates the attL x attR recombination process. TOPO constructs prepared in the previous step were used as entry clones and pGwf (addgene.org/22517) as the destination vector containing an EF1alpha promoter. Due to its resistance to silencing and the capacity to deliver consistent long-term expression, the EF1alpha promoter was chosen over the traditional CMV promoter. It ensures improvement in factors such as

transfection efficiency, transgene expression, positive clone proportion, and episomal vector copy number [212–214].

The LR cloning mix was prepared according to Table 2.12 and incubated for 1 hour at 25°C. Thereafter, 1 µL of Proteinase K solution was added to it and vortexed before being incubated for 10 minutes at 37°C. The transformation into One Shot™ TOP10 *E. coli* cells was performed using the heat shock method. The transformed cells were selected with Zeocin (50 µg/mL). Following colony selection, plasmid extraction was performed, and the obtained plasmid DNA was subjected to enzyme digestion, to confirm the final plasmid size. Selected plasmids were sequenced for the entire coding region of the proteins (including tags). The primers used for sequencing PEX1 and PEX6 are stated in Table 2.2.

Table 2.12: LR cloning components

Components	Quantity
TE buffer, pH 8.0	3 µg
Entry clone (TOPO_PEX1/6)	100 ng
Destination vector (pGwf)	75 ng
LR Clonase II enzyme mix (vortex twice 2s)	1 µL
H_2O	to 10 µL

2.1.5 Site directed mutagenesis

Mutagenesis PCR was performed to introduce the G843D, c.2528 G→A mutation in the pGwf_PEX1.TEV.HIS_6 expression plasmid. Components for this PCR mix are stated in Table 2.13 where the nucleotide to be changed is indicated in bold and underlined in the primer sequences. Thermocycling conditions for the PCR are given in Table 2.14. Primers for this PCR were designed to overlap the region where the single nucleotide change was expected. The annealing and extension steps were run for 3 minutes at each cycle with a final extension time to 5 minutes to ensure that the entire length of the plasmid is amplified.

Table 2.13: Mutagenesis PCR components

Components	Volume (µL)
5X HF buffer	10
10mM dNTPs	1

Fwd Primer (10pmol/µL) 5'-TGG GAC AAG ATT G**A**T GGG TTA CAT GAA -3'	2.5
Rev Primer (10pmol/µL) 5'-TTC ATG TAA CCC A**T**C AAT CTT GTC CCA -3'	2.5
DMSO (5%)	2.5
Template (pGwf_PEx1_TEV_HIS_6)	10ng
Phusion polymerase	1U
H_2O	To 50

Table 2.14: Thermocycling conditions for mutagenesis PCR

Step	Cycles	Temperature (°C)	Time (s)
Initial denaturation	1	98	30
Denaturation	15	98	10
Annealing and Extension		72	180
Final Extension	1	72	600
Hold	1	4	0

After the PCR was completed, DpnI (1U) was added to the mixture and incubated for 1 h at 37°C. This step was done to digest the methylated DNA obtained from the bacteria. From this mixture, 4 µL were transformed into One Shot TOP10 cells. Colonies were selected followed by plasmid purification, enzyme digestion and sequencing to analyze the DNA.

2.1.6 Bacterial transformation by heat shock and storage

For transforming the prepared clones into the chemically competent One Shot™ TOP10 *E. coli* cells, 50 µL aliquots of the cells were first thawed on ice. Then 3 µL of TOPO reaction mixture or 1µL LR reaction mixture (pGwf) were added and incubated on ice for 10 minutes. A heat shock was given for 30 seconds at 42 °C and the cells were immediately put on ice. After 5 minutes, the cells were mixed in 250 µL SOC medium cell suspension was incubated for 2 h at 37 °C in a shaker. Finally, 50 – 200 µL bacterial suspension were plated on agar plates containing low-salt LB-medium with Spectinomycin (100 µg/mL) for the TOPO constructs or Zeocin (50 µg/mL) for pGwf constructs and incubated overnight at 37 °C.

For each construct, 10 single colonies were picked with a pipette tip and streaked onto a new plate. Then the pipette tip was transferred into a Falcon tube containing 6 mL low-salt LB-medium containing appropriate antibiotics and vortexed. Plates and Falcon tubes were then incubated overnight at 37 °C followed by plasmid isolation.

2.1.7 Plasmid amplification and isolation

The method of plasmid isolation was selected based on the type of results needed. A 'quick and dirty' method was used for checking large number of colonies/constructs at once. Mini plasmid extractions were done for selected constructs for sequencing. Midi- or maxi-prep plasmid isolation was performed to transfect mammalian cells for protein production.

2.1.7.1 'Quick and dirty' plasmid extraction (plasmid miniprep)

Bacterial suspensions (2-5 mL) were subjected to centrifugation at 16000 g for 1 minute and the supernatant was discarded. Cell pellets were resuspended in 400 µL of STET buffer (0.1M NaCl, 10mM Tris pH 8.0, 1mM EDTA pH 8.0, 5% Triton X-100) and vortexed. The cell suspensions were heated for 2 minutes at 95 °C after adding 30 µL of Lysozyme (10 mg/mL) and centrifuged at 16000 g for 15 minutes at 4 °C. The resulting supernatant was carefully transferred to a new 1.5 mL reaction tube and 400 µL of isopropanol were added and the sample was vortexed. The samples were centrifuged again at 16000 g for 10 minutes at 4 °C and the supernatant was gently removed using a pipette. After that, 1 mL of 99% ethanol was added to the cell pellet followed by another round of centrifugation at 16000 g for 10 minutes at 4 °C. The cell pellet was dried at 55 °C to remove excess ethanol. 50 µL of TE buffer was added to the pellet and incubated for 5 minutes at 60 °C. After centrifugation, 10 µL of the supernatants were used for the subsequent enzyme digestion (see 2.1.10).

2.1.7.2 Mini plasmid purification (clean plasmid miniprep)

The clean plasmid purifications were performed using the GenElute™ HP Plasmid Miniprep Kit, Sigma Aldrich. Overnight cell cultures (2-5 mL) were centrifuged at 16000 g for 1 minute and plasmid was extracted from the pellet following the instruction manual. The concentration and purity were checked via NanoDrop 1000 Spectrophotometer (Thermo Scientific).

2.1.7.3 Plasmid preparation

Larger plasmid isolation was required for the pGwf expression plasmids expressing PEX1 and PEX6 for transfecting them later into the HEK293TT cells. About 200 mL of low salt

LB medium (0.5% NaCl, 1% pepton, 0.5% yeast extract, 50ug/mL Zeocin) was inoculated with glycerol stocks of One Shot™ TOP10 Chemically Competent *E. coli* cells containing the desired plasmid. The culture was grown over night (37 °C, 160 rpm) and pelleted by centrifuging at 10000 g for 15 minutes. Plasmids were extracted from pelleted bacteria using the NucleoBond™ Xtra Maxi kit (Macherey-Nagel) following the manufacturers protocol. The concentration and purity of the extracted DNA was determined using a Nanodrop. Aliquots of 100-200 µL were stored at -20°C.

2.1.8 Agarose gel electrophoresis

Agarose gels for electrophoresis were prepared by combining the appropriate amount of agarose (agarose standard, ROTH) with 0.5X TBE buffer (4,45 mM Tris pH=8, 4,45 mM Boric acid, 10 mM EDTA), and the mixture was dissolved by heating in a microwave oven. Once dissolved, the agarose solution was allowed to cool down to a temperature between 50-60 °C with occasional stirring. Gel red dye (1:10000) was added to the solution and poured into the electrophoresis chamber, where a comb was inserted to create wells for loading samples. Any trapped air bubbles were carefully eliminated using a pipette tip. After the gel solidified, it was covered with 0.5X TBE buffer and the comb was carefully taken out. Samples mixed in gel loading dye and molecular weight markers were loaded into each well, and the chamber was closed. Electrophoresis was conducted at 100 V until the loading front migrated approximately three quarters of the gel. Finally, the DNA bands were visualized with a ChemiDoc analyzer, and images were recorded.

2.1.9 DNA extraction from agarose gels

Both, plasmids or smaller DNA fragments were extracted using the GenElute™ Gel Extraction Kit (Sigma Aldrich). After running the agarose gel and identifying the correct DNA bands with UV light, they were excised from the gel and kept in 2 mL reaction tubes. DNA was extracted following the instruction manual. The concentrations of the purified DNA samples were measured, and the DNA used for further experiments.

2.1.10 Restriction enzyme digestion

DNA samples (plasmids, PCR products) were digested using suitable restriction enzymes. A master mix was prepared with the following compounds mentioned in Table 2.15.

Table 2.15: Components used in enzyme digest (for 10 reactions)

Component	Volume [µL]
Nuclease-free H_2O	8
10x buffer	12
Restriction enzyme	2

From this master mix, 2 µL were used for each 10 µL DNA sample (max. 2 µg). The reaction mixture was then incubated for 2 hours or overnight at 37 °C. After incubation, samples were mixed with 6x loading dye and separated in an 0.8% agarose gel. Samples in the agarose gel were analyzed via a ChemiDoc analyzer.

2.1.11 RNA extraction from mammalian cells

Mammalian cells transfected with gRNAs or ASOs were lysed after 24 h by adding the appropriate amount of RLT buffer (Qiagen) either directly on the well plate or after pelleting. RNA extraction from the cell lysates was then performed using the Monarch RNA Cleanup Kit (New England Biolabs). Purified RNAs were measured via Nanodrop and used for the following RT-PCR.

2.1.12 One-Step RT-PCR

Purified RNA samples obtained from transfected cells were subjected to reverse transcription and taq PCR in one reaction using the OneTaq® One-Step RT-PCR Kit (25 µL) (New England Biolabs).

About 500 ng of RNA (up to 8 µL), 1.25 µL buffer, 1.25 µL reverse primer (10 µM) and 1 µL sense oligo were mixed and heated at 95 °C for 1 minute and cooled on ice. In absence of the sense oligo, the volume (1 µL) was substituted with H_20 or DMSO and the mixture was heated at 70 °C for 3 minutes.

Finally, 1.25 µL forward primer and 1 µL enzyme mix were added and the PCR was performed under the thermocyclic conditions stated in Table 2.1 using a hot start at 110 °C. Annealing temperature and extension time were chosen based on the primer pairs and the length of the expected PCR product.

Table 2.16: Thermocyclic conditions for One-Step RT-PCR

Step	Temperature	Time	Cycles
Reverse transcription	48 °C	60 min	1
Initial denaturation	94 °C	60 sec	1
Denaturation	94 °C	15 sec	36
Annealing	50 - 60 °C	30 sec	
Extension	68 °C	30 - 60 sec	
Final extension	68 °C	5 min	1
Hold	4 °C	∞	1

Obtained PCR products were run on an agarose gel (0.8%) and correct bands were excised and purified. The concentrations of the purified DNA samples were measured and sent for sequencing.

2.1.13 Sequencing

All Sanger sequencings were carried out using the GATC LightRun Tube service from Eurofins Genomics. 5 µL or purified DNA samples (plasmids or PCR products) were mixed with 5 µL primer in a 1.5 mL reaction tube as recommended in the manual. The reaction tube was labelled with the ordered barcode and sent for sequencing. Results obtained online (eurofinsgenomics.eu) were analyzed by ApE or SnapGene software.

2.2 Cell biology

All mammalian cell lines used in this work are listed in Table 2.17. Stable cell lines of M2H (patient fibroblast cell line with mutation PEX1-c.2528G>A) and PEX1-G843D HEK293(T) were generated during this study using the PiggyBac method to introduce four different SNAP-ADAR variants (see 2.2.3).

Table 2.17: Mammalian cells used in this work

Cell	Source
HEK293TT	Buck *et al.* 2004 [215] (Gift from Bärbel Blaum)
GM05756	Coriell Institute
ΔPEX1 (PBD009)	Collins *et al.*, 1999 [216]/ Gould, Baltimore
ΔPEX6 (PBD010)	Moser & Gould, Baltimore
M2H PEX1-G843D-PTS1 (Fibroblast; Pex1: c. [2528G>A]; [2097_2098insT], p. [G843D]; [0]), Expressing GFP-SKL	Zhang *et al.*, 2010 [141] (Gift from Nancy Braverman)

Hela (ATCC CCL-2)	Gift from Stafforst lab
Flp-In™ T-REx™ 293	Gift from Stafforst lab
Flp-In™-293	Hans Waterham
PEX1-G843D HEK293(T): PEX1-G843D clone B29: mutation 2528G>A (G843D)/2517_2539del	Hans Waterham [217]
PEX1/null-HEK293(T): PEX1 KO: mutation 2541dup/2541dup	Hans Waterham

2.2.1 Cultivation of mammalian cells

Growth media for the mammalian cells was made by adding 10% (v/v) fetal calf serum (FCS), 2 mM glutamine and 50 µg/mL gentamicin in Dulbecco's modified Eagle's medium (DMEM). A constant temperature of 37 °C and CO_2 level of 7.5% CO_2 were maintained for the incubation of cells. Depending on the nature of the cells and the type of experiments additional FCS or antibiotics were supplied. The types of media and buffers used for cell culture are listed in Table 2.18.

Table 2.18: Buffers and media used in cell culture

Name	Ingredients	Purpose
Complete Growth Medium	Dulbecco's Modified Eagle Medium (DMEM) with 10% (v/v) FCS, 2 mM L-Glutamine and 50 µg/mL Gentamicin	Propagation
Serum-reduced Medium	DMEM with 5% (v/v) FCS and 2 mM L-Glutamine	Transfection
Opti-MEM™	Reduced serum medium (Gibco™ 31985062)	Transfection
Hank's Balanced Salt Solution (HBSS)	400 mg/L KCl, 60 mg/L KH2PO4, 350 mg/L NaHCO3, 8 g/L NaCl, 48 mg/L Na2HPO4, 1 g/L D-Glucose, 10 mg/L Phenol-red	Washing
Dulbecco's phosphate-buffered saline (DPBS)	2 g/L KCl, 2 g/L KH2PO4, 80 g/L NaCl, 21,716 g/L Na2HPO4	Washing and storage
Trypsin- EDTA	0,5 g/L Trypsin, 0,2 g/L EDTA in PBS	Detachment

Cells were maintained in culture flasks not exceeding a confluency of 80%. When passaging, the media was discarded, and the cells were washed with HBBS. Trypsin-EDTA solution was added to cover the cell surface and incubated at 37 °C for 5 minutes. Then detached cells were resuspended in fresh media and the required amount was transferred into a new flask (or dish).

2.2.2 Overexpression of recombinant PEX1 and PEX6 (PEI lipofection)

HEK293TT cells were grown in complete media with added hygromycin B (250 µg/mL) to promote maintenance of Large T Antigen expression. The typical doubling time of these cells was 24 h. Cells were split into 175 cm^2 cell culture flasks such that the confluency reaches approx. 70 to 80% before transfection. For this, no antibiotics (gentamicin or hygromycin) were added to the media. Cell passaging was typically performed in the evening and the transfection in the following morning. Before transfection, the media on the cells was replaced by 16 mL fresh media (without antibiotics). For transfection in a 175 cm^2 flask, 35 µg of the respective plasmid DNA (with pGwf backbone, see Table 2.6) and 75 µg of polyethyleneimine (PEI) were mixed in 4 mL serum reduced DMEM and incubated for 5 min at room temperature. The PEI solution was added to the plasmid solution and vortexed for 15 sec. The PEI-DNA mixture was kept for 20 min at RT and then added dropwise to the cells and further incubated overnight (37 °C and 8.5% CO2). The media was replaced (45 mL) the next day (after 18-24 h) and cells were incubated for another 24 to 48 h depending on cell survival before harvesting.

2.2.3 Transfection of PiggyBac plasmids to produce stable cell lines (PEI lipofection)

To prepare the cell for transfection, 200,000 M2H PEX1-G843D cells and 300,000 HEK293(T) PEX1-G843D cells were seeded onto 12 well plates (6 wells for each cell type) and grown in complete media. After 24 h, the media was discarded and 800 µL fresh media without antibiotics was added to each well. The transfection mix was prepared first in two separate reaction tubes. In the first tube, a mixture of plasmids was made as in Table 2.19 and resuspended in OptiMEM to make a volume of 100 µL. Constructs 5 and 6 served as negative controls to check cell survival in presence of the antibiotic Blasticidin. In the second tube, 10 µL of PEI and 90 µL of OptiMEM were mixed. Both mixtures were combined into one tube and incubated at room temperature for 20 min. 200 µL of each mix was added dropwise to individual wells and further incubated. Media was changed after 24 h. Blasticidin (25 µg/ml) was added with the media 48 h after transfection. Cells were trypsinized and transferred to bigger well plates when required. Media with the antibiotic was changed every 3 days. Cells were checked for the

expression of respective SNAP-ADARs via immunofluorescence microscopy and stocks were stored frozen in liquid nitrogen.

Table 2.19: PiggyBac plasmid mix

S. N.	Plasmid 1 (1.6 µg)	Plasmid 2 (0.4 µg)
1	SA1_Xlone_BSD	Transposase
2	SA1EQ__Xlone_BSD	Transposase
3	SA2__Xlone_BSD	Transposase
4	SA2EQ_Xlone_BSD	Transposase
5	SA2EQ_Xlone_BSD	-
6	-	Transposase

2.2.4 Transfection of mammalian cells via electroporation

ASOs and gRNAs were transfected into the mammalian cells via electroporation with the help of Neon™ transfection system (Invitrogen™ MPK5000). Cells were grown in complete media not exceeding the confluency of 80%. For gRNA transfection, 0.5 µg/ml doxycycline HCl (MP Biomedicals, 195044) was added to the media 18-24 hours earlier to induce the expression of the SNAP-ADAR proteins. Cells were harvested and counted with a Neubauer hemocytometer. For one transfection (10 µL), 200,000 to 300,000 cells were taken and centrifuged at 200 g for 5 minutes. The cell pellet was resuspended in electroporation buffer (250 mM Saccharose, 1 mM $MgCl_2$, in D-PBS), the desired substance (ASO or gRNA) was added, and the total volume was made to 10 µL by adding additional buffer. Unless otherwise stated, 25 pmol of ASOs and 5 pmol of gRNAs were taken per 100,000 cells. The mixture was drawn into a 10 µL Neon pipette and transfected with the desired setting with the Neon™ transfection device. The settings used for each type of cells are listed in Table 2.20. Transfected cells were then added to the desired culture flasks/wells with media and incubated until use.

Table 2.20 Transfection settings for mammalian cells

Cell type	Pulse voltage [V]	Pulse width [ms]	Pulse number
GM05756	1350	20	2
M2H PEX1-G843D	1300	30	2
HEK293TT	1100	20	2
Flp-In™-293	1100	20	2
Flp-In™ T-REx™ 293	1100	20	2
HEK293(T) PEX1-G843D	1100	20	2

2.2.5 Transfection of mammalian cells with RNA using lipofection (PEI, RNAiMAX)

Depending on the type of the experiment, ASOs and gRNAs were transfected into the mammalian cells via lipofection method as well. The desired number of cells (100,000 to 150,000) were grown on 24 well plates 24 h before transfection. For RNA transfection, a reaction tube was filled with 25 pmol ASO (or 5 pmol gRNA) in 50 µL OptiMEM and another reaction tube was filled with 1.5 µL RNAiMAX (or 4 µL PEI) in 50 µL OptiMEM. Both mixtures were kept at room temperature for 5 min, then mixed and vortexed briefly. After another incubation time of 20 min, the lipid-RNA mix was added dropwise to the cells in freshly changed media. Cells were incubated at 37 °C until RNA extraction (24 – 48 h) or IF (48 – 72 h).

2.2.6 Flow Cytometry

Flow cytometry is a technique used in rapid analysis of single cells or particles based on various parameters including relative size, shape, number, and fluorescence [218]. Depending upon the type of experiment, cell suspensions were analyzed using laser light scattering and single or more fluorescence parameters. Visible light scatter measurements in flow cytometry are done in two different directions: forward scatter (FSC) and side scatter (SSC). FSC gives insights into the comparative size of cells/particles being measured via light scattering at a small angle, while SSC unveils the internal complexity and granularity [219,220]. Fluorescent channels, such as FITC (490/525 nm) and PE (496/578 nm) are used in a flow cytometer, which are chosen based on the specific fluorophores used. This fluorescence analysis is done by illuminating the cells/particles with a laser that enables the measurement of fluorescence intensity across different populations. In optimal conditions, only one particle is illuminated simultaneously, and the brightness of the illumination is sufficient to generate scattered light or fluorescence of noticeable intensity [218]. The fluorescence signals of the analyte may arise from diverse origins whether intrinsic or after staining with fluorescent dyes. In this study, the signal from EGFP-PTS1 protein was analyzed.

HEK293TT cells transfected with pGwf expression vectors (expressing PEX1 or PEX6 along with EGFP-PTS1) were harvested after 48-72 h and about 200 µL cell suspension was analyzed using a CytoFLEX flow cytometer (Beckman Coulter, California, USA) following the manufacturer's instructions. An area was defined to differentiate cells from

other particles. Then the cell number and transfection efficiency were calculated based on cell populations with and without fluorescence.

2.2.7 Chaperone treatment of M2H cells

M2H cells were detached from the culture flasks with a trypsin-EDTA solution after washing with HBSS and resuspended in complete medium. The cells were counted with a hemocytometer and 50,000 cells were seeded on the wells of a 6-well plate containing cover slips (15 or 18 mm) in 3 mL media. The cells were treated with the respective chemicals (see Table 2.21) and grown for four days. Recovery of peroxisomal import in the cells was then checked via immunofluorescence microscopy.

Table 2.21: Chemicals for treating M2H cells

S. N.	Compound	Stock	Working solution
1	Diosmetin	6 mg/mL in DMSO	10-20 µM in complete media
2	Betaine	4 M in H_2O	100-200 mM in complete media
3	Glycerol	-	5% (v/v) in complete media
4	DMSO	-	1% (v/v) in complete media

2.2.8 Immunostaining and immunofluorescence (IF) microscopy

Cells were seeded and grown on glass cover slips (15 or 18 mm). Weakly attaching cells were grown on cover slips coated with collagen or poly-D-Lysine. Cell confluency was maintained at about 60% confluency during the time of IF preparation and antibody incubation. Without disturbing the cells, the medium was discarded, and the cells were washed 3 times with DPBS. Subsequently, the cells were fixed with freshly prepared 3% formaldehyde solution in DPBS for 20 minutes. Following fixation, two additional washes with DPBS were performed. Cell permeabilization was done with 0.5% Triton X-100 in DPBS for precisely 5 minutes. Two subsequent washes with DPBS were carried out.

For antibody staining, the primary antibodies were diluted in DPBS. Parafilm was spread on the bench, and each coverslip was placed cell-side down with a drop of 30 µL of antibody solution. After 30 min incubation, five washes with DPBS were performed. The procedure was repeated for the secondary fluorescently labelled antibodies, with 10-minute incubation in the dark, followed by five washes with DPBS. The list of antibodies used for immunofluorescence study are listed in Table 2.22.

After washing, a drop (approx. 15 µL) of mounting solution (Mowiol + 2.5% Dabco, ,4-diazabicyclo [2.2.2] octane) was placed on a clean glass slide and the coverslip was carefully placed cell-side down on top of the solution. The coverslip was firmly pressed, and excess mounting solution was removed. The slides prepared as such were kept in dark and left to harden at room temperature for several hours. Finally, the coverslips were sealed with clear nail polish. The samples were then analyzed using a fluorescence microscope with a 63X oil objective using settings as stated in Table 2.23. Images were taken and edited using the software ZEN Pro (Zeiss) and FIJI (IMAGEJ).

Table 2.22 Antibodies used in immunofluorescence microscopy

Antibodies	Species	Origin	Dilution (in DPBS)
Primary antibodies			
α-hsPEX1	rabbit	AG Kunau, Bochum	1:50
α-hsPEX6 (GDA3)	rabbit	AG Dodt, Bochum	1:100
α-AFP (GFP)	mouse	QBiogene/MP Biomedicals	1:100
α-hsCatalase	sheep	Athens Research & Technology	1:100
α-hsPEX14	rabbit	AG Kunau, Bochum	1:400
α-hsPMP70	mouse	Sigma-Aldrich	1:50
α-Thiolase	mouse	Abcam	1:50
Secondary antibodies			
α-rabbit Alexa Fluor-488	donkey	Life technologies	1:200
α-sheep Alexa Fluor-488	donkey	Life technologies	1:200
α-mouse Alexa Fluor-488	donkey	Life technologies	1:200
α-rabbit Alexa Fluor-594	donkey	Life technologies	1:150
α-sheep Alexa Fluor-594	donkey	Life technologies	1:150
α-sheep Alexa Fluor-594	donkey	Molecular Probes	1:150

Table 2.23 Visualization settings for immunofluorescence microscopy

Component	EGFP/ Alexa 488	Alexa 594
Beam splitter (nm)	495	585
Excitation filter (nm)	450 - 490	540 - 580
Emission filter (nm)	500 - 550	593 - 668
Light source	LED-module 475 nm	LED-module 567 nm

2.3 Protein biochemistry

All reagents and materials (columns, magnetic beads and buffers) used in protein purification and analysis were purchased from GE-Healthcare (Frankfurt am Main,

Germany), Sigma Aldrich (München, Germany), IBA Lifesciences (Göttingen, Germany) or Thermo Scientific (Karslruhe, Germany).

2.3.1 Purification of a PEX1/PEX6 complex

Purification of PEX1 and PEX6 recombinant proteins was carried out after using the PEI-transfection method as described in section 0. Cells were harvested with a cell scraper 48 - 72 h after transfection, pooled together with media and taken up in a reaction tube, of which 200 µL were taken for flow cytometry (see 2.2.6). Cell suspensions were centrifuged at 200 g for 5 min and the supernatant was removed. Cell pellets were stored at -80 °C until use.

Frozen cell pellets containing PEX1 and PEX6 proteins were thawed and lysed together in presence of ATP. All buffers and components used in the purification of PEX1/PEX6 are listed in Table 2.24. For all purification experiments the amount of cell pellet containing PEX1 was two to three times higher than that containing PEX6.

Table 2.24 Buffers for protein purification

Name	Contents
Protease inhibitor cocktail	104 mM AEBSF, 80 µM Aprotinin, 4 mM Bestatin, 1.4 mM E-64, 2 mM Leupeptin and 1.5 mM Pepstatin A (Sigma Aldrich, P8340)
Buffer A	25 mM HEPES, 150 mM NaCl, 10% glycerol, pH 7.6
Buffer B	25 mM HEPES, 150 mM NaCl, pH 7.6
Buffer L	Buffer A + 20 mM Imidazole, 0.5% protease inhibitor, 0.75% Triton X-100, 1 mM DTT, 8 mM $MgCl_2$, 3 mM ATP, 1 mM AMP-PNP
Buffer W	Buffer A + 4 mM $MgCl_2$, 2 mM ATP
Buffer HisW	Buffer W + 20mM Imidazole
Buffer HisE	Buffer W + 250mM Imidazole
Buffer FLAGE	Buffer W + 100 µg/mL FLAG peptide
Buffer StrepE	Buffer W + 100 mM biotin

2.3.1.1 Small-scale purification of PEX1/PEX6 complex

A total of 1-2 g combined pellet (PEX1 and PEX6) was taken for test purification with a His SpinTrap column and ANTI-FLAG or MagStrep beads. Both cell pellets were resuspended in the 5-fold amount of lysis Buffer L (5ml/g wet weight) in a falcon tube and then combined. All following steps were done on ice or in a 4 °C cold room. Then the 1.5-fold amount of glass beads (1.5g beads/g wet weight of the combined pellet) was

added to the solution and vortexed 10 times for 1 minute each, with an 1 minute pause on ice in between. The lysate was centrifuged with a table top centrifuge at 3000 g for 5 minutes to separate the glass beads. The supernatant was transferred to another centrifuge tube and spun down again at 16000 g for 30 min to get a cleared lysate. During this time, the His SpinTrap™ column (Cytiva, 28-4013-53) was centrifuged at 100 g for 1 min to get rid of the storage solution and was washed 3 times with 600 µL wash buffer HisW. The cleared lysate (600 µL) was then loaded into the column and incubated in a rotating wheel for 30 min and then centrifuged at 100 g for 1 min. This step was repeated until all lysate was used. The column was then washed 3 times with 500 µL HisW buffer and centrifuged after each round. Finally, the bound proteins were eluted 3 times with 300 µL elution buffer HisE after an incubation time of 10 min at each round. All three elution fractions were pooled together.

For the second round of purification, either 100 µL ANTI-FLAG® M2 Magnetic Beads (Sigma Aldrich, M8823) for PEX6.2xFLAG or 50 µL MagStrep "type3" XT beads (IBA Lifesciences, 2-4090-002) for StrepII.TEV.PEX6 were used depending on the cell pellet taken. The original beads were transferred to a reaction tube and centrifuged (100 g, 5 min), the storage solution was discarded, and the beads were washed 3 times with Buffer W. The pooled His eluate was then added to the tube and incubated for 1-2 h in a rotating wheel. The unbound fraction was taken out after centrifugation and the beads were washed 3 times with 500 µL Buffer. In the last step, the protein complex was eluted from the beads 3 times, by adding 200 µL FLAGE or StrepE elution buffer, incubating for 10 min and centrifugation (100 g, 5 min). The supernatants were collected. SDS samples from all steps were taken and analyzed by silver staining and western blotting.

2.3.1.2 Scaled-up purification of PEX1/PEX6 complex

All steps for the purification were performed either on ice or in a 4 °C refrigerated room. About 10 grams of total pellet (3g PEX6 and 7g PEX1) were taken and resuspended in 20 mL lysis buffer L. The 1.5-fold (w/w) amount of glass beads was added to the suspension and the cells were lysed using a FastPrep-24 5G ™ homogenizer with a BigPrep™ adapter (40 sec at the speed of 6 m/sec). After centrifugation (3220 g, 5 min, 4 °C), the supernatant was transferred into a new container, while the pellet was resuspended in another 20 mL buffer L and lysed again. After centrifugation (3000 g, 7 min, 4 °C), both

supernatants were combined and centrifuged (16000 g, 30 min, 4 °C). The cleared lysate was filtered using a sterile 0.45 µm ROTILABO® PVDF syringe filter (Carl ROTH, P667.1) and loaded into a preequilibrated (with buffer His W) HisTrap™ HP 1 mL column (Cytiva, 17524701) using a peristaltic pump at a flow rate of 0.5 mL/min, twice. The column was connected to the Äkta purifier (Amersham Biosciences) and washed with buffer HisW at a flowrate of 1 mL/min until the A280 nm reached the baseline. Wash fractions were collected in 1 mL aliquots with a fraction collector (Frac-950 Amersham Biosciences). A second wash was done by mixing 90% His W buffer (20 mM Imidazole) and 10% His E buffer (with 250 mM Imidazole). This increased the overall concentration of Imidazole to 43 mM. Fractions were collected as in the first washing step. Then the bound proteins were collected in 1 mL fractions by eluting with 20 mL elution buffer His E in total. A total of 6-8 His elution fractions with the highest amounts of protein (as determined by a Bradford color assay) were pooled together and finally diluted with the same amount of buffer W, dropwise.

The pooled His elution fraction was then run over a preequilibrated Strep-Tactin®XT 4Flow® high capacity FPLC column (1 mL, IBA Lifesciences, 2-5027-001) using a peristaltic pump at approx. 0.5 mL/min. The flow-through was loaded again, completely onto the column as described for the His column. The column was connected to the Äkta purifier and washed with 8 to 10 mL wash buffer FLAG W or Strep W at a flowrate of 0.5 mL/min, until the A280 nm reached the baseline. Elution was then done with 10 mL respective elution buffers, FLAGE or StrepE at a flow rate of 0.5 mL/min. All wash and elution fractions were collected in 1 mL aliquots.

For the purification of the complex with FLAG-tagged PEX6, His eluates were incubated with ANTI-FLAG® M2 Magnetic Beads, washed and eluted as described in 2.3.1.1. Purified protein eluates were then taken for further studies or stored at -80 °C after adding additional glycerol to a final concentration of 10%. This method of purification of the PEX1/PEX6 complex has recently been published [221].

2.3.2 Bicinchoninic acid protein assay

The measurement of total protein concentrations in the samples were done with the modified bicinchoninic acid (BCA) protein assay [222]. The process of protein quantitation in BCA occurs in two sequential steps: first, the reduction of Cu^{2+} ions to Cu^{+}

by the peptide bonds of the proteins (the biuret reaction) and second, the detection of the Cu^{+} ions with a reagent containing BCA. The process of Cu^{2+} reduction is proportional to the number of peptide bonds present in the tested solution and each Cu^{+} ion is chelated by two molecules of BCA. This results in a purple-colored water-soluble complex that has strong absorption at 562 nm. Therefore, the concentration of the desired sample can be efficiently measured by comparing the absorbance value of it with a standard curve prepared from a range of known protein standards. The slow color production in this method also allows for several samples to be tested together.

The Pierce™ BCA Protein Assay Kit (Thermo Scientific) was used to determine the protein concentrations in samples following the manufacturer's instructions. Protein samples were diluted 5-fold using H_2O and 2 µL, 4 µL and 6 µL of the diluted sample were pipetted into wells of a 96 well plate in duplicates. The samples were filled to a volume of 10 µL with H_2O and incubated for 60 min at 37 °C with 190 µL of the BCA reagent. A standard curve was generated with bovine serum albumin (BSA) solutions of known concentrations using H_2O incubated with BCA reagent as a blank value. The absorbances of the colored solutions were measured with the Tecan Infinite 200 microplate reader and the sample protein concentrations were determined by comparing to the BSA standard curve.

2.3.3 Sodium dodecyl sulphate polyacrylamide gel electrophoresis (SDS-PAGE)

Separation of proteins in samples was done by using a modified sodium dodecyl sulphate–polyacrylamide gel electrophoresis (SDS-PAGE), a discontinuous electrophoresis method developed by Laemmli [223]. In SDS-PAGE, proteins undergo denaturation, giving rise to its alternate name, denaturing gel electrophoresis. Samples are combined with a buffer containing sodium dodecyl sulfate (SDS), which binds to proteins, causing them to unfold. SDS binds to the amino acid chain in a stable ratio, proportional to the mass of the protein. Additionally, a reducing agent, commonly β-mercaptoethanol, is introduced to disrupt disulfide bonds, resulting in near-complete denaturation of the protein. Glycerol is also a part of the sample buffer for making the sample easier to load into the wells of the gel. The subsequent electrophoretic separation occurs within a polyacrylamide gel, acting as a molecular sieve. Migration within the gel

primarily depends on the size of the molecule; smaller proteins migrate faster in the gel. The distance traveled is inversely proportional to the logarithm of the molecular mass.

SDS gels (5% stacking gel and 8% resolving gel) with 10 or 15 wells were prepared according to Table 2.26. Whole cell lysates or other protein samples were mixed in 4X Laemmli buffer (Table 2.25) and kept in a heat block at 90 °C for 5-10 min. After short centrifugation, the samples were loaded into the sample wells of the gels and run at 20-30 mA per gel until the loading front reaches the bottom. PageRuler™ Prestained Protein Ladder (Thermo Scientific) was used as a marker to determine the protein mass. Thus, separated gels were used for western blotting or silver staining to detect the proteins.

Table 2.25: Buffers and solutions used in SDS-PAGE analysis

Name	Content
APS	10% Ammonium persulfate in H_2O
TEMED	*N*,*N*,*N*′,*N*′-Tetramethylethylenediamine
Stacking Gel Buffer	0.5 M TRIS, pH 6.8
Separating Gel Buffer	1.5 M TRIS, pH 8.8
SDS-Running Buffer	25 mM TRIS, 192 mM Glycin, 0.1% SDS (w/v)
Laemmli Buffer (4X)	250 mM TRIS, 8% (w/v) SDS, 4% (v/v) Glycerin, 20% (v/v) β-mercaptoethanol, 0.04% (w/v) BPP, pH 6.8

Table 2.26: Composition of polyacrylamide gels

Resolving gel solution (8%)		Stacking gel solution (5%)	
30% Acrylamide:bisacrylamide (37.5:1)	1.33 mL	30% Acrylamide: bisacrylamid (37.5:1)	340 µL
Resolving gel buffer (1.5 M TRIS, pH 8.8)	1.25 mL	Stacking gel buffer (1.5 M TRIS, pH 6.8)	260 µL
H_2O	2.33 mL	H_2O	1.36 mL
SDS 10%	50 µL	SDS 10%	20 µL
TEMED	5 µL	TEMED	2 µL
10% APS	50 µL	10% APS	20 µL

2.3.4 Silver staining

Protein bands separated by the polyacrylamide gel electrophoresis were detected based on the method developed by Blum, Beier and Gross, 1987. All required solutions, 50 mL each for two gels, were freshly prepared (Table 2.27). SDS gels were first fixed using the fixation solution for 2 h (or overnight) and washed thrice with 20 mL H_2O for 20 min each.

Sensitization was done by dipping the gels in Na_2SO_3 solution for 1 min, followed by two brief washes with H_2O. Gels were then incubated in silver staining solution for 20 min in the dark with gentle shaking. The gels were washed twice for 20 s and subsequently developed using the developing solution for 1 to 3 min until clear bands appeared. The reaction was then stopped by washing the gels briefly with water and incubating with the stop solution for 30 min. Finally, the gels were washed with H_2O and pictures were taken with the ChemiDoc analyzer.

Table 2.27: Buffers and solutions used in silver staining

Solution	Composition
Fixation	50% ethanol, 12% acetic acid, 0:05% formaldehyde
Sensitization	0.02% Na_2SO_3
Staining	0.2% $AgNO_3$, 0.075% formaldehyde
Developing	6% Na_2CO_3, 0.0004% $Na_2SO_3 \cdot 5H_2O$, 0.05% formaldehyde
Stopping	1% glycine

2.3.5 Determination of protein concentrations from Silver-stained gels

Protein concentration in samples were determined from silver stained SDS gels according to Merril and Pratt, 1986 [225]. SDS samples of proteins with unknown concentrations and BSA standards were run on a SDS gel and stained by silver staining. After taking the image of the gel with ChemiDoc (Bio-Rad) imager, Image Lab 6.0 (Bio-Rad) software was used for densitometric analysis with the background subtracted using the rolling ball algorithm and a disk size of 0.1 mm. A BSA standard curve was generated by plotting the inverse of the density against the inverse of the protein mass. The unknown protein mass was calculated according to Equation (1).

$$D^{-1} = a + b(P)^{-1} \quad (1)$$

Where D is the protein density, (P) is the protein mass and a and b are standard curve constants.

2.3.6 Western blot analysis

Western blot analysis is a method in protein biochemistry that comprises three steps. Proteins separated in SDS gels are transferred to a membrane, recognized by antibodies

and detected by chemiluminescence. Proteins were transferred and visualized by a modified protocol according to [226] and [227].

For transferring the proteins, a nitrocellulose (NC) membrane, 6 Whatman papers and the SDS gel with proteins were dipped in the transfer buffer (Table 2.28) for 5 minutes. Semi-dry electroblotting was done by stacking the materials from top to bottom (negative to positive) as followed: 3 Whatman papers, SDS gel, NC membrane, 3 Whatman papers. Electroblotting was performed on this "sandwich" at 100 mA for 2 h using the Trans-Blot® SD Semi-Dry Transfer Cell.

Table 2.28: Buffers used in western blot analysis

Name	Content
Transfer buffer	20 mM tris, 150 mM glycine, 0.05% SDS, 20% methanol
PBS	10 mM Na_2HPO_4, 1.8 mM KH_2PO_4, 140 mM NaCl, 2.7 mM KCl
PBS-Tw	PBS + 0.05% (v/v) Tween20
PBS-T	PBS + 0.1% (v/v) Triton X-100
TBS	100 mM Tris, 100 mM NaCl, pH 7.4
TBS-Tw	TBS + 0.05% (v/v) Tween20
TBS-T	TBS + 0.1% (v/v) Triton X-100

Proteins transferred to the NC membrane were identified and then linked through immuno-conjugation using corresponding primary and secondary antibodies [228]. The NC membrane was blocked with milk powder (in blocking solution, Table 2.29) for 1 h and incubated with the primary antibodies (in respective blocking solution) for 1.5 h. The NC membrane was then washed with the corresponding washing buffer (same as blocking buffer without milk protein), twice and incubated with the secondary antibody solutions for 1 h. Secondary antibodies linked to horseradish peroxidase (HRP) bind to the Fc region of primary antibodies [229]. All primary and secondary antibodies used in this work are listed in Table 2.29. After incubation with the secondary antibodies the membrane was washed two times with buffer containing detergent (Triton X-100 or Tween 20) and two times without the detergent. For detection, the Pierce™ ECL Western Blotting Substrate (in 1:1 ratio) was added to the membrane and incubated for approx. 1 min. The substrate solution detects the HRP in secondary antibodies. It consists of luminol which releases visible light of 425 nm wavelength along with an enhancer, that prevents the rapid decay of the chemiluminescence.

Protein bands were visualized from light emitted by chemiluminescence using a ChemiDoc (Bio-Rad) imager. In another method, a photosensitive film (Amersham Hyperfilm™ ECL, GE Healthcare, Munich, Germany) was applied to the membrane for a duration of 1-5 min (until visible bands are seen) seconds and developed in an automated film-processing apparatus (Konica, Langenhagen, Germany).

Table 2.29: Antibody solutions used in western bolt assays

Antibody	Species	Origin	Dilution
Primary antibodies			
α-hsPEX1	rabbit	Kunau lab, Bochum	1:4000
α-hsPEX6 (GDA3)	rabbit	Dodt lab, Bochum	1:2000
α-SNAP	rabbit	NEB / Invitrogen	1:1000
α-hsMAPK100	mouse	MyBiosource.com	1:2000
α-Tubulin I&II	mouse	Sigma-Aldrich	1:2000
α-FLAG	mouse	Sigma-Aldrich	1:2000
α-HIS	rabbit	Rapaport lab, IFIB	1:4000
α-ADAR	rabbit	Sigma-Aldrich	1:1000
Secondary antibodies			
α-Rabbit-HRP	Goat	Sigma-Aldrich	1:15000
α-Mouse-HRP	Goat	Sigma-Aldrich	1:15000

2.3.7 ATPase Assay

The ATPase assay was performed by measuring the amount of inorganic phosphate (Pi) released from ATP hydrolysis, using the PiColorLock™ detection reagent (Innova Biosciences, 303-0030). An acidified dye reagent (orange) was added to stop the reaction, turning green or yellow in the presence or absence of inorganic phosphate. Substrate aliquots containing 20 mM ATP and 40 mM $MgCl_2$ were prepared in assay buffer (25 mM HEPES, 150 mM NaCl, pH 7.6) and frozen at -20°C. The purified PEX1/PEX6 complex was diluted to a concentration of 500 ng/µL with assay buffer and kept on ice. The assay buffer was placed in a thermomixer at 37 °C.

A substrate aliquot was taken from the freezer and 80 µL buffer (at 37 °C) were added. The reaction was initiated by adding 10µL of enzyme (5 µg) to the reaction tube and placed in the thermomixer with gentle shaking at 650 rpm for 5 to 30 min. PNS (1:100) was used as a positive control instead of PEX1/PEX6. One set of assays was performed without the enzyme for blank measurement. A standard curve was prepared using the 0.1 mM Pi standard from the kit.

The reaction was stopped with 25µL of PiColorLock™ reagent mix (PiColorLock and Accelerator in the ratio 100:1) and gently mixed. After waiting for 5 minutes, 10µL stabilizer was added and the reaction mixed. The samples were transferred into a 96-well plate and left for 1 hour for color production. Absorbance was measured at 635 nm and the amount of Pi produced by the enzyme over-time was calculated.

2.3.8 Microscale thermophoresis

MicroScale Thermophoresis (MST) is regarded as a robust method for precisely characterizing the binding affinities between molecules within solutions. This method is highly effective at measuring interactions between biomolecules and can determine equilibrium constants, even in complex biological samples like cell lysates. A distinctive feature of MST is its reliance on fluorescence, necessitating one binding partner to be fluorescent, usually achieved by labeling target proteins with a suitable fluorophore. MST operates on the principle of thermophoresis (also called Ludwig-Soret effect), wherein molecules undergo directed movement in a temperature gradient induced by an infrared laser [230]. The resulting variation in the fluorescence signal is meticulously measured. Importantly, these molecular movements depend not just upon the size or charge of the molecules but also on their hydration shell or conformation [231], enabling MST to detect events like the binding of small molecules to proteins, substrates to enzymes, or ligands to liposomes [232]. The degree of fluorescence variation serves as a direct indicator of the binding affinity of the ligand to the fluorescent partner. Furthermore, MST's versatility extends to its ability to operate in various buffers, including plasma and cell lysate, making it highly adaptable. Notably, MST facilitates the determination of equilibrium dissociation constants (K_D) between interacting molecules, solidifying its utility in probing molecular interactions across diverse biological contexts.

During this study, the interaction between the HIS-tagged PEX1 (from the PEX1/PEX6 complex), the target, and the identified drug partners betaine or diosmetin, the ligand, was analyzed. To measure and quantify such interaction, the MST setup depicted in Figure 12 was used. The variation observed in thermophoresis could be graphed against the ligand concentration and analyzed to generate a binding curve depicting the interaction between the ligand and the target [232].

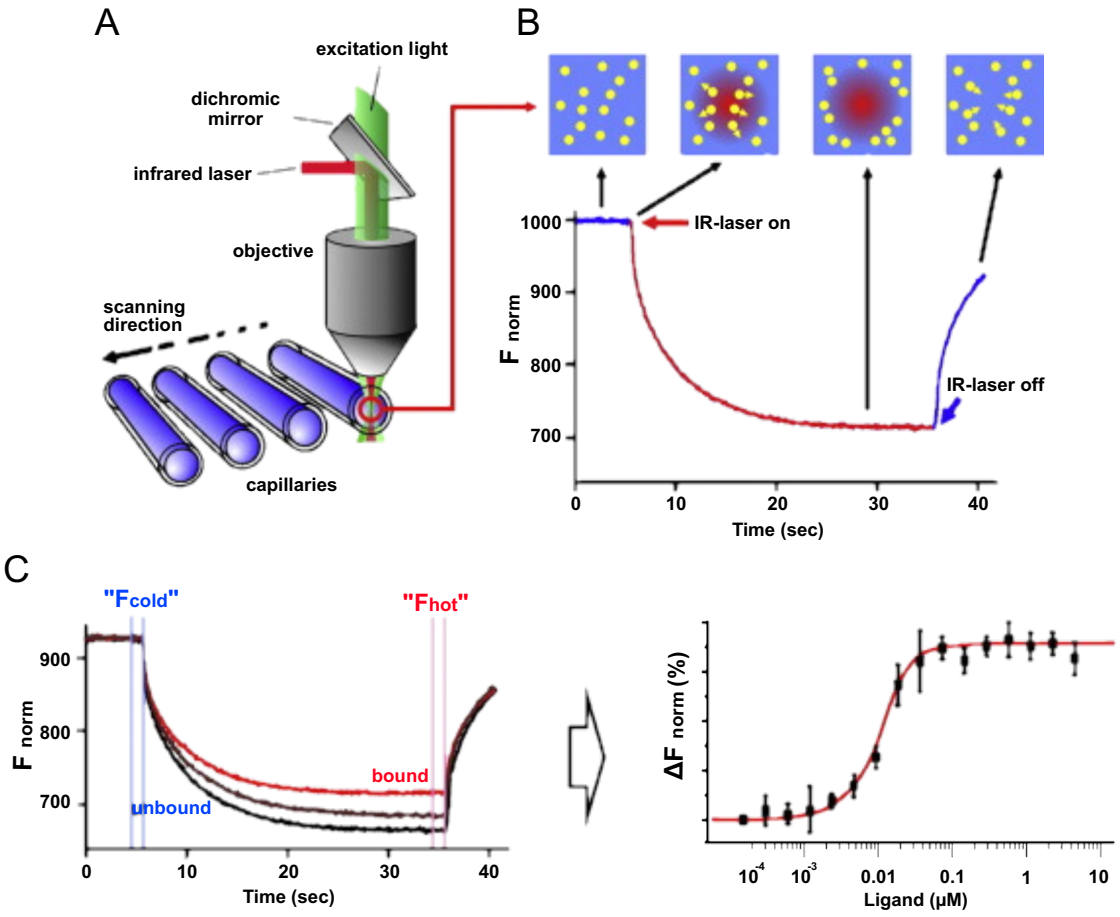

Figure 12: Overview of the MST setup and experiments. (A) Schematic representation of MST optics. MST is measured in capillaries with a total volume of about 4 µL. The fluorescence within the capillary is excited and detected through the same objective. A focused IR-Laser is used to locally heat a defined sample volume. Thermophoresis of fluorescent molecules through the temperature gradient is detected. (B) Typical signal of an MST experiment. Initially, the molecules are homogeneously distributed, and a constant ''initial fluorescence'' is detected. Within the first second after activation of the IR laser, the ''T-Jump'' is observed, which corresponds to a rapid change in fluorophore properties due to the fast temperature change. Subsequently, thermophoretic movement of the fluorescently labeled molecules out of the heated sample volume can be detected. After deactivation of the IR-Laser, an inverse T-Jump occurs, followed by the ''backdiffusion'' of molecules, which is solely driven by mass diffusion. MST, Microscale Thermophoresis; IR, infrared; T-Jump, temperature jump. (C) Typical binding experiment. The thermophoretic movement of a fluorescent molecule (black trace; ''unbound'') changes upon binding to a non-fluorescent ligand (red trace; ''bound''), resulting in different traces. For analysis, the change in thermophoresis is expressed as the change in the normalized fluoresence (ΔF_{norm}), which is defined as F_{hot}/F_{cold} (F-values correspond to average fluorescence values between defined areas marked by the red and blue cursors, respectively). Titration of the non-fluroescent ligand results in a gradual change in thermophoresis, which is plotted as ΔF_{norm} to yield a binding curve, which can be fitted to derive binding constants. Adopted from Jerabek-Willemsen *et al.*, 2014 **[232]**.

In this study, the fluorescent dye RED-tris-NTA was employed. This dye comprises the red-fluorescing dye NT-647, which is chemically bonded to a complex of

tris(hydroxymethyl)aminomethane (tris) and nitrilotriacetic acid (NTA) preloaded with Ni^{2+}. This setup facilitated the binding of the dye to HIS_6-tags coordinatively [233]. All MST experiments were performed by adapting the NanoTemper manuals [234,235]. The Monolith NT.115 instrument was set up and controlled using the MO.Control software. Data analysis was performed using the MO.Affinity Analysis software. RED-tris-NTA dye was prepared in HEPES-T buffer (Table 2.30) and stored in aliquots as 5 µM solution at -20 °C. Prior to usage, all stock solutions were centrifuged at 13000 g for 5 minutes at 4 °C to remove any aggregates. All solutions and dilutions were prepared on ice. Incubations and measurements were done as specified.

Table 2.30: Buffers used in MST assay

Buffer	**Composition**
HEPES-T	25mM HEPES (pH 7.6), 150mM NaCl, 0.05% Tween 20
AB1	HEPES-T + 4mM MgCl2, 2mM ATP, 10% glycerol, 100mM biotin
AB2	HEPES-T + 4mM MgCl2, 2mM ATP

Since the RED-tris-NTA recognizes and binds to the HIS-tag, PEX1.TEV.HIS_6 from the purified complex was labelled with it. For this the RED-tris-NTA stock solution was diluted to 100 nM in AB2 and added to the protein in a 1:2 molar ratio of dye to protein. The mix was incubated for 30 minutes at room temperature, followed by centrifugation at 15000 g for 10 minutes at 4 °C. The supernatant was then transferred to a new reaction tube.

Binding assays of the compounds (diosmetin or betaine) to the labelled protein were done first by making the dilution series of the compound (ligand). Starting concentrations for diosmetin and betaine were kept at 200 µM and 2 M respectively and subsequent 1:2 dilutions (10 µL) were made in the assay buffer AB2 (up to 16 dilutions). All dilutions were adjusted, such that only the ligand concentration is altered, and other components are constant. 10 µL of the labeled protein were added to each dilution and mixed by pipetting. The reagents were incubated for 30 to 60 minutes at 4 °C, followed by 5 minutes at room temperature. The samples were loaded into standard capillaries and measured using the Monolith NT.115 at 100% LED power and varying MST powers.

The fluorescence measurements were normalized (F_{norm}) according to Equation 2:

$$F_{norm} = \frac{F_1}{F_0}\,, [F_{norm}] = \% \tag{2}$$

Here, F_0 represents the fluorescence before the IR-laser is turned on, while F1 represents the fluorescence after the laser is activated. The relative fluorescence values were plotted in percentages.

The K_D value, representing the dissociation constant, was determined using the law of mass action and a quadratic formula described by Equation (3) [48]:

$$y = F_u + \frac{(F_b - F_u) \cdot \left(x + c_t + K_d - \sqrt{(x + c_t + K_d)^2 - 4 \cdot x \cdot c_t}\right)}{2 \cdot c_t} \tag{3}$$

In Equation (3), F_u is the normalized fluorescence of the unbound state in percent, F_b is the normalized fluorescence of the bound state in percent, x is the concentration of the ligand, c_t is the concentration of the labeled protein (target), and K_D represents the dissociation constant.

When the concentration of the ligand was unknown, the EC50 (half-maximal effective concentration) was determined using Equation (4), derived from the Hill equation [48]:

$$y = F_u + \frac{F_b - F_u}{1 + \left(\frac{EC_{50}}{x}\right)^n} \tag{4}$$

In Equation (4), EC_{50} denotes the dose at which half of the maximum response is observed, and n represents the Hill coefficient.

3 Results

A trimer-dimer complex of PEX1 and PEX6 along with its membrane tether PEX26 form the export complex in peroxisomes. PEX1 and PEX6 belong to a group of AAA+ ATPases and the PEX1/PEX6 ATPase complex helps to extract the monoubiquitinated import receptor protein PEX5 out of the peroxisomal membrane [119,129,236]. Mutations in one or both of the two ATPases lead to a defect in the import of peroxisomal matrix proteins resulting in a spectrum of peroxisomal biogenesis disorders (PBDs) [121,122,237].

A crucial component of this work involved the development of an approach to establish the expression of recombinant human PEX1 and PEX6 in HEK293TT cells. In order to study the functions and interactions of the PEX1/PEX6 complex, it was necessary to purify the complex with sufficient purity and yield. The purification is based on the knowledge that a heterohexameric AAA+ ATPase complex is formed by 3 subunits of PEX1 and 3 subunits PEX6 proteins. The purified protein complex was analyzed by an ATPase assay and by MicroScale thermophoresis (MST) to examine possible pharmacological partners.

The second part of the thesis covers the correction of the *PEX1-G843D* (c.[2528G>A]) missense mutation at the mRNA level in cells to facilitate the translation of correctly folded PEX1 protein leading to a fully functional PEX1/PEX6 complex. One approach used ectopically expressed SNAP-ADAR proteins and transfected guide RNAs. In another approach endogenous ADAR proteins were utilized in combination with transfected antisense nucleotides (ASOs). In both methods the guide RNAs/ASOs specific to the point mutation site were able to partially correct the adenosine to inosine, which is read as guanosine during protein translation, thus forming the wildtype PEX1 protein. The results were confirmed via Sanger sequencing and fluorescence microscopy.

Together, the aim of this project was to find possible therapies for treating mild PBDs resulting from the *PEX1-G843D* mutation.

3.1 Purification and analysis of the PEX1/PEX6 AAA+ ATPase complex

This part of the project was focused in developing methods to purify the hsPEX1/hsPEX6 protein complex. HEK293TT (or 293TT) cells were chosen for protein production. Rapid over-replication of SV40 Ori+ plasmids in 293TT cells make them useful for the production of papillomavirus or polyomavirus reporter vectors as well as for production of recombinant proteins of interest. While using the 293TT cells, protein production is best achieved by placing the gene of interest under control of human elongation factor 1 alpha (EF1α). Therefore, the vector plasmid pGwf (with EF1α promotor) was taken to insert the ORFs of PEX1 and PEX6 by Gateway cloning methods. After the transfection of 293TT cells with the respective expression vectors, the cells were harvested and the PEX1/PEX6 complex was purified. This complex was later used for an ATPase assay and for MST experiments.

3.1.1 Preparation of expression vectors via Gateway® cloning

Existing pcDNA3.1 vector plasmids with the coding sequences of hsPEX1 and hsPEX6 were the starting point of preparing the expression vectors required for this study. The Gateway cloning method was used for this purpose which eliminates the need for using several restriction enzymes and ligases. This method is based on first preparing a donor vector harboring the required coding sequence and later switching it with the acceptor (expression) plasmid.

As seen in Figure 13, PEX1 and PEX6 coding regions from the pcDNA3.1 vectors were first amplified using suitable primers (see Table 2.1). In presence of a taq polymerase, 3'A overhangs were introduced to the PCR product which was then paired to the linear vector pCR™8/GW/TOPO® to generate the donor vector with the help of the attached topoisomerase. The donor and the acceptor vector (pGwf) were mixed as a part of the LR reaction along with the LR Clonase® II enzyme mix, which switches the protein coding sequence in the donor vector with the ccdB coding sequence in the expression vector. Thus, the final expression pGwf vectors with individual coding sequences of PEX1 and PEX6 along with the respective N- or C-terminal tags were prepared (see Table 2.6). As listed in Table 3.1, five different expression plasmids were prepared encoding PEX1.TEV.HIS_6, PEX1(G843D).TEV.HIS_6, PEX6.2xFLAG, StrepII.TEV.PEX6 and

PEX6.StrepII, respectively. The expression vector pGwf additionally encodes EGFP. This was used to determine the transfection efficiency of the vectors. The correct sequence of these plasmids was confirmed by sequencing using primers listed in Table 2.2.

Table 3.1: Mammalian expressions plasmids generated

S.N.	Plasmid	Protein	Tag	No. of AA	Size (kDa)	pI
1	pGwf_PEX1.TEV.HIS_6	hsPEX1	C-terminal HIS_6	1296	144.54	5.99
2	pGwf_PEX1(G843D). TEV.HIS_6	hsPEX1	C-terminal HIS_6	1296	144.60	5.95
3	pGwf_PEX6.2xFLAG	hsPEX6	C-terminal 2xFLAG	1005	106.93	5.63
4	pGwf_StrepII.TEV.PEX6	hsPEX6	N-terminal StrepII	998	106.25	5.93
5	pGwf_PEX6.StrepII	hsPEX6	C-terminal StrepII	988	105.10	5.99

3.1.2 Transfection of HEK293TT cells by PEI lipofection

HEK293TT cells express both the Large T antigen, and the small t antigen. The combination of 293TT cells and plasmids with EF1α promotor system can result in extremely high expression of the recombinant protein. The transfection of 293TT cells with the pGwf expression vectors encoding recombinant PEX1 and PEX6 proteins was carried out as described in the methods section (see 2.2.2). For protein production, 35 µg of each plasmid was transfected separately into T175 culture flasks with 70-80% confluent cells via PEI lipofection. The amount of PEI used in the transfection was optimized after performing the transfection with different plasmid to PEI ratios (data not shown). The final ratio was kept roughly at 1:2, 35 µg plasmid and 75 µg PEI. Transfected cells were harvested after 48 h and small fractions of the cell suspension (100-200 µL) were taken for flow cytometry analysis. The cell pellets were stored frozen at -80 °C until use.

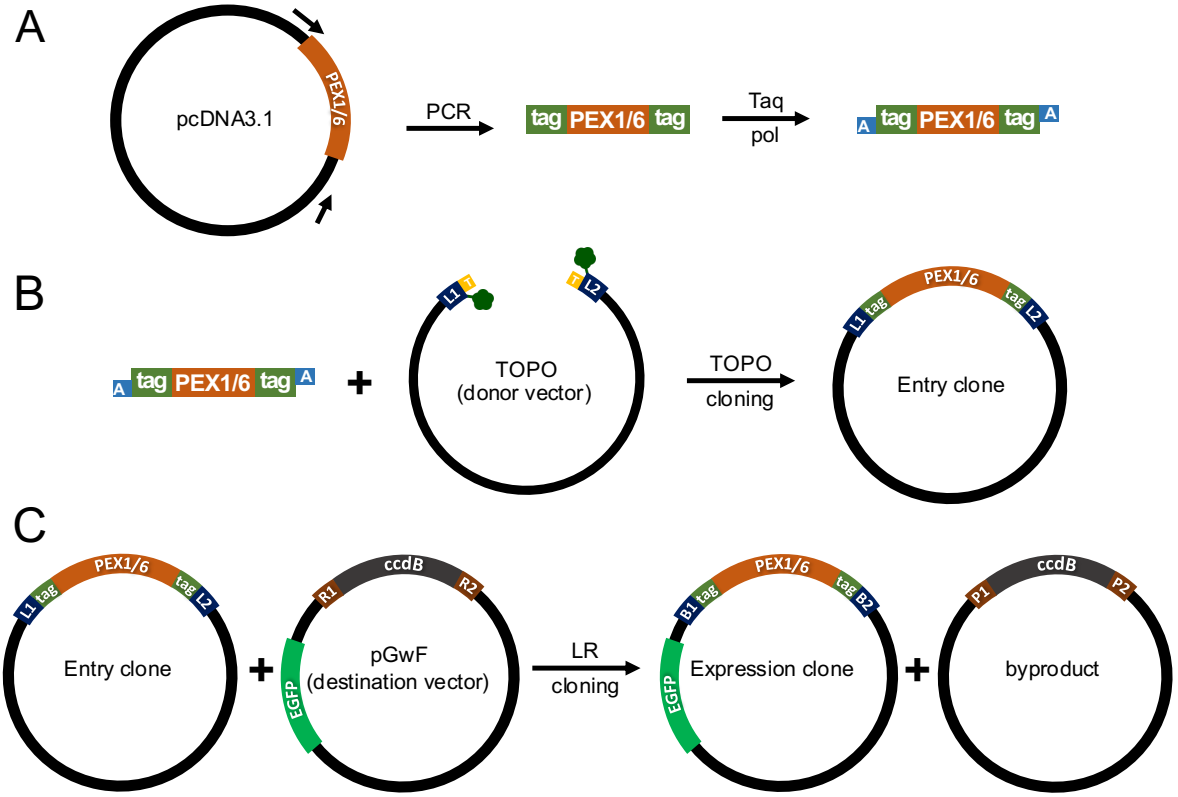

Figure 13: Gateway cloning strategy. (A) Open reading frames of the PEX1 and PEX6 genes were amplified from the pcDNA3.1 vectors with suitable primers including tags. In the presence of dATPs and *Taq* polymerase, 3' A overhangs were introduced to the PCR products. (B) PCR products were incubated with the TOPO vector to prepare the entry clone. (C) Entry clones containing the respective ORFs of PEX1 and PEX6 along with the tags were treated with the destination vector pGwf in presence of LR Clonase II enzyme mix thus resulting in the expression clones.

3.1.2.1 Flow cytometry analysis showed high translation of EGFP encoded by the plasmids.

The expression vector (pGwf) used in this study for encoding the recombinant hsPEX1 and hsPEX6 proteins also encodes the EGFP protein. Hence the transfected cells also separately translate this protein. To test the transfection efficiency, the number of cells harboring the EGFP protein was estimated by flow cytometry analysis. Cells harvested 48 hours post transfection were resuspended in culture media and a small amount (100 – 200 µL) was used for flow cytometry analysis (see 2.2.6). A total of 10,000 cells each was analyzed for EGFP expression. As observed from a representative experiment, in Figure 14, 48.62% of the cells were expressing the EGFP when transfected with the pGwf_PEX1.TEV.His_6 plasmid and 62.02% cells were expressing the EGFP when

transfected with the pGwf_StrepII.TEV.PEX6 plasmid. Typical expression rates for the vectors ranged from 40% to 60%, with some reaching up to 80%.

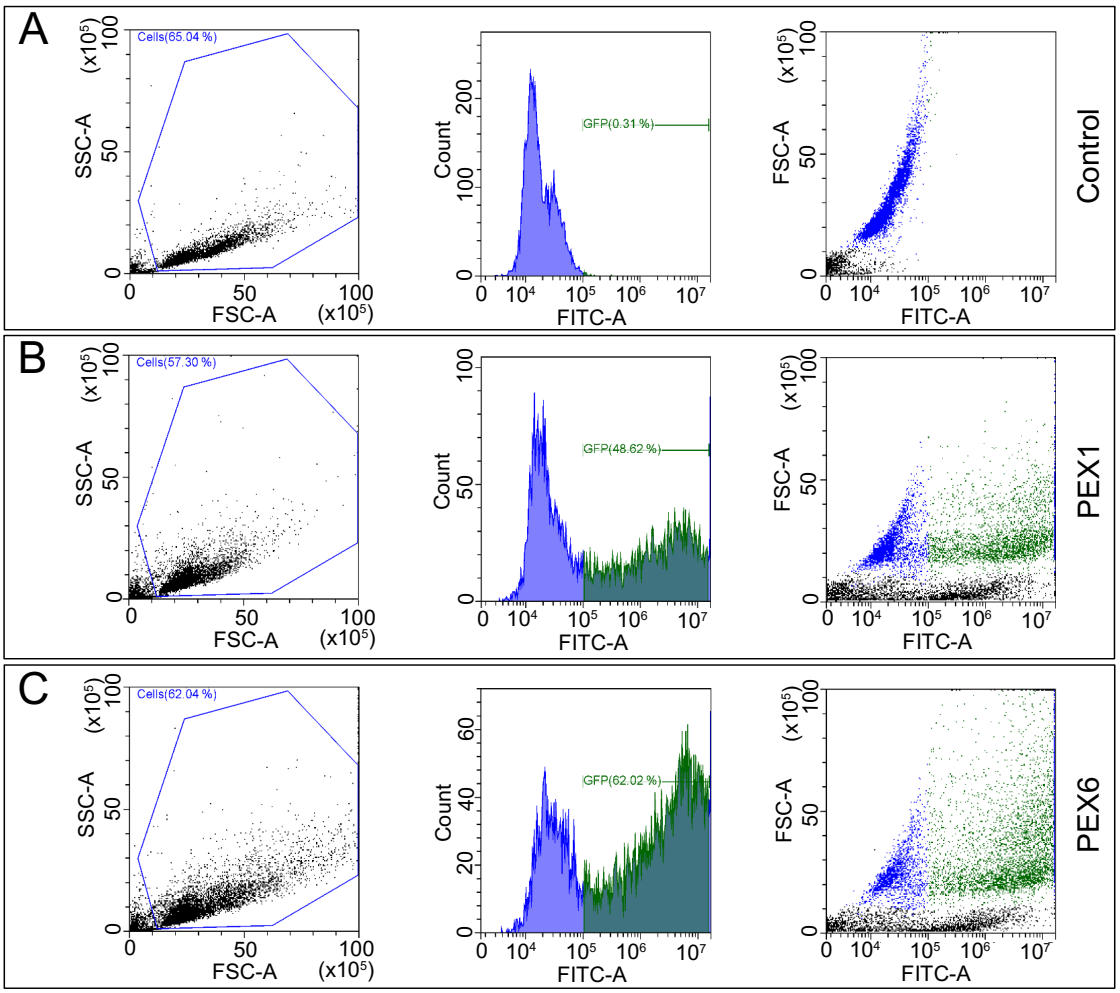

Figure 14: Flow cytometry of HEK293TT cells transfected with pGwf plasmids encoding EGFP and PEX1 or PEX6. A total of 10000 events from the cell suspension containing (A) untransfected HEK293TT cells and those transfected with (B) pGwf_PEX1.TEV.His_6 plasmid and (C) pGwf_StrepII.TEV.PEX6 plasmid were counted and analyzed using a flow cytometer. The left plots show the distribution of cells the side-scatter cytogram area (SSC-A) (granularity) versus the forward-scatter cytogram area (FSC-A) (size). Cell debris (area outside the blue frame) is excluded to compare the cells expressing and not expressing EGFP. Middle plots show the fluorescence intensity of the EGFP (FITC-A) distributions of the cells. Right plots show the FSC-A versus FITC-A dot-plots indicating the populations of cells with (green) and without (blue) EGFP. Untransfected cells (A) resemble the negative control that was used to define the regions of transfected and untransfected cells. Adopted from Pandey and Dodt, 2023 **[221]**.

3.1.2.2 Vector plasmid pGwf enhances the translation of PEX1 and PEX6 proteins

An expression test was done to compare the amounts of protein translated when the HEK293TT cells were transfected with different plasmids coding for PEX1 and PEX6 proteins.

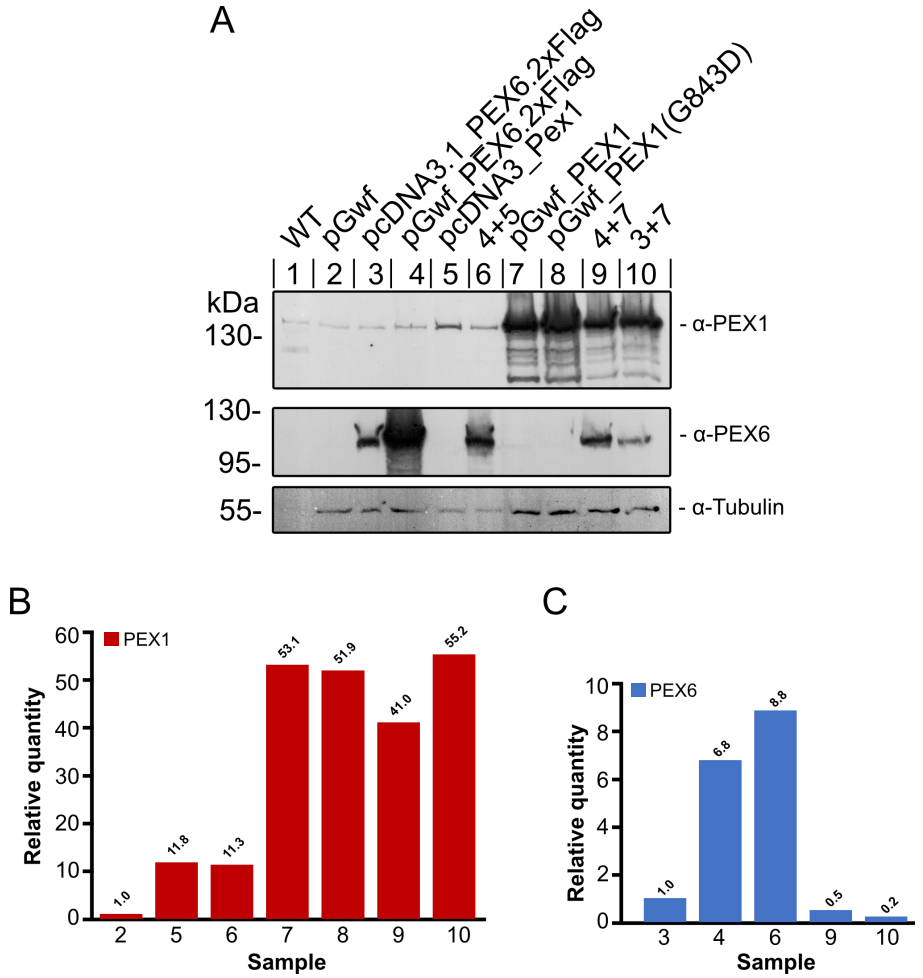

Figure 15: Comparison of protein expressed by various plasmids. Western blot image of the corresponding proteins (A) and their relative quantities (B and C). (A) HEK293TT cells in 25 cm^2 cell culture flasks were transfected with 10 µg plasmids (5 µg each for co-transfection) by PEI lipofection and harvested after 48 h. 20 µg of the cell lysates were run on two identical SDS gels and transferred onto nitrocellulose membranes. The membranes were cut and incubated with respective primary and secondary antibodies. One membrane was incubated with antibody solution against PEX1 and the other against PEX6 and Tubulin. The molecular mass of protein in kDa are shown in the left and the primary antibodies used are shown in the right alongside the corresponding protein bands. The chemiluminescence signals were detected on a photosensitive film (Amersham Hyperfilm™ ECL) with the help of a film imager (Konica, Langenhagen, Germany). Protein standard used: Pre-stained Protein Ladder, Thermo Scientific 26616. (B) Relative quantities of PEX1 proteins detected

in A corresponding to the wildtype value (lane 1). (C) Relative quantities of detected PEX6 proteins corresponding to the amount generated by pcDNA3.1_PEX6.2xFLAG transfection.

The amount of PEX1 and PEX6 proteins expressed in the cells untransfected or transfected with different plasmids is shown in Figure 15. Wildtype cells (lane 1) appeared to have low levels of PEX1, while the amount of PEX6 was below the detection limit. Comparing lane 3 with 4 and 5 with 7, it is clear that the amounts of proteins expressed by the pGwf vectors were higher than those expressed by the pcDNA3.1 vectors. Even the PEX1 (G843D) mutant (lane 8) showed high translation efficiency with the pGwf vector. Compared to the amount of endogenous PEX1, transfection with the pGwf_PEX1.TEV.HIS_6 plasmid resulted in a 50 times higher level of PEX1 and transfection of the pcDNA3.1 vector gave a four times higher yield (Figure 15B). The difference for PEX6 protein produced was even higher (>six times) when the two vectors were compared (Figure 15C). Interestingly, when these plasmids are co-transfected with half the amount of each plasmid, the amount of PEX1 produced remained fairly the same, while that of PEX6 was severely reduced (lanes 9 and 10). It seems that the expression of PEX1 is suppressing the expression of PEX6 in the cells. Furthermore, co-transfection also cannot ensure that the plasmids are equally distributed among the cells. Owing to these observations, it was decided to transfect the PEX1 and PEX6 plasmids separately and combine the pellets together for purification. This strategy has also been used for purifying the yeast Pex1/Pex6 complex [130,238].

Next, the cells were harvested at 24-, 48- and 72-hours post transfection to find the optimal time for protein production in the cells. As seen in Figure 16, the amounts of recombinant PEX1 and PEX6 proteins translated in the cells after 24 h were severalfold higher than in untransfected cells. The amounts get even higher when harvested at 48 or 72 h. Separately translated EGFP levels are the highest at 72 h. Depending on cell confluency, cells were harvested between 48 and 72 h for protein purification.

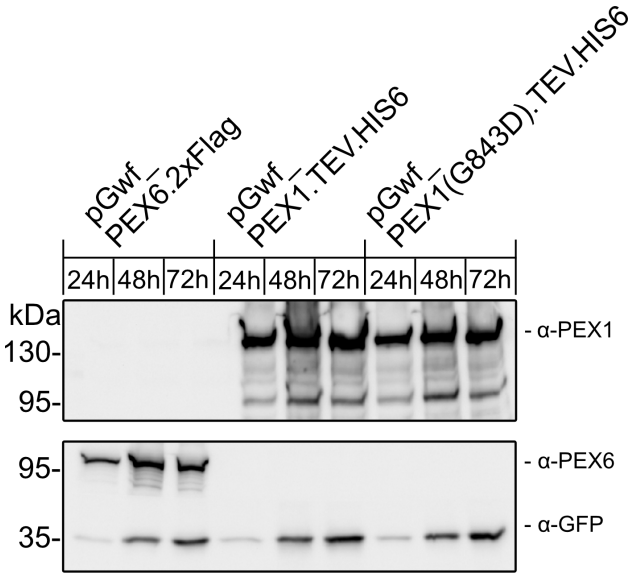

Figure 16: Optimal time for harvesting cells with expressed proteins. HEK293TT cells in 25 cm^2 cell culture flasks were transfected with 10 µg plasmids by PEI lipofection and harvested after 24, 48 and 72 h. 20 µg of the cell lysates were run on two identical SDS gels and transferred onto nitrocellulose membranes. One membrane was incubated with antibody against PEX1, and the other was cut and incubated with antibodies against PEX6 and GFP. The chemiluminescence signals were detected on a photosensitive film (Amersham Hyperfilm) with the help of Konica Imager. The molecular mass of proteins in kDa are shown on the left and the primary antibodies used are shown on the right, alongside the corresponding protein bands.

3.1.3 PEX1 and PEX6 deficient fibroblasts were complemented by the expression vectors

Complementation assays were performed in deficient cell lines to assess whether the constructed expression plasmids function properly in the cells. The plasmids were transfected into the respective ΔPEX1 (PBD009) or ΔPEX6 (PBD010) deficient cell lines. After 48 h transfected cells were stained using specific antibodies against marker proteins, namely Pex14, representing peroxisomal membrane proteins, as well as against catalase, representing matrix proteins with PTS1 import signal. Cellular localization and expression patterns of these marker and matrix proteins were then examined via immunofluorescence microscopy (Figure 17A and B). This assay allowed for the evaluation of whether the constructed plasmids successfully complemented the deficient cell lines by restoring the peroxisomal import/export. In wildtype cells the PEX14 (magenta) and catalase (light blue) punctate structures overlap, which confirms that both proteins are at peroxisomes and the peroxisomal import-export is functioning well. Similarly, such overlaps were also observed in PEX1 and PEX6 deficient fibroblast cells

when transfected with plasmids encoding the corresponding proteins. Some cells also displayed bright green fluorescence with the different pGwf plasmids, which is due to the expression of the EGFP.

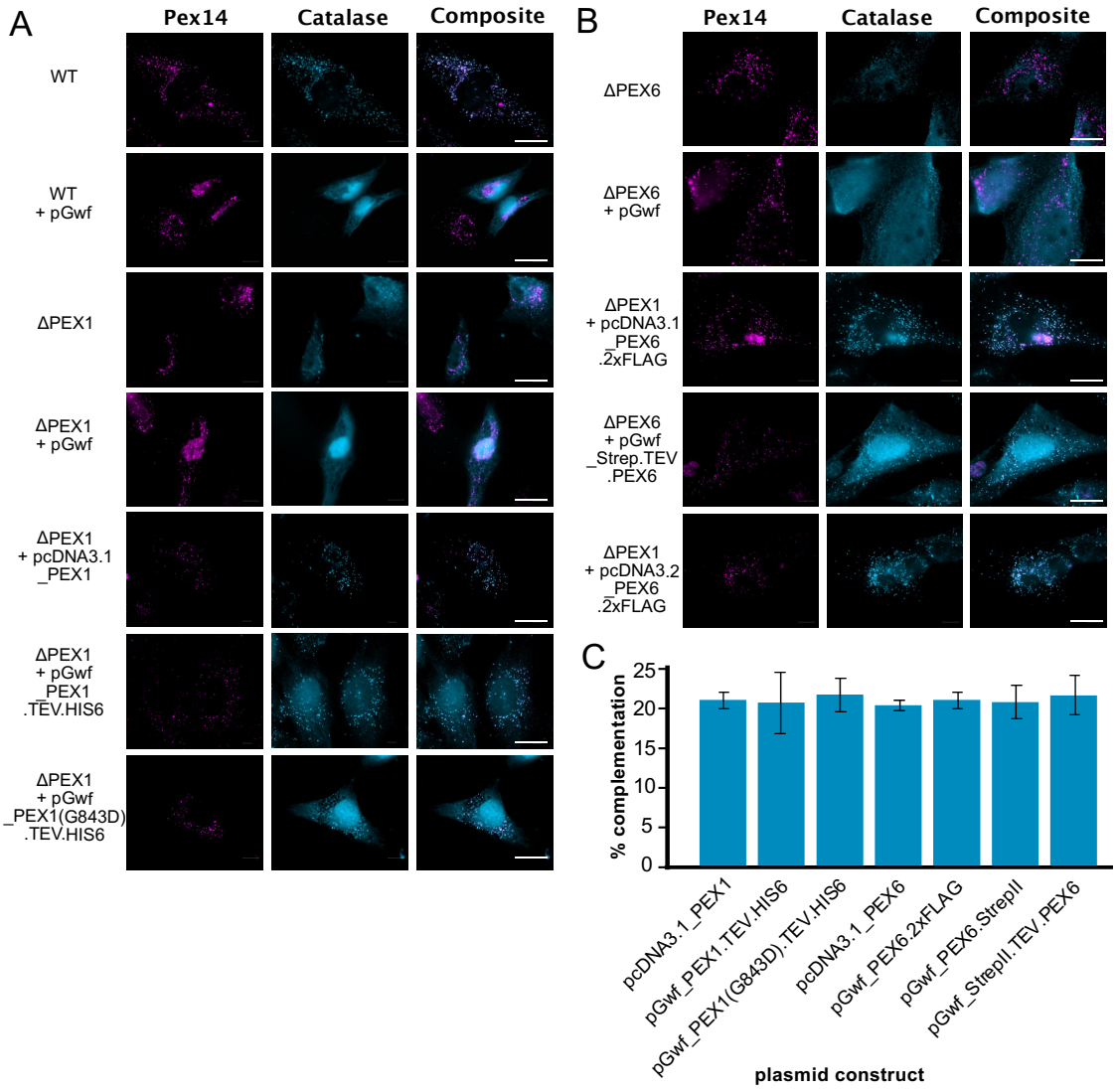

Figure 17: Complementation assay for the expressed plasmids: Immunofluorescence microscopy images from control cells and cells transfected with vectors encoding the PEX1 constructs (A) and PEX6 constructs (B); percentage of complemented cells after transfection (C). Wildtype fibroblast cells or the corresponding ΔPEX1 or ΔPEX6 cells were seeded onto 15 mm or 18 mm cover slips in 6cm dishes and grown in full media until 50-60% confluency. Corresponding plasmids (3 µg) and PEI (6 µg) were mixed and added to the cells and incubated overnight. Media was changed and the cells were grown for another 24 h. Cells were treated with indicated primary antibodies and the corresponding secondary antibodies and visualized using a Zeiss Axio Observer microscope with a 63X oil objective. Between 300 and 500 cells were counted for each construct and values are represented as average and SD of 3 independent experiments. Values are taken after deducting the values for the corresponding negative controls.

Complementation efficiency was calculated by counting the cells successfully importing the matrix protein catalase versus those not importing (Figure 17C). While the quantity of proteins observed through western blotting displayed significant variations, when employing the pcDNA3.1 or pGwf vector backbones, the percentage of cells complemented by these vectors showed minimal differences. About one fifth of the cells counted were complemented for all plasmids. Even the plasmid expressing the mutant PEX1 (G843D) had a similar complementation rate. This might be due to the correct folding of a small fraction of the large amount of the PEX1 protein produced in the cell.

Observations from the expression test and the complementation test suggested, that although the classical pcDNA3.1 vectors with the CMV promoters can complement similar fractions of cells as those with the pGwf backbone, the amount of protein produced by the pGwf vector is severalfold higher. They also suggested that overexpression of only one of the proteins PEX1 or PEX6 was not sufficient to achieve higher complementation rates. This meant that the use pGwf vector in plasmid preparation and protein production would be a favorable option.

3.1.4 Small scale purification and optimization

Until this stage, the conditions for transfection of the expression plasmids and cell harvest had been determined. For each transfection in a 175 cm^2 flask, 35 µg plasmid (pGwf_PEX1.TEV.HIS_6 or pGwf_PEX6.2xFLAG) and 75 µg of PEI were resuspended in 4 mL of serum-reduced media and added to the cells giving a total volume of 20 mL. The media was replaced after 18-24 h and cells were harvested at 48-72 h.

Before performing the purification of the PEX1/PEX6 complex with the ÄKTA system, small-scale extractions were performed. Cell disruption methods, buffer components and incubation times were optimized during the process using FLAG tagged PEX6 and His-tagged PEX1. Strep tagged PEX6 was cloned in the pGwf vector later and was used during buffer pH optimization.

3.1.4.1 Cell disruption with glass beads outperformed homogenizer and 27G needle

Three different methods were taken to break the transfected HEK293TT cells, so as to determine a stable and reproducible disruption scheme. For each approach, 1 g (approx.

10^8 cells) of cell pellet was resuspended in 4 mL buffer with varying amounts of detergent (Triton X-100).

i. Glass beads (0.25-0.5 mm in size), 1.5 times the weight of cell pellet were added to the cell suspension and vortexed ten times for one minute, each with one minute interval in between.
ii. A pre-cooled ball-bearing homogenizer was loaded with the cell suspension with 5 mL syringes at both ends. The suspension was pushed with the syringes forth and back 3 times.
iii. A 27 G needle attached to a syringe was loaded with the cell suspension and passed through the needle 30 times.

After cell disruption, SDS samples were taken, and the homogenates generated by each method were centrifuged at 16000 g for 15 min. Supernatants were separated and pellets were resuspended in buffer 4 mL buffer to take the SDS samples.

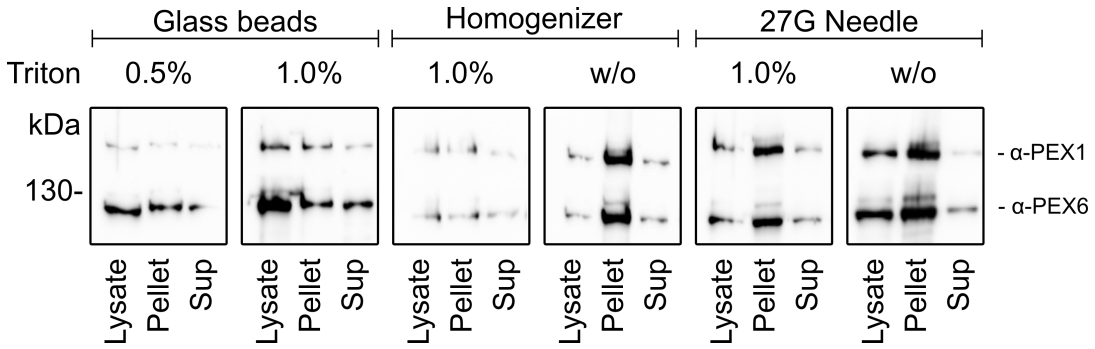

Figure 18: Comparison of cell disruption methods. One gram of transfected cell pellets (0.5 g with PEX1 and 0.5 g with PEX6) were resuspended in 4 mL lysis buffer with or without Triton X-100. Homogenization was done with glass beads, a ball-bearing homogenizer, or a 27 G needle. The resulting lysates were centrifuged at 16000 g for 15 min and supernatants separated. SDS samples were loaded on an 8% gel and transferred onto a nitrocellulose membrane before incubating with antibodies against PEX1 and PEX6. Chemiluminescence signals were obtained after incubating with the secondary antibodies (α-rabbit HRP) via a ChemiDoc analyzer (Bio-Rad).

Figure 18 shows the western blot images of the lysate, pellet and supernatant samples stained against the respective PEX1 and PEX6 antibodies obtained after each disruption methods. Out of all approaches, cell disruption with the glass beads using 1% Triton X-100 seemed to be the most effective. The amounts of proteins (PEX1 and PEX6) in the supernatant fraction from this method was the highest. Furthermore, the other two

methods (with homogenizer and needle) were not reproducible, and some cell suspensions were lost in the process. Therefore, it was decided to use glass beads in combination with 1% Triton X-100 in the following experiments. For scaling up, the cell suspension (up to 50 mL) was homogenized with a bead beater instead of a tabletop vortex.

3.1.4.2 Two-step purification yielded relatively pure PEX1/PEX6 complex

After the successful complementation of the proteins and determining a reliable cell disruption method, the purification of the PEX1/PEX6 protein complex was performed as described in 2.3.1.1. Harvested cell pellets containing PEX1.TEV.HIS$_6$ and PEX6.2xFLAG were resuspended in lysis buffer along with glass beads. The suspension was vortexed to break the cells and centrifuged. The supernatant was filtered, and the filtrate was run on a mini HisTrap HP column for 1.5 h before washing with the wash buffer. Eluates extracted with the His elution buffer (containing 250 mM imidazole) were pooled and incubated with ANTI-FLAG M2 magnetic beads. The eluates were extracted after washing the beads with wash buffer.

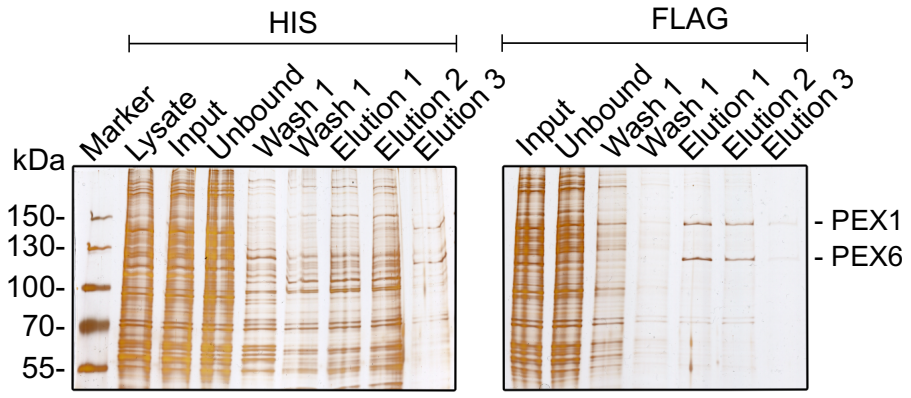

Figure 19: Small-scale purification of PEX1/PEX6 complex. The PEX1/PEX6 complex was purified from HEK293TT cell by sequential HisTrap HP column and anti-FLAG M2 magnetic beads. SDS gels (8%) were loaded with protein samples from each purification step: 0.01% each of lysate, input, and unbound fractions, 0.2% of HisTrap wash fractions, 0.8% of HisTrap elution fractions, 0.03% each of FLAG input and unbound fractions, 1.5% FLAG wash fractions and 3% FLAG elution fractions were used. Gels were stained using the silver staining method (see 2.3.4).

A typical silver stained SDS gel from a small-scale purification is provided in Figure 19. The quantity of proteins got reduced from the unbound fraction to the wash fractions on the His column. The first two His elution fractions still had a lot of proteins, while two

prominent protein bands were seen in the third fraction. Most of these weakly bound proteins on the His column did not bind to the anti-FLAG beads and were released in the unbound fraction. Washing the anti-FLAG beads got rid of many more proteins and two dominant bands of PEX1 and PEX6 could be observed in the FLAG elution fractions.

Although the amount of the proteins achieved by this method is very low, it is evident that the two proteins form a complex and can be purified together.

3.1.4.3 Recombinant PEX1 and PEX6 were correctly translated with tags

The open reading frame of the PEX1.TEV.HIS$_6$ translates to a 144.54 kDa protein and that of the PEX6.2xFLAG to a 106.93 kDa protein. As seen in the silver-stained gel of the purified samples, PEX1.TEV.HIS$_6$ appeared at the correct size and PEX6.2xFLAG appeared slightly higher than expected. This was also confirmed by western blotting.

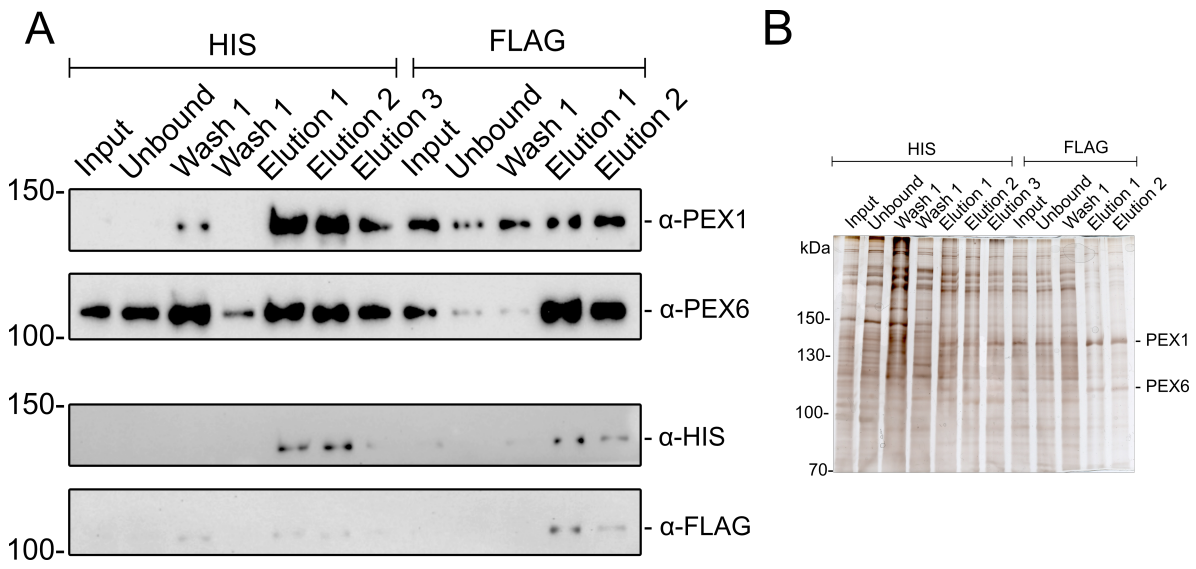

Figure 20: Recombinant PEX1 and PEX6 are correctly translated with tags. (A) Western blot of the protein fractions taken from each step from the His-tag purification of PEX1.TEV.HIS$_6$/PEX6.2xFLAG complex. Samples were separated in an SDS gel and transferred onto a nitrocellulose membrane. Corresponding membrane sections were incubated with α-PEX1 and α-PEX6 antibodies. Chemiluminescence signals were obtained from the membranes using the ChemiDoc Analyzer (Bio-Rad) after incubation with secondary antibodies (upper two sections). The membrane parts were stripped and stained with the antibodies against corresponding His and FLAG tags (lower sections) and detected similarly. (B) Remaining proteins in the gel after the western blot transfer were stained with via silver staining.

To further confirm that the purified proteins are indeed the desired PEX1 and PEX6, the nitrocellulose membranes stained with the respective PEX1 and PEX6 antibodies were stripped and stained with antibodies against the tags (α-Hisand α-FLAG). As expected, the bands appear exactly at the same spot as the α-PEX1 and α-PEX6 antibodies (Figure 20 A). Therefore, it was confirmed that both recombinant proteins were correctly expressed in the HEK293TT cells and could be purified along with their tags.

3.1.4.4 PEX1/PEX6 complexes are more stable at pH 7.6 than at pH 8.0

Stability of the purified PEX1/PEX6 complex is necessary to further evaluate its performance in functional assays after purification. It was also necessary to investigate the stability and performance of the complex with and without the PEX1-G843D mutation. It has been shown that the mutation *PEX1-G843D* disrupts the folding of PEX1 and diminishes the essential interaction between PEX1 and PEX6 by 70% [122,141] thereby hampering the peroxisomal protein import. Therefore, the purification of both, the wildtype complex (PEX1.TEV.HIS_6/StrepII.TEV.PEX6) and the mutated complex (PEX1-G843D) TEV.HIS_6/StrepII.TEV.PEX6) were checked at two different pH values.

At this point of the thesis the purification was continued with Strep-tagged PEX6 instead of the FLAG-tagged one. One reason for this was the better binding affinity of the Strep-tag II compared to the FLAG-tag. The Strep-tag II is also smaller and is less likely to disrupt the native protein folding. Furthermore, the readily available Strep-tag affinity column was more suitable for the purification process compared to the FLAG-agarose beads.

Each of the cell pellets were lysed and run on HisTrap HP columns at pH 7.6 and 8.0, separately. Figure 21 illustrates the immuno-staining against PEX1 and PEX6 for each purification setting. The wildtype complex at pH 7.6 appears to be the most stable. At pH 8.0, small quantities of both proteins are lost in the unbound and wash fractions. The proteins in the mutated complex on the other hand are already lost in the unbound and wash fractions at pH 7.6, with disproportionate amounts in the elution fractions. At pH 8.0, the amount of PEX6 recovered in the elution fraction is even lower. Furthermore, the complex appears to disintegrate even more, when the His-tag elutions are further purified with the Strep tag (figure not shown). These observations for the mutated complex were supported by the fact that the PEX1-G843D interacts with PEX6 very

weakly [122]. All further purifications were therefore done using the wildtype PEX1 and PEX6 at pH 7.6.

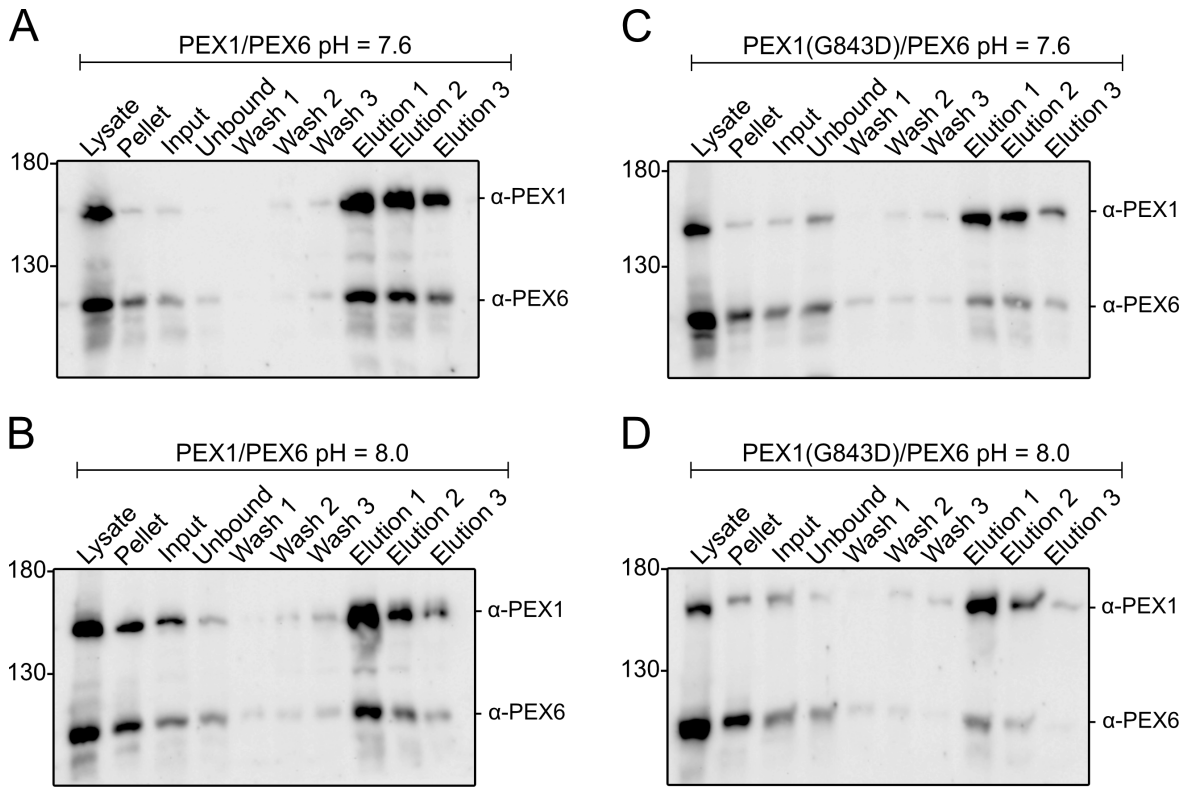

Figure 21: Effect of pH in the PEX1/PEX6 and PEX1(G843D)/PEX6 complexes. Cell lysates were loaded onto HisSpinTrap columns, washed and eluted. Both complexes were treated and purified at two different pH values; PEX1/PEX6 at pH 7.6 (A) and ph 8.0 (B); PEX1(G843D)/PEX6 also at pH 7.6 (C) and pH 8.0 (D). Samples separated on SDS gels were transferred onto NC membranes and incubated with α-PEX1 and α-PEX6 antibodies. After incubating with the secondary antibodies, chemiluminescence signals were obtained from the membranes using the ChemiDoc analyzer (Bio-Rad).

A PEX1 to PEX6 ratio of 1:1 in the purified sample is important for downstream assays. Therefore, the amount of PEX1 cell pellet in the first stage of purification (cell disruption) was increased to at least twice as high as for PEX6. This ensured that most of the PEX6 was bound to the PEX1 in the first stage, which increased the chance that the complex stayed stable during the second purification stage.

AMP-PNP was added to the lysis buffer to keep the PEX1/PEX6 ATPase complex locked. PEX1 and PEX6 assemble only in the presence of ATP. AMP-PNP is an analogue of ATP which cannot be cleaved between the β- and γ-phosphorus atom of the molecule. Due to its non-hydrolysable nature, the stability of the PEX1/PEX6 complex seemed to be increased [239].

During the optimization steps, several other parameters and buffer components were also tested. The amount of Triton X-100 (detergent) was maintained at 0.75%, DTT at 1 mM and the protease inhibitor cocktail at 0.5%. ATP and $MgCl_2$ were used in all buffers. All final buffer components used for purification are listed in Table 2.24.

The next step in the project was to analyze whether the purified complexes could be stabilized by pharmacological and chemical chaperones. However, as the purification of the mutated complex was incredibly challenging, it was decided to continue with the wildtype complex, only.

3.1.5 Scaled-up purification of the PEX1/PEX6 complex

After confirming the expression of the designed plasmids and optimizing the methods and conditions, the PEX1/PEX6 protein purification was scaled-up from SpinTrap columns to 1 mL columns using the ÄKTA Purifier FPLC system.

3.1.5.1 The Recombinant PEX1/PEX6 protein complex could be purified by sequential purification

The purification is based on the principle described earlier. Here, 6 g of PEX1.TEV.HIS_6 pellet and 3 g of StrepII.TEV.PEX6 pellet were lysed together by glass beads in lysis buffer in presence of 4 mM ATP. The cleared lysate was run twice over a HisTrap HP column and washed sequentially with buffer containing 20 mM and 50 mM Imidazole using an ÄKTA Purifier FPLC system. Proteins bound to the column were eluted with 250 mM Imidazole (HisE), pooled and loaded onto a StrepTactin™ XT 4Flow™ HC cartridge for another two cycles. Protein complexes were eluted with buffer containing 100 mM biotin (StrepE). Eluted proteins were either used directly for assays or aliquoted in 100 – 500 µL fractions, snap-frozen in liquid nitrogen and stored at -80 °C.

SDS samples from each step of purification were analyzed by silver staining and western blotting. Silver staining of the protein from each purification steps can be seen in Figure 22. A seemingly prominent band of PEX1 could be detected above the 130 kDa marker in the lysate and supernatant fractions. Both, PEX1 and PEX6 proteins are lost after centrifugation in the pellet fraction. The amount of PEX1 in the input fraction got reduced in the unbound fractions after two loading cycles, indicating that most of the PEX1 was bound to the column via its HIS_6 tag. As the washing steps got rid of weakly bound protein

from the column, large amounts of other proteins were still present in the elution fractions along with the desired PEX1 and PEX6 proteins. Pooled elution fractions from the His column were run over the Strep column again to trap the PEX6 protein with its Strep-tag II. It could be observed that both PEX1 and PEX6 proteins are lost in the unbound and wash fraction along with most of other proteins. However, a relatively pure PEX1/PEX6 protein complex was recovered in the elution fractions.

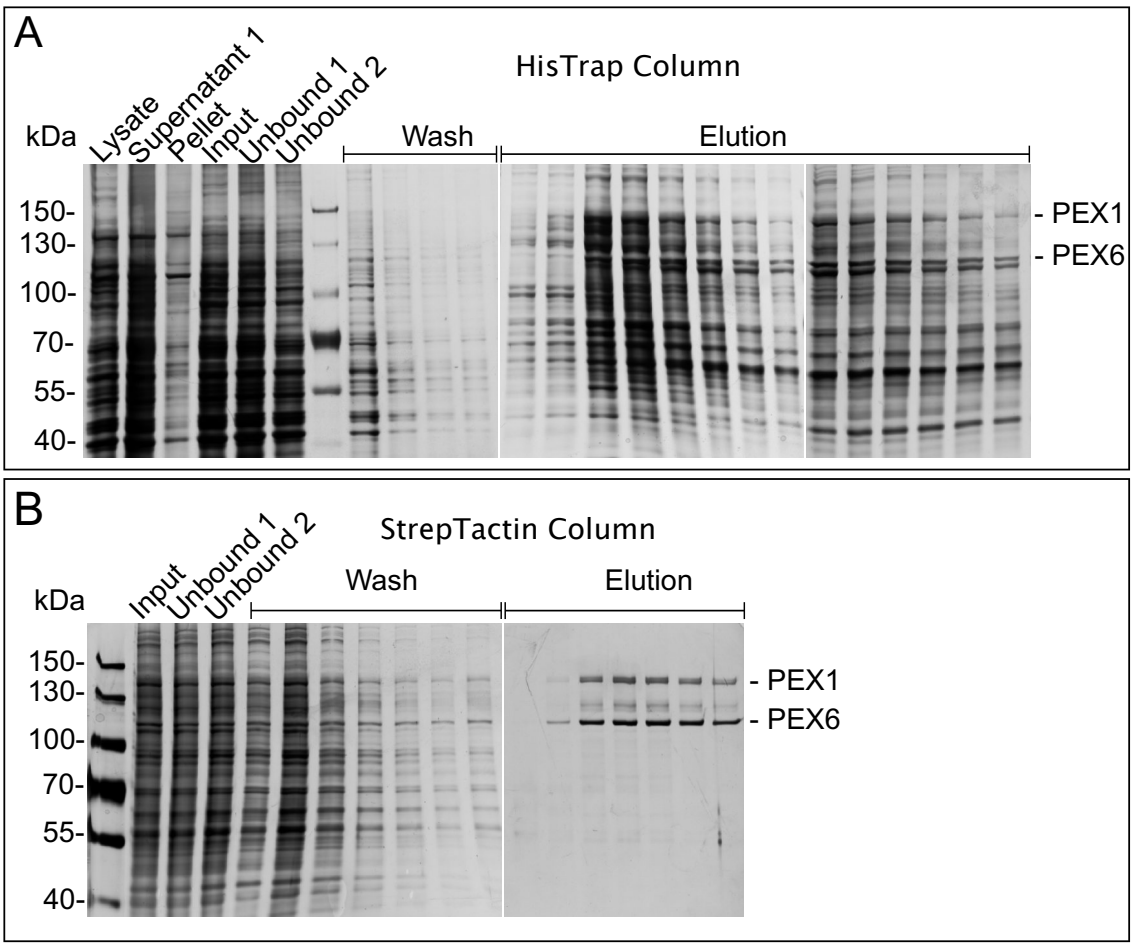

Figure 22: The PEX1 / PEX6 complex is purified from HEK293TT cell by sequential HisTrap and StrepTactin column chromatography. SDS-PAGE (8% gels) of (A) Cell lysis and HisTrap purification and (B) StrepTactin purification. Gels were loaded with protein samples from each purification step. The amount of sample loaded depends on the working volumes at each step. We used 0.01% each of whole cell lysate, supernatant 1, lysate, pellet, input and two unbound fractions, 0.2% of HisTrap wash fractions, 0.8% of HisTrap elution fractions, 0.03% each of StrepTactin input and unbound fractions, 1.5% StrepTactin wash fractions and 3% StrepTactin elution fractions. Gels were stained via Silver Staining. The theoretical molecular mass of PEX1-TEV-HIS6 and Strep-tagII-TEV-PEX6 were 144.54 kDa and 106.25 kDa, respectively. Numbers on the left indicate the molecular mass of proteins in kDa (Ladder, Thermo Scientific). Adopted from Pandey and Dodt, 2023 **[221]**.

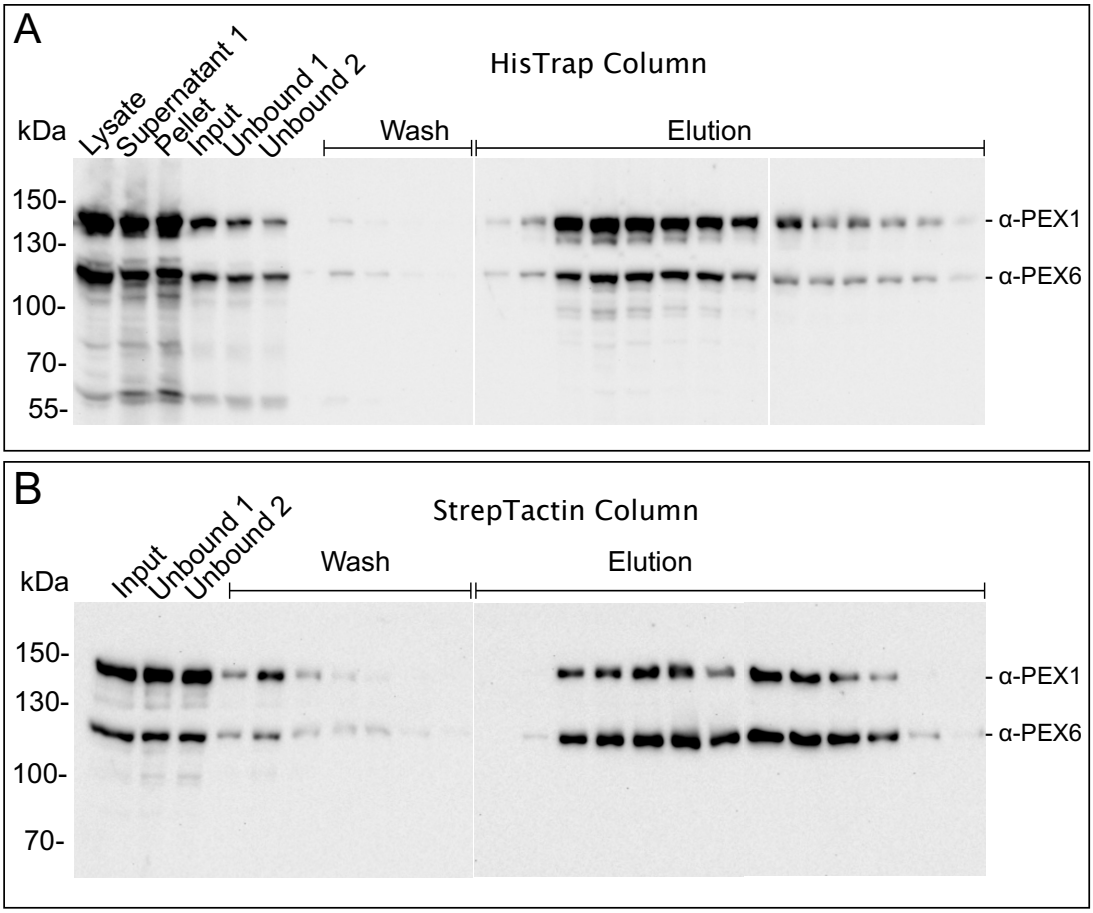

Figure 23: Immunoblots corresponding to the purification of the PEX1/PEX6 complex. (A) Cell lysis and HisTrap purification. (B) StrepTactin purification. SDS gels (8%) were loaded with protein samples from each step. The amount of sample loaded depended on the working volumes at each step. We loaded 0.01% each of whole cell lysate, supernatant 1, pellet, input and two unbound fractions, 0.2% of His wash fractions, 0.4% of His elution fractions, 0.04% each of StrepTactin input and unbound fractions, 0.8% StrepTactin wash fractions and 2% StrepTactin elution fractions. Western blot analysis of the gels was done using antibodies against PEX1 and PEX6 proteins. Chemiluminescence signals from secondary antibodies were obtained using a ChemiDoc Analyzer (Bio-Rad). The theoretical molecular mass of PEX1-TEV-HIS6 and Strep-TagII-TEV-PEX6 are 144.54 kDa and 106.25 kDa, respectively. Numbers on the left indicate the molecular mass of proteins in kDa (Ladder, Thermo Scientific). Adopted from Pandey and Dodt, 2023 **[221]**.

The fractions were also studied by treating with antibodies against PEX1 and PEX6 (Figure 23). Both recombinant PEX1 and PEX6 obtained in the cleared lysate after centrifugation and filtering (with 0.45 µm filter) were bound to the His column with some loss in the unbound fractions. Most of these two proteins were eluted with minimal loss in the wash fractions. It could be observed that the ratio of PEX1 to PEX6 got reduced in the His elution fractions, indicating that there are more PEX1 molecules that are not in complex with PEX6. Since only the proteins with an affinity to the HIS_6 tag are trapped in

the Ni-NTA column, all PEX6 molecules obtained in this step were recovered as a part of the PEX1/PEX6 complex. After loading the His eluates onto the StrepTactin column and washing, the protein complex was obtained by elution with 100 mM biotin. In this process, the Strep-tag II in the PEX6 binds to the column while PEX1 binds to PEX6. Therefore, the amount of PEX1 lost was higher than the amount of PEX6.

In conclusion, the sequential HIS- and Strep-tag purification of the recombinant PEX1 and PEX6 proteins together let to the recovery of relatively pure PEX1/PEX6 complex. As described earlier [238], PEX1 and PEX6 form a heterohexameric complex in yeast and are also thought to adopt a similar hexameric complex at human peroxisomes during receptor recycling [240].

3.1.6 ATPase Assay

After the successful purification of the PEX1/PEX6 complex, an ATPase assay was performed to check the activity of the complex (see 2.3.7). The amount of inorganic phosphate (Pi) released by ATP hydrolysis was measured using the PiColorLock™ detection reagent.

The reaction was started by adding the PEX1.TEV.HIS_6/PEX6.2xFLAG complex (5 µg) to the substrate (2 mM ATP, 4mM $MgCl_2$, final concentration) in assay buffer (25 mM HEPES, 150 mM NaCl, pH 7.6) at 37 °C. Reaction tubes were kept in a thermomixer at 37 °C and the reaction was stopped by adding 25 µL PiColorLock™ reagent mix followed by 10 µL stabilizer. The Color production was measured after 1 h by measuring the absorbance at 635 nm. With the help of the standard curve (with inorganic phosphate, Pi), the amount of Pi released from the enzyme was calculated. The reaction was carried out at an incubation time of 5 – 30 minutes. Control reactions were also done in absence of PEX1/PEX6 complex. The presence of post nuclear supernatant (PNS) from mouse liver was taken as a positive control.

A

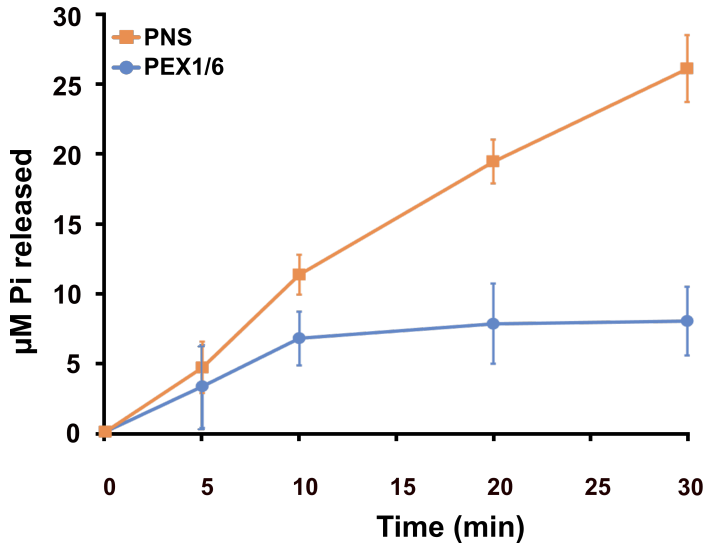

B

ATPase activity (after 10 min) pmol Pi min^{-1} μg^{-1}	
PEX1/6	6.69 ± 1.93
PNS	28.13 ± 3.54

Figure 24: ATPase activity of PEX1.TEV.HIS$_6$/PEX6.2xFLAG and mouse liver PNS. (A) Time course of ATP hydrolysis (B) ATPase activity after 10 min. Reactions containing 5 µg PEX1/PEX6 complex (or 2 µg PNS), 2 mM ATP and 4mM $MgCl_2$, were performed in assay buffer (25 mM HEPES, 150 mM NaCl, pH 7.6) at 37 °C and stopped by the addition of PiColorLock reagent mix. After 5 min a stabilizer was added and incubated for 1 h for color development. Absorbance was measured at 635 nm and the amount of Pi released calculated comparing the standard curve after background subtraction. Values represent mean ± SD, n=3.

As seen in Figure 24A, ATPases in the PNS were able to efficiently hydrolyze ATP in a time-dependent manner until 30 min. On the contrary, ATPase activity of PEX1/PEX6 ceases after 10 minutes. After 10 minutes, the ATPase activity of proteins in the PNS was calculated to be 28.13 ± 3.54 pmol Pi min^{-1} µg $^{-1}$ whereas that of PEX1/PEX6 complex was 6.69 ± 1.93 pmol Pi min^{-1} µg $^{-1}$ (Figure 24B). This ATPase activity of human PEX1/PEX6 complex is about 500 folds lower than the activity of yeast PEX1/PEX6 complex as measured by Ciniawsky *et al.*, 2015. Since the activity of the protein in PNS is steady, it confirms that the assay conditions are optimal.

With the assay results, it cannot be concluded that the human PEX1/PEX6 complex purified during this work is active especially because the ATP hydrolysis drastically reduces after 10 minutes. Addition of other interaction partners (PEX5-Ub and PEX19/26 complex) or the use of also Strep-tag II in PEX6 instead of FLAG-tag did not improve the activity (data not shown). The yeast Pex1/Pex6 complex with tags in one or both of the proteins complex have been shown to efficiently hydrolyze ATP [130,131,137]. In addition, it cannot be ruled out that the tags in the proteins used in this work might have

hindered the enzyme activity. PEX1 is known to be an unstable protein, and fragments resulting from its degradation are frequently observed in SDS gels. The stability of the isolated PEX1/PEX6 complex may begin to decline shortly after purification, potentially influencing the ATPase assay results. It is therefore advisable to replicate the assay, considering alterations in other factors such as ATP concentration, temperature, and involvement of other interaction partners.

3.1.7 Some chemical compounds can recover the function of PEX1-G843D

One of the aims of this project was to find the possible treatment of the Zellweger spectrum disorder (ZSD) caused by the PEX1-G843D mutation. Previous studies indicate that there is partial or near full recovery in the functions of PEX1-G843D by the use of chemical chaperones and/or flavones [141,148]. A similar setup was used to examine the effect of some of these chemicals in the recovery of this mutant PEX1 leading to the improvement in peroxisomal import mechanism.

A patient fibroblast cell line with mutation PEX1-c.2528G>A; p.G843D also expressing EGFP-PTS1, hereafter named as M2H cells was taken for further studies. The translated EGFP-PTS1 protein is predominantly in the cytosol [141]. Chemical chaperones like glycerol and betaine as well as the flavone diosmetin were added to the cell culture media and the cells were grown for 72 h. Afterwards, the cells were fixed, immuno-stained and imaged using immunofluorescence microscopy. While dimethyl sulfoxide (DMSO) served as a negative control in this assay, both glycerol and betaine functioned as chemical chaperones, specifically as osmolytes. Their role involves enhancing the hydration of proteins through unfavorable interactions between the protein and the osmolyte. This outcome leads to the reinforcement of the more compactly folded protein state while weakening the stability of unfolded states. While it has been established [148] that diosmetin enhances the function of PEX1(G843D), the exact mechanism behind this effect remains unknown.

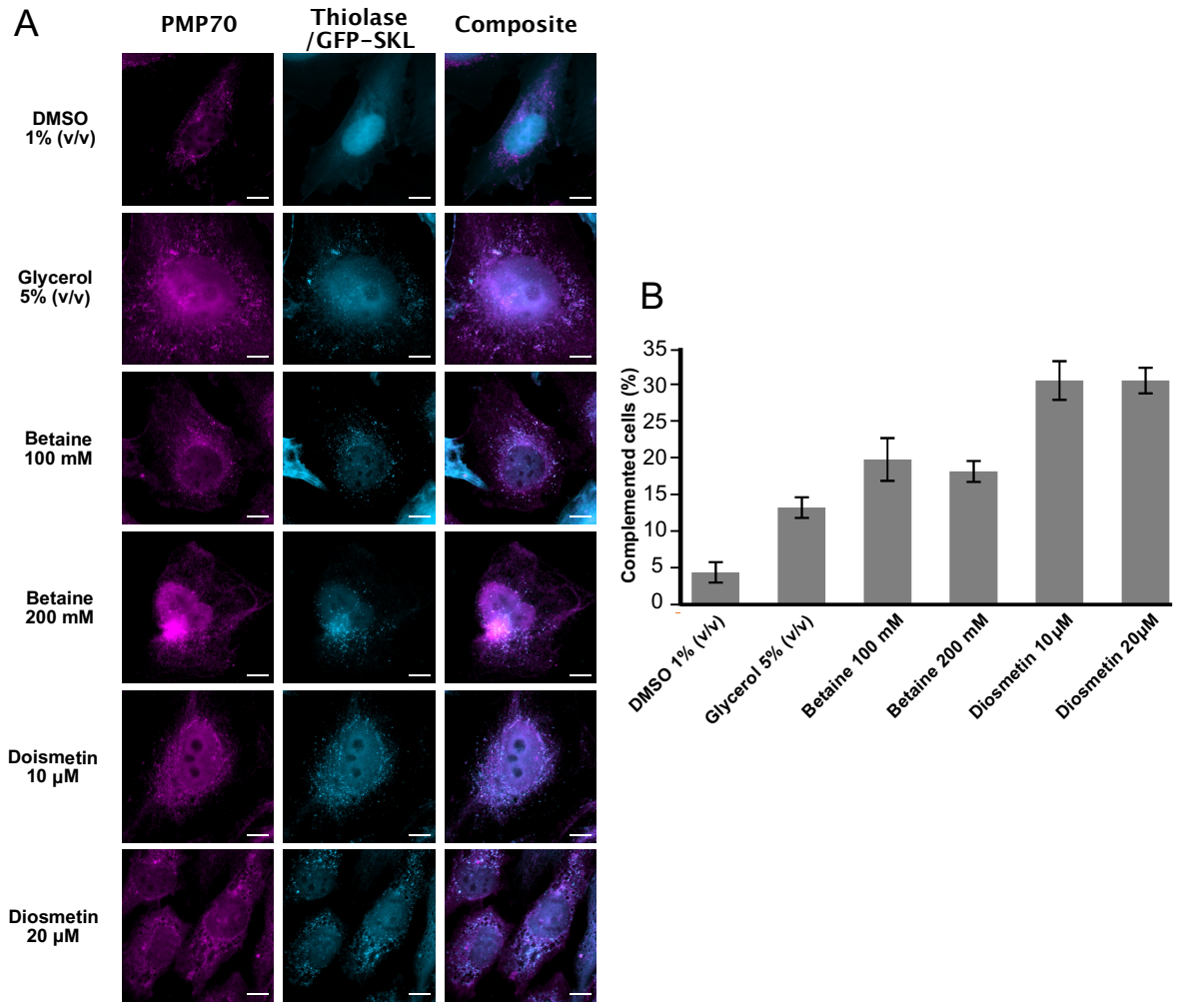

Figure 25: Effect of chaperones in peroxisomal protein import. (A) Immunofluorescence of treated cells, (B) Percentage of cells importing thiolase. M2H cells were grown in cell culture media with DMSO, glycerol, betaine or diosmetin (in indicated concentrations) for 72 h and immunostained against PMP70 (magenta) and thiolase (light blue). GFP-SKL is also visualized in light blue color. Cells were fixed with 3% formaldehyde, permeabilized with 0.5% Triton X-100 and stained with corresponding primary and secondary antibodies. The stained cells were visualized using a 63X oil objective (A). Scale bars represent 10 µm. The graph represents the percentage of cells with restored peroxisomal import given as the mean and SD of 3 independent experiments (B).

Although a significant number of cells show peroxisomal localization of the EGFP-SKL protein when observed by live cell imaging (seen as green punctates) after treating with diosmetin and betaine, the import was not detected after immunostaining the EGFP protein (data not shown). The reason behind this could be the loss of cells during immunostaining while treating with formaldehyde and Triton X-100solutions. Highly expressing cells tend to detach from the surface faster than untransfected cells or cells with low expression rates. Therefore, the treated cells were immunostained against PMP70 and thiolase (Figure 25), where PMP70 is a peroxisomal marker protein and

thiolase is a matrix protein that gets imported into the peroxisomes utilizing the recognition sequence PTS2. Here thiolase was stained with secondary antibodies false colored in light blue, the same way as the expressed pEGFP-PTS1, that means that PTS1 or PTS2 import can't be distinguished. In Figure 25A, PMP70 can be seen in magenta whereas thiolase and the expressed EGFP-PTS1 are colored light blue. The percentage of cells successfully importing the matrix proteins, indicated by the colocalization of proteins in both channels, are quantified in Figure 25B. Treatment with 1% DMSO served as the negative control where thiolase import was seen in 4.33 ± 1.53% of the cells. This small amount of import could be the result of cell handling outside of the incubator, as it known that the PEX1(G843D) is temperature sensitive and could recover its function at 30 °C [138,140,141]. The percentage of cells with colocalized PMP70 and thiolase/EGFP-SKL were found to be 13.33 ± 1.53% with glycerol, 20.00 ± 3.00% with 100 mM betaine, 18.33 ± 1.53% with 200 mM betaine, 31.00 ± 2.65% with 10 µM diosmetin and 30.67 ± 2.08% for 20 µM diosmetin. As can be seen, diosmetin was the most effective agent in restoring the peroxisomal import. An increase in the concentration of diosmetin from 10 µM to 20 µM or that of betaine from 100 mM to 200 mM did not seem to rise the efficiency of the import machinery. Therefore, the lower concentrations of these compounds were used in the following MST experiments.

3.1.8 Microscale Thermophoresis (MST)

After determining the positive effects of the pharmacological agents in aiding the import of peroxisomal proteins in PEX1 (G843D) mutant cells, it was decided to study the interaction of these compounds (betaine and diosmetin) with the purified PEX1/PEX6 complex via microscale thermophoresis (MST). MST is a technique to determine the interaction of molecules based on a temperature gradient. To be able to measure the thermophoretic response, the PEX1 protein in the complex was labelled with a fluorescent dye RED-tris-NTA, which specifically binds to HIS_6-tags. For assessing binding affinity, a series of dilutions of the ligand (betaine or diosmetin) around the anticipated K_D value was made. Following this, the target (PEX1.TEV.HIS_6, in complex with Strep.TEV.PEX6) labeled with fluorescent dye was introduced into each step of the dilution series and measured. Any alteration in the thermophoretic response of the labeled target can then be linked to variations in the ligand concentration.

3.1.8.1 Capillary positions can be determined with low IR power before MST measurement

Before measuring the protein-ligand interactions, positions of the capillaries were determined using the fluorescent signal. Reaction mixtures including the fluorescently labelled protein and the dilution series of the ligand were loaded into the standard glass capillary tubes and measured. Peak positions were taken as references for the capillary location during the measurement (Figure 26A). This procedure was carried out both before and after the measurement, aimed at identifying any attachment of labeled protein to the capillary. A minor decrease in the fluorescent signal was observed after the measurement due to the photobleaching of the dye. Normalized scans of the capillaries with uniform peaks can be seen in Figure 26B. If fluorescently labeled protein adhered to the capillary walls, this would manifest as an asymmetric and distorted peak.

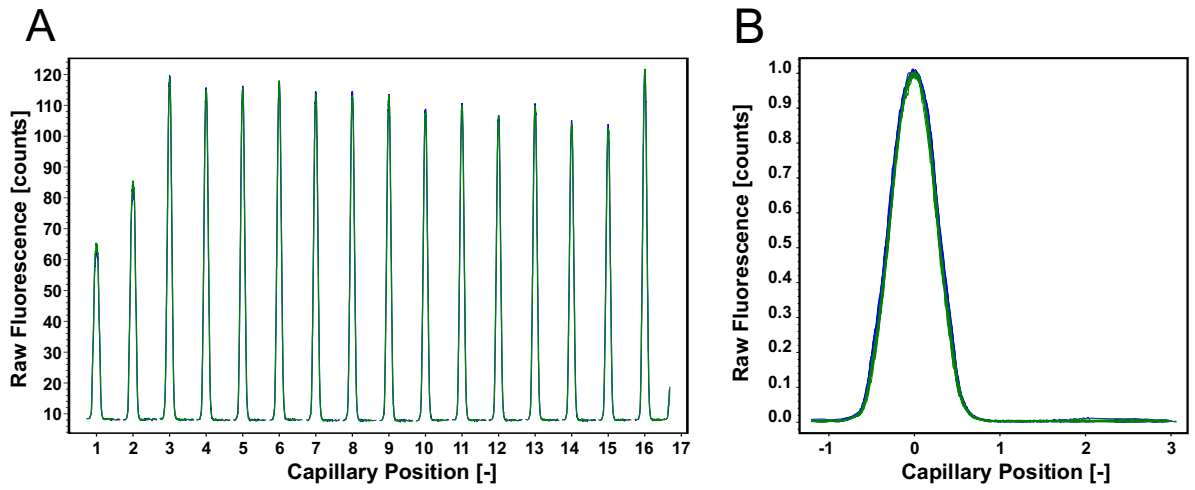

Figure 26: Representative scan and shape of capillaries. (A) original fluorescence, (B) normalized fluorescence. Photodiode of the Monolith NT.115 was used to scan the capillaries, with the LED power set at 100% and a concentration of 5 nM for RED-tris-NTA. The original fluorescence is displayed against the capillary's location (A). The fluorescence, normalized and superimposed onto the capillary's position, is used to determine its shape (B). Fluorescence before MST measurement is shown in green that after MST measurement is shown in blue.

To compute the change in normalized fluorescence (F_{norm}) at each concentration, two regions were selected: a region prior to activating the laser (cold region) and a region after the laser was activated (hot region). These two regions are indicated with blue (cold) and red (hot) bars in Figure 27. For all experiments, the cold region was defined between -1 to 0 seconds, while the hot region was adjusted to achieve a favorable signal-

to-noise ratio and mitigate the impact of interfering factors like convective flow. This approach ensured that the initial fluorescence change (temperature jump) as well as the actual thermophoretic effects were considered.

The lowest feasible infrared (IR) laser power that still enabled the observation of binding events was chosen to minimize the established temperature gradient and prevent any disruptive effects from interfering with the measurements. Actual MST measurements were done after this preliminary procedure.

3.1.8.2 K_D values for betaine and diosmetin binding to PEX1.TEV.HIS$_6$ were different

After confirming the positive effects of betaine and diosmetin in PEX1 (G843D) mutant cells in the recovery of peroxisomal import-export machinery, it was decided to examine the interaction of these compounds with the purified PEX1/PEX6 complex. To this end, MST analysis was performed as described in section 2.3.8. The tested chemical compounds could influence the PEX1/PEX6 complex either by binding directly to the proteins or by changing the chemical environment of the complex. Either way, the change in the complex could be detected by a change in the thermophoretic movement. Since the HIS-tag in the PEX1.TEV.HIS$_6$ was labelled with the dye, K_D values of the compounds binding to the PEX1 protein in the complex was then determined by plotting the normalized fluorescence values against the concentration.

Representative MST measurements of betaine and diosmetin with the PEX1.TEV.HIS$_6$ are depicted in Figure 27. Purified protein complexes (Figure 27 A and D) were used for the MST measurements after determining the concentration of each PEX1 and PEX6 protein in the complex via silver staining (see 2.3.5). PEX1/PEX6 complex was titrated with each compound and the thermophoretic effect was measured using the Monolith NT.115 (NanoTemper) at 100% LED power and medium IR laser power. The concentration of betaine and diosmetin were taken in the range where they were able to recover peroxisomal activity in PEX1 mutant cells (see Figure 25).

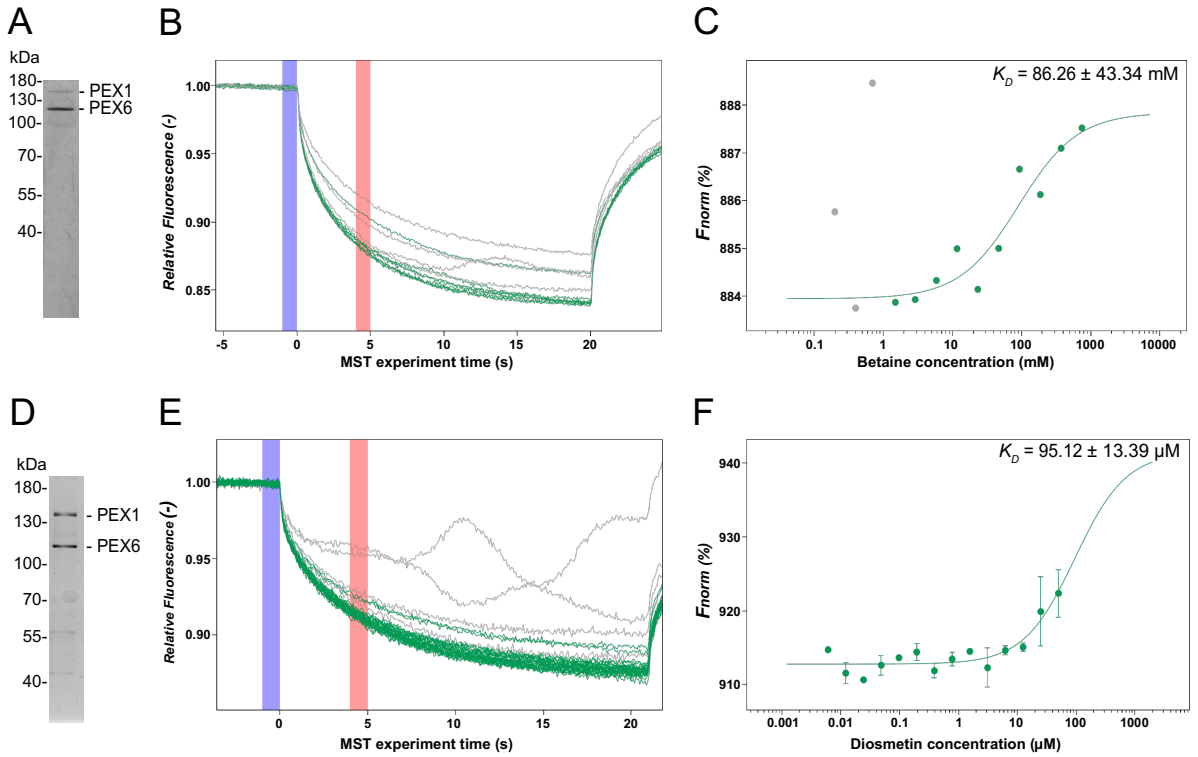

Figure 27: Interaction of betaine and diosmetin with PEX1.TEV.HIS$_6$. MST analysis for betaine (top) and diosmetin (bottom) with PEX1/PEX6 complex. (A, D) Silver-stain of purified PEX1/PEX6 complex, (B, E) MST traces, and (C, F) dose-response-curves. Serial dilutions of both compounds were made in 16 reaction tubes and purified PEX1/PEX6 complex was incubated with RED-tris-NTA for 30 min and centrifuged for 10 min. The supernatant was added to the serial dilutions of each compound and further incubated for 30 min at room temperature. The mixtures were taken in separate capillary tubes and measured with 100% LED power and medium laser power. MST traces (B and E) plotted are the normalized fluorescence F_{norm} against time. Outliers are marked in gray. The IR laser was turned on at 0 s (blue line). The resulting dose-response curves (averaged F_{norm} from 1.5 s to 2.5 s plotted against the compound concentration) were fitted (red line) to a one-site binding model for K_D determination (C and F). Measurement for betaine was done once and that for diosmetin was twice (with same samples, before and after centrifugation). Error bars = SD.

After fitting the dose response plot, a K_D value of 86.26 ± 43.34 mM was obtained for betaine (Figure 27 C) and 95.12 ± 133.92 µM for diosmetin (Figure 27 F). Outliers, as indicated by gray colored MST traces (Figure 27 B and E), were omitted while fitting the plots. The diosmetin curve is unsatisfactory due to significant fluctuations in values at higher concentrations. This inconsistency is often attributed to the limited solubility of diosmetin, leading to frequent precipitation issues.

The measurements were done multiple times using the same settings. The K_D values obtained for both betaine and diosmetin along with the S_E and the concentration of PEX1.TEV.HIS$_6$ are listed in Table 3.2, where the measurements displayed in Figure 27

are marked with an asterisk (*). The K_D values of betaine fall in the millimolar range while that of diosmetin fall in the micromolar range. Although the K_D values of the same compound vary in different experiments, the K_D value of betaine differs from that of diosmetin by a factor of around 1000 when same protein sample used. This indicates that the interaction of the PEX1/PEX6 complex with diosmetin is more specific than with betaine. The difference in values in different experiments could be explained by the fact that the protein preparations used differ in purity and the ratio of the two proteins, PEX1 and PEX6, in the protein sample. Furthermore, the concentrations of protein samples used seem to be at the lower end of the experiment sensitivity and use of concentrated protein complex could produce more reliable data.

Table 3.2: Comparison of K_D values of betaine and diosmetin with PEX1.TEV.HIS$_6$

Exp.	PEX1.TEV.HIS$_6$ concentration	Betaine		Diosmetin	
		K_D	S_E	K_D	S_E
1.	9.72 nM	3.47 ± 2.23 mM	0.8878	3.15 ± 5.38 µM	2.1225
2.	7.02 nM	-	-	95.12 ± 133.92 µM*	1.3601
3.	2.31 nM	86.26 ± 43.34 mM*	0.4521	64.20 ± 94.49 µM	1.2229
4.	2.28 nM	337.04 ± 221.37 mM	1.0511	-	-

where, K_D is the dissociation constant, S_E is the standard error of mean, and * indicate the values taken in Figure 27.

This result also comes in line with the proposal that diosmetin binds at the ATP-binding site of PEX1(G843D) and stabilizes the protein [148]. However, it is not clear how diosmetin could reach the ATP binding site of PEX1 due to the compact structure of the complex (more in discussion). Chemical chaperones like betaine indiscriminately provide stability to misfolded proteins through relatively weak thermodynamic interactions that necessitate high concentrations to exert their efficacy [146].

3.2 Targeting the PEX1-G843D mutation by RNA editing

Pathogenic mutations in any one of the 14 PEX genes result in disorders of peroxisome assembly which lead to Zellweger spectrum disorder (ZSD), a heterogenous group of multi-system disorders [11,241]. Of these, almost 60% of the affected patients have mutations in the *PEX1* gene [89,242] and the *PEX1-G843D* (PEX1-p.Gly843Asp; PEX1-c.[2528G>A]) is the most common disease-causing *PEX1* allele present predominantly in patients of European origin [121,140,216,243].

This part of the project was concentrated in targeting this *PEX1-G843D* mutation in the patient cell lines with different approaches of site directed mRNA editing thus resulting in the translation of correctly folded PEX1 protein. For this purpose, cells lines with this particular mutation were used.

i. M2H PEX1-G843D-PTS1 (Pex1: c.[2528G>A]; [2097_2098insT], p.[G843D]; [0]): One allele of the *PEX1* gene in these cells contain the desired mutation while the second allele has a frame shift mutation with a thymidine insertion at 2097 bp. This frameshift mutation causes the translation of a non-functional protein. Additionally, these cells also expressed EGFP-PTS1, prepared by integrating pEGFP-PTS1 (Clontech) using an adenoviral transfection system [141].
ii. HEK293 Flp-In PEX1-G843D (Pex1: c.[2528G>A]; [2517_2539del], p.[G843D]; [0]): This cell line also has one allele with the desired G843D mutation while the other allele has a deletion of 20 nucleotides flanking the mutation site [217].

Unlike DNA base editing, modifications made to RNA are non-permanent and non-heritable. Instead, they offer reversible and dosable effects, which are desirable for a range of therapeutic uses. After transfection of specific gRNAs to these cells, the efficiency of RNA editing was examined by sequencing the target region after RNA extraction and cDNA synthesis. Successful translation and complementation of the functional PEX1 protein was also checked by fluorescence microscopy.

3.2.1 SNAP-ADAR based RNA editing

One approach of RNA editing was the use of SNAP-tagged (self-labeling protein tag) deaminases guided by chemically stabilized specific guide RNA to edit the adenosine (A) to inosine (I) in endogenous transcripts, which is then later read as guanosine (G) by the

translation machinery. It has been shown that SNAP-tagged ADARs (adenosine deaminases acting on RNA) can be used to replace adenosine by inosine in specific RNA positions [200,201].

3.2.1.1 SNAP-ADAR proteins are stably expressed after PiggyBac transfection

For utilizing the SNAP-ADAR system, copies of four different SNAP-ADAR enzymes (SNAP–ADAR1 (SA1) and SNAP-ADAR2 (SA2), and their respective hyperactive E>Q variants SA1Q and SA2Q) were integrated separately into the genome of M2H cells under control of the doxycycline-inducible CMV promoter [197]. M2H cells grown in 12-well plates were transfected (PEI lipofection) with the two plasmids, one encoding corresponding SNAP-ADAR enzyme and the other encoding a transposase (see Table 2.19) with the help of polyethyleneimine (PEI). Cells were selected with media containing Blasticidin (25 µg/mL). Media with the antibiotic was changed every 3 days. Cells were checked for the expression of respective SNAP-ADARs, and correct samples were stored frozen in liquid nitrogen.

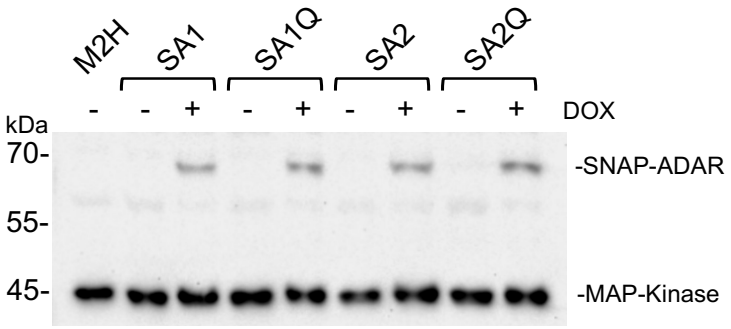

Figure 28: Expression of SNAP-ADAR proteins in M2H cells. Stable cell lines generated by the PiggyBac transfection of each variant of SNAP-ADAR proteins were grown in presence (+) or absence (-) of doxycycline (DOX) (500 ng/mL) and harvested the next day. 20 µg of whole cell lysates were run on an 8% SDS gel and transferred to a NC membrane by western blotting. Thereafter, SNAP-ADAR and MAP-Kinase proteins were stained using corresponding α-SNAP (1:1000) and α-MAPK (1:2000) antibodies. After incubating with the secondary antibody solutions, chemiluminescence signals were obtained from the membranes using a ChemiDoc Analyzer (Bio-Rad).

Cells grown in presence of doxycycline produce the SNAP-ADAR proteins after overnight incubation. As seen in Figure 28, all cells treated with the antibiotic show the presence of the protein in the cell lysate. All variants of the SNAP-ADAR appear just below the 70 kDa mark when treated with α-SNAP antibody after SDS gel separation and western blotting.

MAP-Kinase protein was stained as a loading control. The cells were thus ready to be treated with the specific BB-guide RNA for RNA editing.

3.2.1.2 Specific guide RNA and SNAP-ADARs partially avert the *PEX1-G843D* mutation

SNAP-ADAR proteins engineered into the patient cell lines are artificial editases comprising a deaminase domain (wildtype or hyperactive mutant) of ADAR1 or ADAR2 and an N-terminal SNAP-tag protein. The SNAP-tag is originated from O^6-alkylguanine-DNA alkyltransferase (hAGT) [244,245] and can bind to O^6-benzylguanine (BG) with high specificity. Therefore, this BG moiety when conjugated to a guide RNA (gRNA) can covalently bind to the SNAP-ADAR in a 1:1 ratio [200]. For this project, chemically modified gRNA specific to the PEX1-G843D site was prepared and a BisBG moiety was conjugated to its NH_2-terminal (kindly provided by the lab of Prof. Stafforst, IFIB). BisBG is a dimeric linker that helps attach two SNAP-ADAR proteins to either 3'- or 5'- end of a single gRNA. This modified gRNA (named BB283 hereafter) was transfected into the M2H cells stably expressing the SNAP-ADAR proteins after induction. As a control, another modified gRNA (BB180) specific for the STAT1 Y701 was used.

The workflow for the transfection of the modified gRNAs into the cells and the sequencing results are illustrated in Figure 29. M2H cells with or without the SNAP-ADAR sequence were seeded in each well of a 24-well plate and incubated for 6 h until they settled. Doxycycline (500 ng/mL) was added to all wells (except for the original M2H cells) for SNAP-ADAR induction. Media was discarded after overnight incubation (18 h) and treated with PEI-gRNA mixture in 100 µL OptiMEM (see 2.2.5) for 6 h. The mixture was replaced with fresh media and the cells were incubated for another 18 h. Media was discarded, and the cells were lysed with 100 µL of RLT buffer (Qiagen), directly on the well plate and transferred into a reaction tube. RNA from the cell lysates was extracted using the Monarch RNA Cleanup Kit (NEB). A One-Step RT-PCR was performed using 500 ng of each purified RNA and the PCR products were separated in an 1.4% agarose gel. Correct products were excised and purified using a gel extraction kit (Sigma). Thus obtained DNA samples were sent for Sanger sequencing. A forward primer (STAT1 seq #fw) was used for STAT1, and a reverse primer (G843D_10_rv) was used for the PEX1 construct (see Table 2.5). For the control experiment in M2H_SA2Q cells, the STAT1 Y701

site specific gRNA (BB180) was able to correct the site with 81.0% efficiency. Similarly, the PEX1-G843D specific gRNA (BB283) was able to correct the nucleotide by 18.9% in M2H_SA1, 18.6% in M2H_SA1Q, 18.4% in M2H_SA2 and 16.4% in M2H_SA2Q cells. Since there was a large difference in the correction efficiency in the control and the experimental groups and the repetitive experiments yielded inconsistent results (data not shown), it was decided to use a different transfection method.

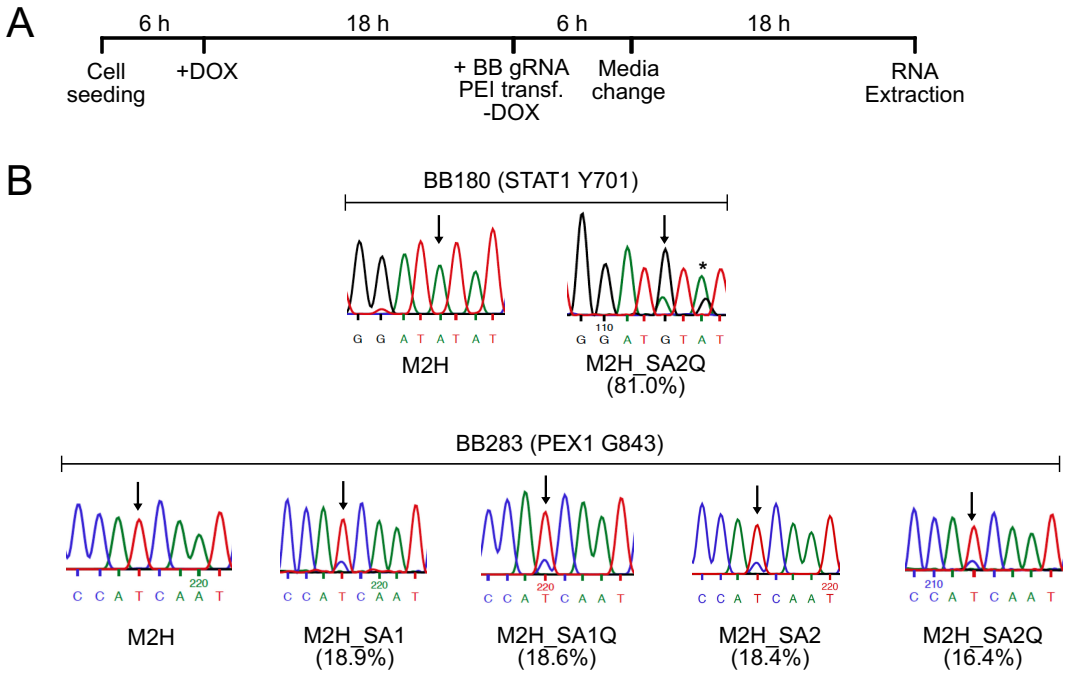

Figure 29: Editing of endogenous transcripts with SNAP-tagged ADARs. (A) Workflow for the transfection of gRNA into the SNAP-ADAR expressing cells and (B) sanger sequencing traces of the corresponding targets. In each well of a 24-well plate, 100,000 cells (as indicated) were seeded and incubated in 1 mL media until the cells settled. After about 6 h, 0.5 µL doxycycline (1µg/µL) was added to each well to induce SNAP-ADAR expression and incubated overnight. After 18 h of incubation, the media was discarded and a mixture of 10 pmol gRNA and 4 µg PEI mixture in 100 µL OptiMEM was added dropwise to the cells. Cells were treated with the PEI-gRNA mixture for 6 h and then the media was replaced. RNA extraction was done after another 18 h of growth. A One-Step RT-PCR was done using 500 ng of RNA from each construct with corresponding primers for PEX1 and STAT1. The obtained PCR products were purified on an agarose gel and sent for sequencing. Arrows indicate the target sites and asterisk indicate an off-target site. Editing efficiency is written in parentheses for each construct.

In the next phase, the cells were electrotransfected using a Neon™ transfection system (see 2.2.4). Cells were treated with doxycycline a day before transfection. All variants of the M2H cells were transfected with gRNAs specific to STAT1 Y701 (BB180) and PEX1-G843D (BB283) sites. One batch of the cells was used for RNA extraction after 24 h and

the other batch was used for live cell imaging 48 h after transfection (Figure 30). Purified RNA samples were used for One-Step RT-PCR and the resulting products (DNA) were sent for sequencing after purification from an agarose gel. Live cell imaging was done after 48 h using a 63X oil objective with a Zeiss Axio Observer microscope.

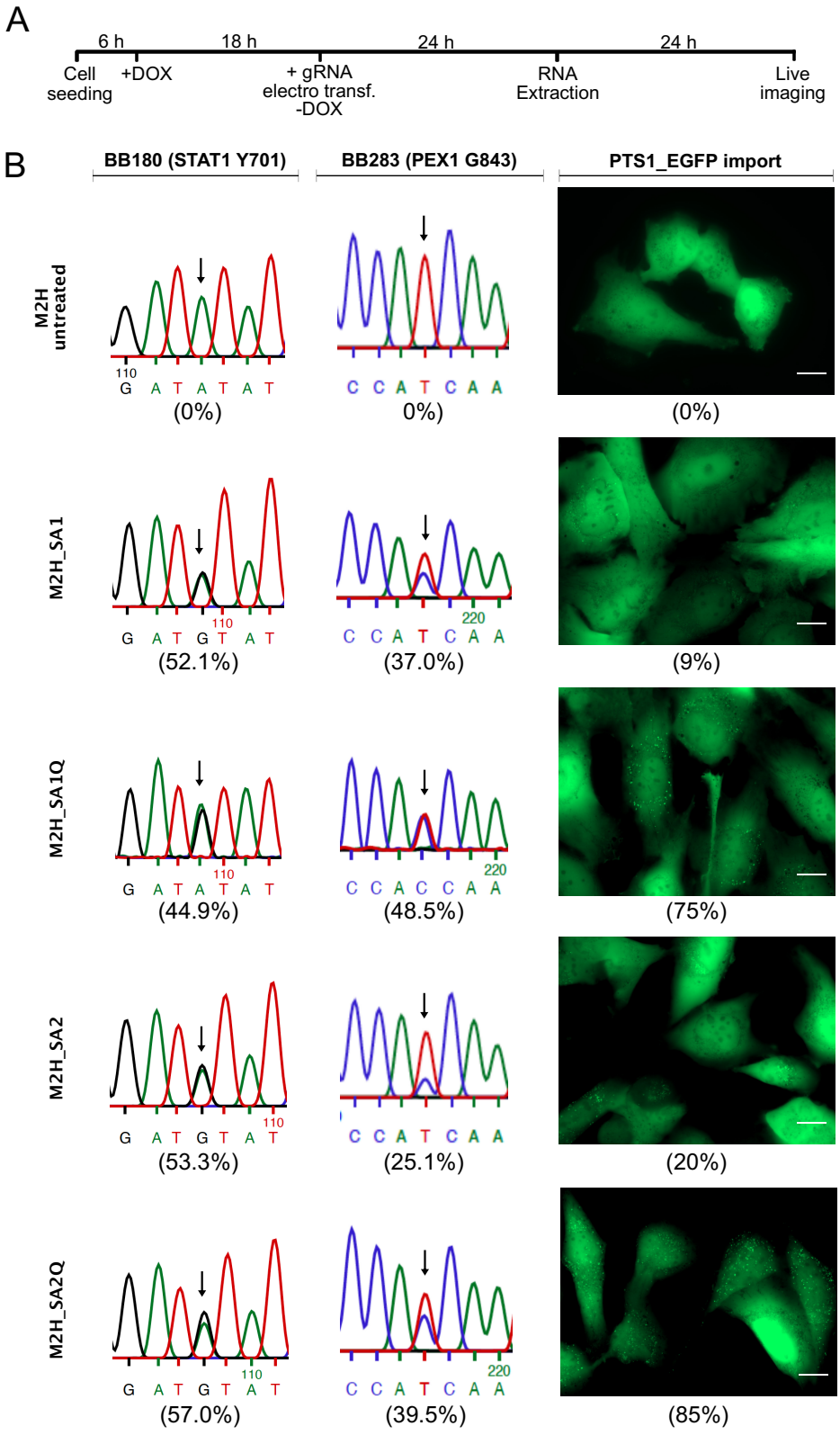

Figure 30: Editing of endogenous transcripts with SNAP-ADARs after gRNA electroporation. Workflow for the transfection of gRNA into the SNAP-ADAR expressing cells (A) and sanger sequencing traces of the corresponding targets along with live cell imaging (B). Actively growing M2H cell variants were split into new culture flasks. After about 6 h, doxycycline (1µg/µL) was added to each flask to express SNAP-ADAR and incubated overnight. The following day, cells were detached again and counted. A total of 100,000 cells were electroporated with the corresponding 5 pmol gRNAs with 1300 V power for 30 ms and 2 pulses. Cells were resuspended in fresh culture media and grown in two separate dishes. Glass-bottom dishes were used for live cell imaging. RNA extraction was done after another 24 h using one batch of cells. A One-Step RT-PCR was done using 500 ng of RNA from each construct with corresponding primers for PEX1 and STAT1. Obtained PCR products were run in an agarose gel. The correct products were purified using a gel-extraction kit and sent for sequencing. Arrows indicate the target sites. Live cell imaging was done using Zeiss Axio Observer microscope with a 63X oil objective. Editing efficiency is written in parentheses for each construct.

As can be seen in Figure 30 B, A to I (G) correction in STAT1 Y701 position were 52.1% in M2H_SA1, 44.9% in M2H_SA1Q, 53.3% in M2H_SA2 and 57.0% in M2H_SA2Q cells. Similarly, the correction at PEX1-G843D position was 37.0% in M2H_SA1, 48.5% in M2H_SA1Q, 25.1% in M2H_SA2 and 39.5% in M2H_SA2Q cells. The correction efficiency of BB180 gRNA seems fairly consistent for all cell types, ranging between 44-57%. This efficiency was however lower than the efficiency obtained by PEI-lipofection. The transfection of BB283 gRNA on the other hand resulted in a higher transfection efficiency in presence of the hyperactive variants SA1Q and SA2Q. A similar effect was also seen in live cell imaging, where green punctates of peroxisomes were seen in 9% of M2H_SA1, 75% of M2H_SA1Q, 20% of M2H_SA2 and 85% of M2H_SA2Q cells. Overall green fluorescence in the cytosol and the nucleus was seen in the M2H cells due to the presence of EGFP-PTS1 protein, which is only transported into the peroxisomes when the import machinery functions properly. Since both, the sequencing results and the IF experiments indicated that the hyperactive SNAP-ADAR variants are better in correcting the mutation site, it was decided to further investigate the process using the cells with these variants (SA1Q and SA2Q), only.

3.2.1.3 Peroxisomal import remains functional 7 days after *PEX1-G843D* mRNA correction

Next, the M2H cells expressing SA1Q and SA2Q variants were tested to see if the effect of the *PEX1-G843D* mRNA correction persists for several days at the protein level. For this the cells were transfected with the BB283 gRNA as described earlier. One set of cells were

harvested for RNA extraction (after 24 h) and RT-PCR while the other set of cells were grown in glass-bottom dishes for live imaging. Live cells were observed 48 h following transfection, split, and grown until 7 days for another round of imaging.

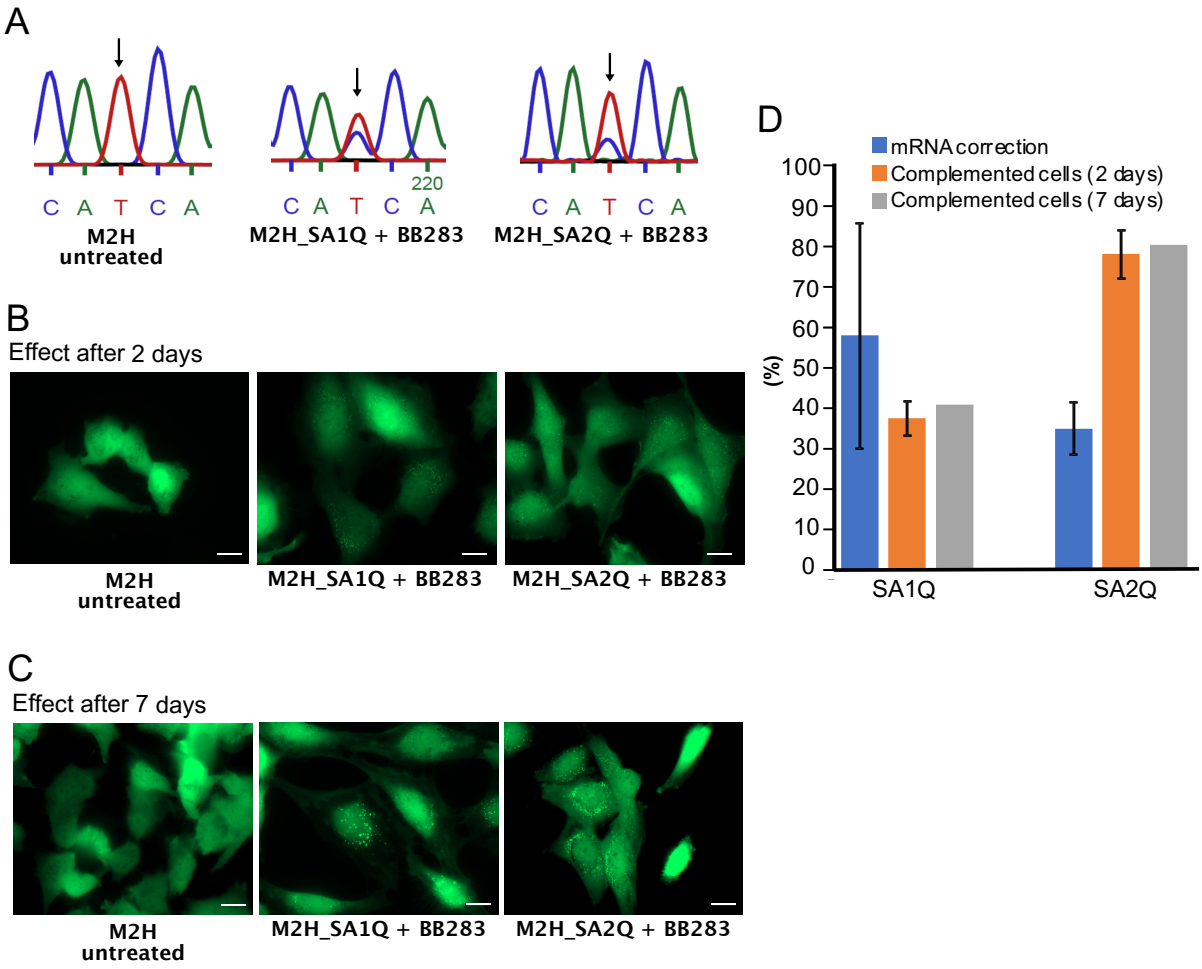

Figure 31: Restoration of peroxisomal matrix protein import in M2H *PEX1-G843D* mutant cells. M2H cells expressing SA1Q and SA2Q were transfected with BB283 gRNA one day after doxycycline induction. M2H cells were taken as a negative control. Extraction of RNA was done after 24 h followed by OneStep RT-PCR to yield DNA fragments which were run on an 8% agarose gel and the correct band sizes were purified. DNA samples were sanger sequenced using the reverse PCR primer (A). Another set of cells grown in glass-bottom dishes were observed under 63X oil objective 2 days (B) and 7 days (C) after transfection. The graph represents the fraction of mRNA editing and the percentage of cells importing the GFP-PTS1 protein into the peroxisomes (D). Sequencing result and live cell imaging data for two days are given as the mean +/- SD of 3 independent experiments (orange bars) and the data for 7-day imaging (grey bars) are given for one experiment only. Values from untransfected M2H cells were normalized to zero.

The amount of mRNA correction and the fraction of cells restoring the peroxisomal import are shown in Figure 31. Sequencing results show that both SA1Q and SA2Q variants of the deaminase were able to consistently edit the target site *PEX1-G843D* in

presence of the guide RNA. As an average of 3 independent experiments, 58.1 ± 28.2% edit was observed for SA1Q and 35.0 ± 6.4% for SA2Q variant at the mRNA level. Similarly, 37.6 ± 4.0% in M2H_SA1Q cells and 78.4 ± 5.7% M2H_SA2Q cells show the import of GFP-PTS1 protein into the peroxisome 2 days after gRNA transfection. In one experiment, the import of the GFP-PTS1 protein was retained even after 7 days post-transfection as observed in 41% M2H_SA1Q cells and 81% M2H_SA2Q cells. As the life span of peroxisomes lasts only a few days [246,247], the transfer of gRNA, mRNA and/or the translated protein might be reason for functional peroxisomes even after 7 days of gRNA transfection.

While comparing the correction rates with the sequencing data to the IF data, it is seen that SA1Q variant has less cells importing the GFP-PTS1 protein while the SA2Q variant has significantly higher number of cells with peroxisomal import. The reason for this could be that the higher mRNA edits result in higher peroxisomal import which will import most of the highly expressing GFP-PTS1 proteins into the peroxisomes. This might have affected the organelles resulting in early cell death, thus decreasing the percentage of cells with the import. Some of these cells can be seen with larger green punctates under live imaging indicating the stress on the peroxisomes (Figure 31C).

3.2.1.4 HEK *PEX1-G843D* mutant cells regain peroxisomal import after gRNA transfection

The presence of GFP-PTS1 made it difficult to reliably stain and visualize other peroxisomal matrix proteins. Some cells were blown up with bright green fluorescence even under live cell imaging. Upon successful editing of the *PEX1-G843D* site, this EGFP protein might overload the peroxisomes, blocking the import of other essential matrix proteins, eventually hampering the peroxisomal function. Further lipid measurement and other biochemical assays might also be affected due to this effect. This posed a need for other cell types without the overexpression of EGFP-PTS1. Therefore, a HEK Flp-In cell line with the G843D mutation (c.2528G>A) was used in the following experiments. The cell line was kindly provided by the group of Prof. Dr. Hans Waterham, Amsterdam. These cells were grown and maintained in complete media with 15% FCS instead of 10% as they weakly attach to the culture flask surface. Immunofluorescence of these cells was also done by growing them on glass cover slips coated with poly-D-Lysine.

As described for the M2H cell line, copies of the SNAP-ADAR enzyme variants were integrated into the genome of the HEK *PEX1-G843D* cells via PiggyBac transfection (see 2.2.3). Cells were checked for the production of the SA1Q and SA2Q enzymes by doxycycline (500 ng/mL) induction. As seen in Figure 32A, the cells treated with doxycycline (DOX) successfully translated the respective deaminase enzymes. Similar expressions of the SA1 and SA2 enzymes were also observed (data not shown). However, only the cells with the hyperactive variants (SA1Q and SA2Q) were taken for the study. The cells were transfected with the gRNA BB283 to analyze the effect on mRNA editing. A total of 100,000 cells were transfected with 5 pmol of gRNA after 18 h of doxycycline induction. Cells were harvested for RNA extraction, followed by OneStep RT-PCR and agarose gel separation of the products. Primers G843D_53_Fw (forward) and G843D_53_Rv (reverse) were used for the PCR. The PCR products were sequenced (Figure 32B and D). Correction of the *PEX1-G843D* mutation at the mRNA level was observed in 20.8 ± 2.5% with SA1Q and 17.5 ± 1.1 with the SA2Q variant (Figure 32D). Transfected cells were also stained with antibodies against PMP70 and catalase proteins after 3 days. Since PMP70 is an essential peroxisomal membrane protein, it is always present in mature peroxisomes and is regarded as one of the marker proteins for the peroxisomes. PMP70 proteins can be seen as bright violet punctates in Figure 32C. Catalase, being a matrix protein, is only inserted into the peroxisome when the import/export machinery is functioning properly. Cells transfected with the specific gRNA for the mutation were able to translate the correctly folded PEX1 protein thus maintaining the import/export machinery. In these cells, catalase was also seen as punctates (light blue) indicating its successful entry into the peroxisomes. The number of cells importing the matrix protein catalase was calculated to be 28.4 ± 2.0% and 22.3 ± 2.3% in SA1Q and SA2Q expressing cells respectively. In addition, thiolase, a PTS2 protein, was also imported to the cells (not shown as the data were incomplete). This proves that the method was reliable in correcting the import of both PTS1 and PTS2 containing proteins.

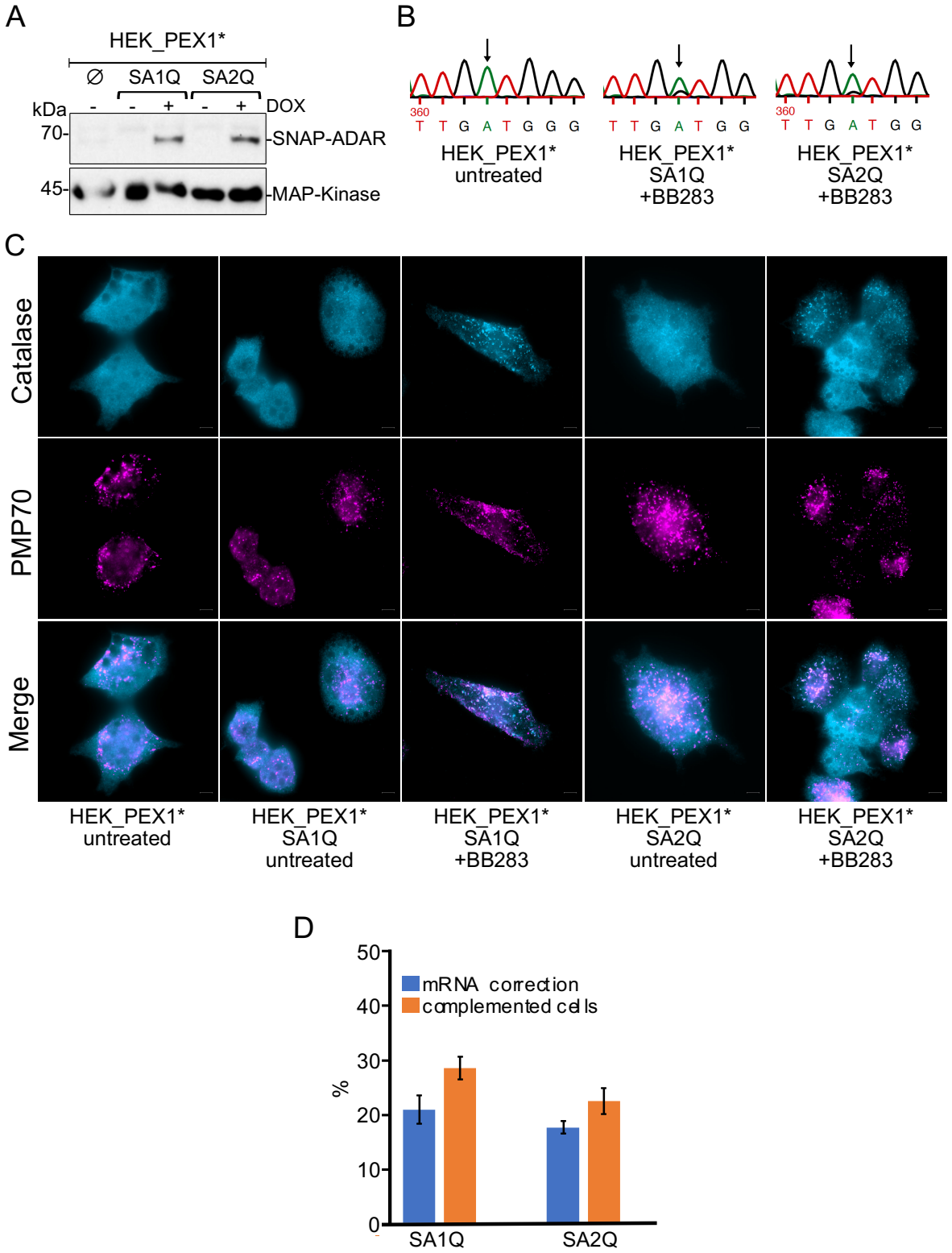

Figure 32: Restoration of peroxisomal matrix protein import in HEK *PEX1-G843D* mutant cells. Expression of SNAP-tagged ADARs in HEK Flp-In_PEX1-G843D cells (A), correction of mutant mRNA (B), immunofluorescence microscopy of the cells (C) and fraction of corrected mRNA and complemented cells (D). Stable cell lines generated by the PiggyBac transfection of each SNAP-ADAR variant were grown with (+) or without (-) doxycycline induction (500 ng/mL) and harvested the next day. 20 µg of whole cell lysates were separated on an 8% SDS gel and transferred to an NC membrane. Subsequently, SNAP-

ADAR and MAP-Kinase proteins were stained using corresponding α-SNAP (1:1000) and α-MAPK (1:2000) antibodies (A). A total of 100,000 cells (doxycycline induced and uninduced) were electroporated with the corresponding 5 pmol gRNAs with 1200 V power for 20 ms and 2 pulses. RNA extraction was done after 24 h followed by One-Step RT-PCR, agarose gel separation and sequencing (B). Arrows indicate the target sites. A set of cells were grown on cover slips coated with poly-D-Lysine and used for immunofluorescence microscopy by staining with PMP70 and catalase antibodies followed by the corresponding secondary antibodies after three days. Cells were visualized using a Zeiss Axio Observer microscope with an 63X oil objective. Catalase staining is shown in light blue and PMP70 in violet. The lower panel depicts the composite image of both channels (C). The graph represents the fraction of mRNA editing and the percentage of cells importing catalase into peroxisomes (D). Sequencing results and live cell imaging data are given as the mean and SD of 3 independent experiments. Values from untreated cells were normalized to zero. PEX1*: PEX1-G843D, DOX: doxycycline

When comparing correction efficiency in HEK cells to that in M2H cells, HEK cells tend to have lower mRNA correction as well as lower matrix protein import. However, since these were only preliminary experiments done in the HEK cells, further optimization might increase the efficiency of the system.

3.2.2 RESTORE based ASO mediated editing

Apart from editing the RNA with the help of overexpressed proteins, advances have also been made to harness the endogenous ADAR proteins to reverse desired point mutations. Without the co-delivery of any exogenous proteins (like SNAP-ADARs), only the recruitment of chemically modified antisense oligonucleotides (ASOs) can now enable programmable A-to-I RNA editing in an approach known as RESTORE (recruiting endogenous ADAR to specific transcripts for oligonucleotide-mediated RNA editing) [164]. The ASOs are comprised of two parts: an invariant ADAR recruiting domain and a programmable specificity domain. The specificity domain is prepared/modified according to the target site. All the ASOs (see Table 2.4) used in this study were kindly provided by the lab of Prof. Dr. Thorsten Stafforst, IFIB Tübingen.

3.2.2.1 ASO mediated editing of *PEX1-G843D* mutation in M2H cells

During the first phase of this project, two ASOs (TMR177 and TMR178) were transfected into the M2H cells and studied. The ASO TMR177 is 59 nt long while TMR178 is 45 nt long. Both ASOs have very few chemical modifications. Cells were seeded and grown. Transfection was done to the actively growing cells via electroporation. An ASO concentration of 20 pmol per 100,000 cells in electroporation buffer was used to

electroporate the cells with 1300 V for 20 ms and 2 pulses (see section 2.2.4). Cells were incubated and grown in culture media for 24 h and harvested for RNA transfection. Extracted RNA was then used for reverse transcription and PCR. Primer pairs SP09/SP10 were used in the PCR for these constructs. Correct PCR products were purified from an agarose gel and sent for sequencing using the reverse primer SP10. Another set of transfected cells was grown in glass bottom dishes and visualized live under the microscope (Figure 33 A and B). Sequencing results of 3 independent experiments revealed 8.2 ± 1.1% correction of the *PEX1-G843D* mutation with TMR177 and 8.9 ± 1.7% correction with TMR178. Similarly, live cell imaging 2 days after transfection showed import of GFP-PTS1 protein into the peroxisomes in 15.4 ± 1.4% of the cells with TMR177 treatment and in 18.4 ± 2.4% of the cells with TMR178 treatment (Figure 33D).

Two more ASOs (TMR204 and TMR205) were also transfected into the M2H cells. Both ASOs are 59 nt in length and have more chemical modifications than TMR177/TMR178 with slightly different combinations. The same method as described above was deployed for transfection of the cells with these ASOs. However, a different set of primers (SP43/SP44) was used for PCR. This was done to get cleaner sequencing data (more in discussion). Sequencing data revealed 16.8 ± 8.4% mRNA correction with TMR204 and 34.0 ± 13.4 correction with TMR205. As seen in the chromatogram (Figure 33 C), the negative control also showed correction of the nucleotide (T to C, reverse). The reason did not lie in the actual correction of the mRNA but is due to the genetic composition of the M2H cells. One allele of the *PEX1* gene in these cells contains the desired mutation, while the second allele has a frame shift mutation with a thymidine insertion at 2097 bp (Pex1: c. [2528G>A]; [2097_2098insT], p. [G843D]; [0]). Although this frame shift leads prevents protein translation, mRNA might still be present and might lead to a PCR product with the used primer pair (SP43/SP44). The correction rates presented for TMR204 and TMR205 (Figure 33 D) have been normalized to that of the untreated cells.

Overall, the transfection of M2H cells with different ASOs revealed that the ASOs with higher chemical modifications were more efficient in correcting the desired mutation in the PEX1 mRNA.

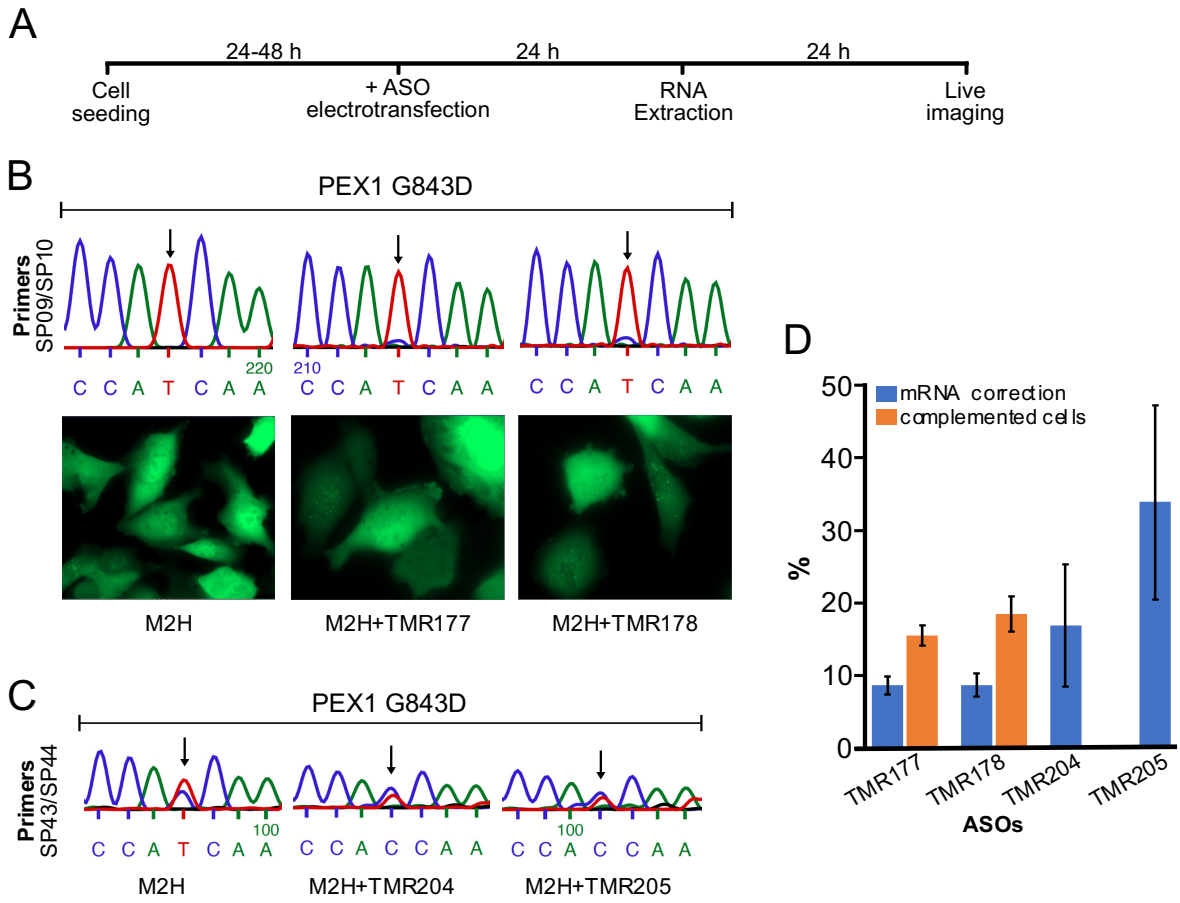

Figure 33: ASO mediated editing of *PEX1-G843D* mutation. Workflow for the transfection of ASOs into M2H cells (A), Sanger sequencing traces of the *PEX1-G843* site (B, C) along with live cell imaging (B) and percentage of corrected mRNA and complemented cells (D). For one electroporation, 200,000 cells were resuspended in 10 µL buffer and 40 pmol of the respective ASOs. Cells for negative controls were transfected without the ASOs. RNA extraction was done after 24 h followed by One-Step RT-PCR, agarose gel separation and sequencing. Arrows indicate the target sites (B, C). A set of cells were grown in glass bottom dishes and visualized via live microscopy 48h after electroporation under 63X oil objective (B). The graph represents the fraction of mRNA editing and the percentage of cells importing catalase into the peroxisomes (D). Sequencing results and live cell imaging data are given as the mean and SD of 3 independent experiments. Values from untreated cells were normalized to zero. PEX1*: PEX1-G843D

3.2.2.2 Need for cells with more endogenous ADAR levels

As mentioned earlier, the presence of GFP-PTS1 in the M2H cells posed a hinderance in visualizing live cells and in the immunolabeling of the marker proteins. It was also observed that these cells contained significantly lower amounts of the endogenous ADAR proteins as compared to other cells such as Hela and HEK293TT (Figure 34A). Both

reasons indicated a need for a cell line with higher endogenous ADAR levels and the absence of any interfering proteins. As stated earlier, a HEK Flp-In cell line with the same mutation was used for the next experiments.

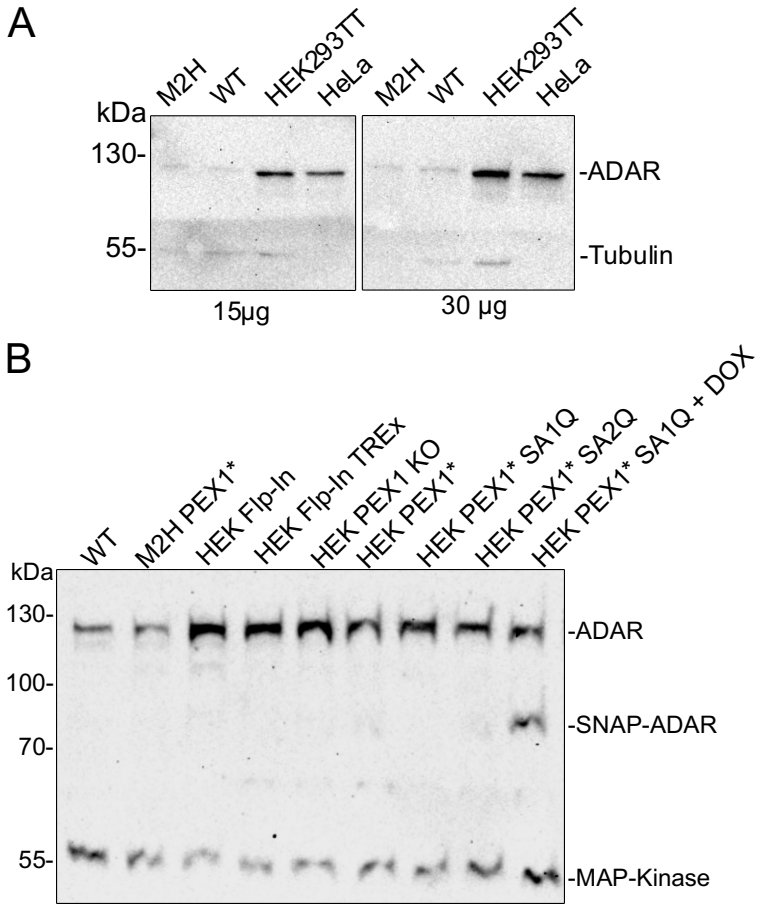

Figure 34: Comparison of endogenous ADAR levels in different cell types. ADAR levels in M2H (PEX1-G843D) cells compared to wildtype fibroblasts, HEK 293TT and Hela cells (A) and compared to HEK PEX1-G843D along with the corresponding wildtype and SNAP-ADAR variants (B). Cells were grown and harvested during active growth phase. Whole cell lysates were run on an 8% SDS gel and transferred to a nitrocellulose membrane by western blotting. Subsequently, ADAR, Tubulin and MAP-Kinase proteins were stained using corresponding α-ADAR (1:1000), α-Tubulin (1:2000) and α-MAPK (1:2000) antibodies. After incubating with the secondary antibody solutions, chemiluminescence signals were obtained from the membranes using a ChemiDoc Analyzer (Bio-Rad).

Immunoblotting of the whole cell lysates with α-ADAR antibodies showed that the HEK Flp-In PEX1-G843D cells contained a significantly higher amount of the ADAR protein as the M2H cell line (Figure 34B). While the wildtype fibroblasts and the M2H cells have low ADAR levels, all of the HEK cell lines (Flp-In, T-REx, PEX1 KO, PEX1-G843D) have higher amounts of ADAR. Please note, that the HEK Flp-In PEX1-G843D cell line with induced SNAP-ADAR SA1Q protein showed both proteins, the endogenous ADAR and the induced

variant. Due to the results shown, it was decided to use the HEK Flp-In PEX1-G843D cell line to evaluate the RESTORE technique.

3.2.2.3 Effect in HEK Flp-In cells

Before using the ASOs targeted against the desired mutation, some controls were needed to check the efficiency of the technique in the HEK Flp-In PEX1-G843D cells. At first, two ASOs (TMR141 and TMR174) specific to the STAT1 Y701C were used. Both ASOs are 59 nt long, but TMR141 has fewer chemical modifications than TMR174. A total of 300,000 cells were mixed with 60 pmol of the ASO in a total volume of 10 µL with electroporation buffer. Transfection of the cells was done via electroporation at 1100 V for 20 ms and 2 pulses. RNA extraction was done after 24 h followed by One-Step RT-PCR and purification of the fragments from an agarose gel. A different set of primers (SP53/SP54) was taken for the PCR reaction in the HEK cells, due to differences in the genotype (see discussion for more information). After sequencing analysis, the desired A to G change was seen with a 21.3 ± 7.1% correction rate for TMR141 and a 5.9 ± 3.9% correction rate for TMR174 (Figure 35).

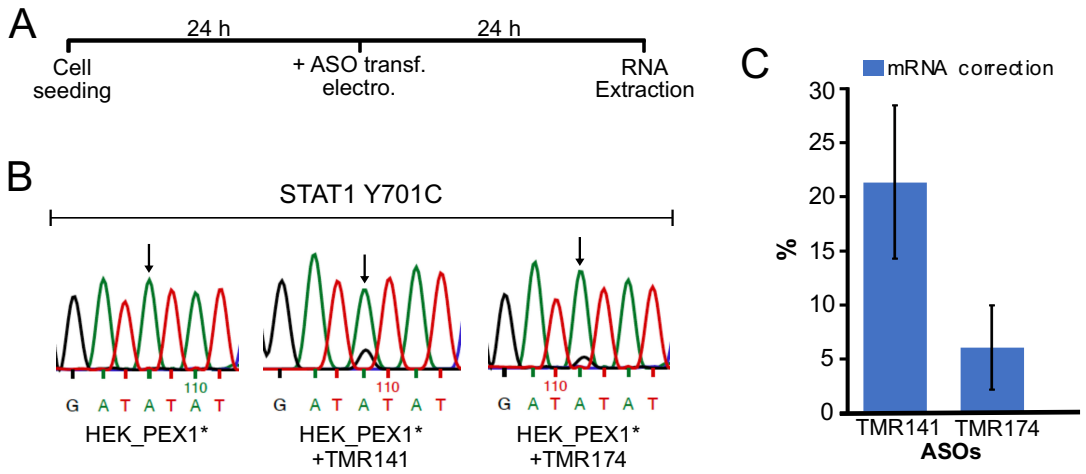

Figure 35: STAT1 Y701C correction with different ASOs. Scheme for transfection and RNA extraction of the cells (A), chromatograms obtained after sequencing the PCR products (B) and graph with mean correction rate and SD (C). For each transfection, 60 pmol ASO was mixed with 300,000 HEK_PEX1* cells in electroporation buffer and transfected with a Neon electroporator. Cells were transfected without the ASOs for negative controls. RNA extraction was done after 24 h followed by One-Step RT-PCR and purification from agarose gel. DNA samples were then sent for sequencing. HEK_PEX1*: HEK Flp-In PEX1-G843D.

Similarly, two more ASOs targeting the β-Actin 3‘-UTR (AI-0111) and GAPDH L157L (TMR84) were also checked for their efficiency in replacing the desired nucleotide in the mRNA. HEK Flp-In PEX1-G843D and HEK Flp-In T-REx cells were transfected with these ASOs exactly as the ASOs against STAT1 mRNA. Single transfection experiment showed the correction efficiency of AI-0111 on mutant HEK cells to be 56.8% and on the HEK T-REx cells to be 54.6%. TMR84 yielded 28.1% correction in the PEX1 mutant cells and 16.2% correction in the HEK T-REx cells.

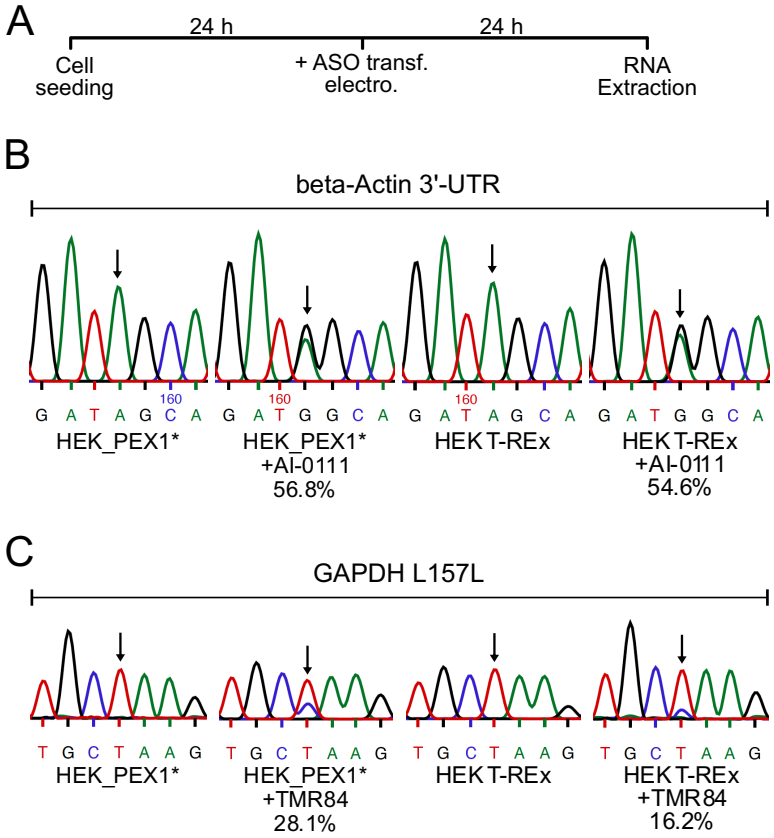

Figure 36: Correction of β-Actin 3‘-UTR and GAPDH L157L sites. Scheme for transfection and RNA extraction of the cells (A), chromatograms obtained after sequencing the PCR products using the extracted RNA at β-Actin 3‘-UTR (B) and GAPDH L157L (C) regions. For each transfection, 60 pmol ASO was mixed with either 300,000 HEK_PEX1* cells or HEK T-REx cells in electroporation buffer and transfected. Cells were transfected without the ASOs for negative controls. RNA extraction was done after 24 h followed by One-Step RT-PCR and purification from agarose gel. DNA samples were then sent for sequencing. Transfected ASOs with correction efficiency are written below corresponding chromatograms. Values are obtained from single experiments. HEK_PEX1*: HEK Flp-In PEX1-G843D, HEK T-Rex: HEK Flp-In T-Rex.

This control experiment suggests that the correction efficiency depends on various factors such as the correction site, the type of ASO use and the type of modifications they exhibit. The efficiency can also be altered by the cell type and the growth and transfection conditions. All in all, these data suggested that the used cell lines contain endogenous ADAR levels in sufficient amounts for the desired correction at specific positions in the mRNA.

3.2.2.4 Correction of the *PEX1-G843D* mutation in HEK Flp-In cells with an ASO

Due to time constraints, not a lot of experiments were done on the HEK cells for the correction of the PEX1-G843D mutation. Some of the ASOs transfected into the cells did not have any effect on the mutation. However, one experiment with the ASO TMR205 yielded a correction efficiency of 32.8% (Figure 37). This result along with the correction rates observed in the M2H cells pave way for more optimizations and modifications that could lead to the production of stable ASOs which could then be used in clinical studies.

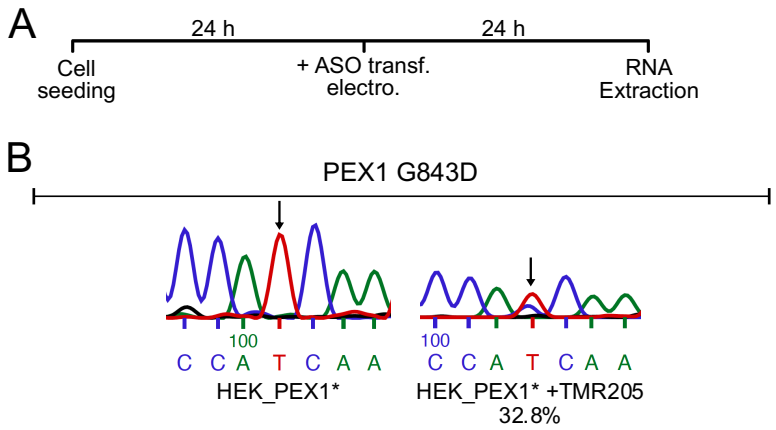

Figure 37: ASO mediated correction of PEX1-G843D mutation in HEK Flp-In cell line. Scheme for transfection and RNA extraction of the cells (A), chromatograms obtained after sequencing the PCR products (B). For each transfection, 60 pmol the ASO TMR205 was mixed with 300,000 HEK Flp-In PEX1-G843D cells in electroporation buffer and transfected. Cells were transfected without the ASOs for negative controls. RNA extraction was done after 24 h followed by One-Step RT-PCR and purification from agarose gel. DNA samples were then sent for sequencing. Correction efficiency is written below corresponding chromatogram. Value obtained from single experiment. HEK_PEX1*: HEK Flp-In PEX1-G843D

After these optimizations, the next step in the project will be to check whether the import of proteins could be restored and whether this would lead to a correction of the disturbed peroxisomal metabolism. For this, the amount of lipid oxidation and plasmalogen synthesis will be analyzed. This will make sure that the correctly folded PEX1 will not only help to improve the import machinery but also guarantees the smooth functioning of the peroxisomal metabolism.

4 Discussion

The formation and maintenance of peroxisomes rely on the crucial presence of the heterohexameric PEX1/PEX6 complex, classified as type II AAA+ ATPases due to their two ATPase domains [137,248]. Like other AAA-ATPases, the PEX1/PEX6 complex utilizes the energy derived from ATP hydrolysis to intricately guide substrate proteins through its central pore, causing them to unfold in the process. The PEX1/PEX6 complex, attached to the peroxisomal membrane via a tail anchored protein PEX26 (Pex15 in yeast), recognizes the ubiquitinated PEX5 [119,137,249], processes and pulls it back to the cytosol [137,239]. The import receptor protein PEX5 recognizes proteins with the PTS1 signal [33] via its C-terminal TPR domain and guides them toward a docking complex situated at the peroxisomal membrane [52]. An impairment or loss of PEX1 and/or PEX6 leads to the accumulation of PEX5 in the peroxisomal membrane, triggering pexophagy and peroxisomal biogenesis disorders (PBDs) [250–253]. The PEX1-c.2528G>A missense mutation (PEX1-G843D) is the most frequent mutation leading to Zellweger spectrum disorders (ZSD) and results in a mild phenotype. This point mutation leads to a misfolded and instable PEX1 that loses the ability to efficiently bind to PEX6. These discoveries highlight the crucial significance of PEX1/PEX6 in regular cellular development and maintaining homeostasis.

The first part of this project focused on the purification of the human PEX1/PEX6 complex and its interaction with some chemical chaperones and pharmacological agents that have been found to help import the peroxisomal proteins in PEX1 mutant cells [141,148]. Purified and fluorescently labeled PEX1-His_6/StrepII-PEX6 complex showed interaction with betaine and diosmetin as suggested by Microscale Thermophoresis (MST) experiments. The results show that diosmetin has a much stronger and more specific interaction with the PEX1/PEX6 complex compared to betaine. This supports the idea that diosmetin binds to the ATP-binding site of PEX1(G843D) and stabilizes the protein, while betaine provides stability indiscriminately through weaker interactions, requiring higher concentrations for efficacy.

The aim of the other part of the project was to correct the PEX1-G843D mutation directly at the mRNA level so that correctly folded protein is translated in the cells. Both ectopically induced and endogenous ADAR proteins were able to correct this mutation to

some extent in presence of suitable guide RNAs. The SNAP-ADAR method yielded an editing of up to 80% and the RESTORE method up to 50% of the PEX1-G43D mRNA. The effects were also seen in the import of the peroxisomal matrix proteins as observed via fluorescence microscopy. Both of the RNA editing techniques look promising and could be used developed for therapeutic purposes in the future.

4.1 Analysis the human PEX1/PEX6 complex

4.1.1 Purification of the human PEX1/PEX6 complex

In this project, both PEX1 and PEX6 proteins were individually overexpressed in HEK293TT cells, and the pellets were combined during purification. The complex was purified through two consecutive affinity chromatography steps utilizing distinct affinity tags on PEX1 and PEX6. The purified protein complex is relatively pure, and both the proteins are easily detected by silver staining and western blot. This method of purification of the human PEX1/PEX6 has also recently been published [221].

The yeast Pex1/Pex6 complex has previously been purified by several groups and structures have been reported [120,130,135,137]. The structure of the human PEX1/PEX6 is not yet known, but models have been predicted [123,254]. The work presented in this thesis could pave a way for such structural analysis. Optimization can still be done to increase the quantity of the proteins achieved. While attempting to express human PEX1 and PEX6 in an alternative host like *S. cerevisiae* or *E. coli* to boost protein quantity is a possibility, challenges may arise due to the size of the proteins.

4.1.2 ATPase assay

The activity of the purified AAA+ ATPase PEX1/PEX6 complex was measured by the amount of inorganic phosphate (Pi) released after ATP hydrolysis (Figure 24). Compared to the activity of the yeast Pex1/Pex6 complex [130], the activity of human PEX1/PEX6 measured during this study is about 500 times lower. This suggests that the purified complex is not fully active and further optimization is required.

Using ATP with different purity or omitting ATP during the elution of the complex also did not seem to change the result. The use of freshly eluted complex instead of a frozen one also did not make much difference. In most ATPase assays, the amount of free

phosphate released was still significantly lower than in the control with PNS. Altogether, this led to the conclusion that the purified samples had little to no ATPase activity and that the measured changes in phosphate amount could represent baseline fluctuations.

One reason for the inactivity of the complex might be due to the presence of the added tags that might have hindered the complex formation between the PEX1 and PEX6 proteins. However, similar tags have already been used to purify the yeast Pex1/Pex6 complex where they remain active [120,130,131,137]. To further examine the activity of the purified PEX1/PEX6 complex, it can be transferred into cells lacking these proteins. The type and position of the tags can also be optimized in order to purify an active complex. In addition, it might be possible, that other interacting proteins are needed to activate the complex.

4.1.3 Chaperones and their interaction with the PEX1/PEX6 complex

Currently, the primary focus of treatment involves enhancing the folding of PEX1 using chemical compounds. The PEX1-G843D mutation, characterized by a missense mutation, induces misfolding and protein destabilization. Notably, a significant improvement in protein folding is observed when cells are incubated at a reduced temperature of 30 °C [138,140]. If temperature reduction proves effective in repairing misfolding, there is potential for chaperone treatment. Chemical chaperones, such as glycerol, DMSO, and betaine, have shown promise by binding non-selectively to the protein and stabilizing the misfolded PEX1. Zhang *et al.* [141] demonstrated that the chemical chaperones glycerol and betaine can restore peroxisome function impaired by the PEX1-G843D mutation, while MacLean *et al.* [148] identified the flavone diosmetin as a compound capable of recovering peroxisomal function. A drawback of chemical chaperones is the need for high concentrations to achieve improvement, as their stabilization relies on general, weak thermodynamic interactions. In contrast, pharmacological chaperones, such as diosmetin, exhibit greater efficiency at lower concentrations due to their more selective action on the target.

In cell-based assays aiming to restore PEX1-G843D function, betaine proved effective at millimolar concentrations, while diosmetin demonstrated effectiveness at micromolar concentrations. To assess the effects of these compounds, M2H cells were exposed to them and the localization of EGFP-PTS1 and thiolase was determined through

fluorescence microscopy. Compared to the effect of DMSO, cells treated with betaine and diosmetin showed improved punctate localization of GFP-PTS1 and thiolase in peroxisomes (Figure 25). These results with thiolase were more pronounced compared to the analysis of catalase import (data not shown). Thiolase is among the four identified proteins in mammalian cells that undergo import using a PTS2 signal peptide and the receptor PEX7 [255–257]. Due to this, there is minimal competition for the import receptor, resulting in rapid import once matrix import has been restored. In contrast, catalase must compete with numerous other PTS1-dependent proteins, leading to a slower import into peroxisomes. In addition, catalase has a somewhat weaker PTS1-signal. Consequently, it might be possible that the chosen timeframe for fixation was sufficient for thiolase import but too early for catalase.

The effects of betaine and diosmetin were additionally supported by microscale thermophoresis experiments, where the gap in K_D values when employing diosmetin versus betaine was significant, spanning three orders of magnitude (Figure 27). Although the actual concentrations within the cell remain unknown, the determined dissociation constants appear to be in an appropriate order of magnitude. This observation aligns with the acting mechanisms of chemical [146] and pharmacological [147] chaperones. Despite betaine being categorized as an osmolyte, suggesting it should not bind to PEX1-His_6/StrepII-PEX6, a change in thermophoresis was observed. This change may not be attributed to direct binding but rather to alterations in the hydration shell of the complex in response to varying betaine concentrations. Betaine, classified as a chemical chaperone and specifically as an osmolyte, exerts its effects in a nonspecific manner, necessitating higher concentrations for efficacy. In contrast, diosmetin appears to interact more selectively with PEX1-His_6/StrepII-PEX6. However, it is still unclear how exactly the flavonoids like diosmetin interact with the complex, whether they stabilize PEX1, increase interaction with PEX6 or other mechanisms. There has been no proof of the direct interaction of diosmetin with the PEX1/PEX6 complex yet.

PEX1/PEX6 ATP binding domains exhibit a characteristic structure of the AAA-ATPase domains. Each ATPase domain is made of two subdomains: a large subdomain forming a βαβ sandwich, and a small subdomain with an α-helical bundle. These subdomains interact with each other and with neighboring subunits in the assembled hexamer [258]. ATP binds at the junction between the large and small subdomains, as well as to the large

subdomain of a neighboring subunit. Specifically, the Walker A motif in the large subdomain is essential for ATP binding, while hydrolysis of ATP requires the presence of a Walker B (WB) motif in the large subdomain and an adjacent "arginine finger" from the neighboring ATPase domain [116]. These conserved arginine fingers in PEX1 and PEX6 are also crucial for the complex formation [130].

A study conducted by introducing mutation to the Walker B motifs of yeast Pex1 and Pex6 suggested that the mutation in Pex1 WB mutation cause slight reduction in ATP hydrolysis while Pex6 WB mutation results in no ATP hydrolysis [130]. This suggests that while both PEX1 and PEX6 WB domains are required for complex formation, the PEX6 WB domain accounts for the main ATPase activity of the complex. Owing to these results, it can be speculated that diosmetin might first be binding to the PEX1 ATPase binding site and the stable protein would bind to PEX6 to make the complex. Therefore, it would be better to test the interaction with pure PEX1 and PEX1-G843D proteins alone rather than using the complex. The presence of ATP in the purified PEX1/PEX6 complex might as well be a hinderance for diosmetin interaction. As diosmetin and ATP are similar in structure, the chance of diosmetin reaching PEX1 in an already formed complex bound to ATP is low. In absence of ATP diosmetin could interact earlier with PEX1 and stabilize it.

Additionally, the MST analysis during this project solely utilized wildtype PEX1 protein, while the impact of diosmetin primarily pertains to PEX1-G843D. Nevertheless, if diosmetin functions as a pharmacological chaperone by binding to the ATP-binding Walker A motif, as suggested by MacLean *et al.* [148], it should also interact with the motif of PEX1. Previous research has demonstrated that other flavonoids can bind to and modulate the activity of ATP-binding cassette (ABC) transporters [259].

As an alternative approach to explore new treatment options, inhibiting pexophagy has also been considered. Initially it was believed that the accumulation of ubiquitylated PEX5 in the peroxisomal matrix signals pexophagy, as the use of autophagy inhibitors like hydroxychloroquine seemed to have the potential to restore the number of peroxisomes, as shown by Law, Bronte-Tinkew *et al.* in 2017 [252]. However, the lack of "multiple, complimentary functional assays" including biochemical assays, raises concerns about the sufficiency of evidence supporting this claim, as highlighted by Klouwer, Falkenberg

et al. in 2021 [217], based on which, autophagy inhibitors are not considered promising therapeutic compounds.

4.1.4 Developing therapies for PBDs using small-molecule compounds

The *PEX1-G843D* mutation partially impairs the function of PEX1 resulting in PBD of mild severity. Due to this reason, there is a potential for pharmacological interventions to increase the quality of life as well as the lifespan of the patients carrying this mutation. Studies have been made to identify compounds that can recover the peroxisomal import affected due to the improper functioning of PEX1-G843D. Compounds like betaine, diosmetin and arginine with chaperone activity have been found to enhance the folding of PEX1 as well as its localization in the peroxisomes, thereby partially restoring protein import and metabolic functions of peroxisomes [141,260].

Another high-throughput study identified S-nitrosoglutathione (GSNO), a nitrogen oxide donor, as a prospective treatment for this mild type of PBD. GSNO was shown to improve the number of peroxisomes as well as the function in PEX1-G843D mutant fibroblasts. Humanized Drosophila model carrying the PEX1-G843D mutation also displayed enhanced survival and longer lifespan when treated with GSNO [261].

Drug-protein interaction assays like MST are therefore valuable methods to find out the binding sites of pharmacological compounds with the related proteins. This will later help in determining the exact mechanism of action of the drugs. Tissue or organ-specific treatment strategies can further be optimized to treat different forms of peroxisomal disorders.

Overall, the development of targeted therapies for peroxisomal disorders holds promise for improving patient outcomes and quality of life. Ongoing research efforts continue to discover the underlying molecular mechanisms of these disorders and identify novel therapeutic targets and treatment strategies.

4.2 Correction of the PEX1-G843D mutation at the mRNA level

With the rise of site-directed RNA editing as a promising post-transcriptional modification tool, it offers the potential to induce significant changes in RNA function through A-to-I base substitutions. Consequently, it presents an extremely beneficial opportunity to correct inaccurate genetic data at the RNA level.

During this study, the utilization of the SNAP-ADAR system and the recruitment of the endogenous ADAR using RESTORE gRNAs were employed to reverse the PEX1-G843D mutation in mammalian cells. The outcomes observed from both methods look promising for the continued progress of this technology, paving the way for potential therapeutic approaches that could benefit individuals impacted by the mutation-induced disease.

4.2.1 The SNAP-ADAR editing system has a high correction efficiency

The SNAP-ADAR (SA) enzyme can be encoded into the genome and expressed in mammalian cells by transfecting plasmids. The gRNA modified with O^6-benzylguanine is then transfected into the cells to recruit the SA to the target site [200]. In this project, the SNAP-ADAR enzymes SA1 and SA2 along with their hyperactive variants, SA1Q and SA2Q, were expressed in the PEX1-G843D mutant cells aiming to correct the mutation. When transfected with the modified gRNA BB283 against this mutation in M2H cells, mRNA correction was seen with all SA enzymes where the hyperactive variants were more effective. Due to this correction, peroxisomal import was rescued as seen by fluorescence microscopy (Figure 31) implying the translation of the correctly folded PEX1 protein. The peroxisomal import was still functional after 7 days of BB-gRNA transfection in cells with the hyperactive SA variants (Figure 32).

A significant challenge in implementing RNA editing systems lies in preserving the integrity of the A-to-I RNA editome within the cell. Deviations in A-to-I editing have been linked to various human diseases, such as cancer, neurodegeneration, and autoimmunity [190,262]. An optimal RNA editing system therefore should not interfere with the functions of the endogenous ADARs while effectively catalyzing editing at the target sites. Apart from the dedicated target site, a lot of other sites also have been found to be edited while using the overexpressed deaminases especially when the hyperactive domains are employed [reviewed in 79]. This often happens when there is a high sequence similarity

to the target site. During this study, such off-target effects were rarely seen. In one of the experiments, a minor off-target edit of A-to-G was seen (PEX1-c.2331A>G). This was however attributed to a silence edit as the codon GGA was changed to GGG, both coding for the amino acid glycine. Apart from some inconsistencies in sequencing chromatograms, which might result from impure samples, no other off-target edits were seen. This however cannot rule out the possibility of other sites where unwanted edits have occurred as only a fraction of the nucleotide chains have been sequenced around the target site. Before using the modified gRNAs in clinical studies, a deep-RNA sequencing might be essential to check for such edits as suggested by Merkle *et al.,* 2019 [164].

4.2.2 RNA editing by endogenous ADARs via the RESTORE approach looks promising

The use of endogenous ADAR enzymes in editing the mRNA targets eliminates the need for artificial protein production in the cells. Introduction of target-specific antisense nucleotides (ASOs) into the cells is enough for this method of editing. This RESTORE method reduces the steps in the editing process and is more promising for developing therapies [164]. The ASOs (or gRNAs) used in this method include a 20-40 nt region that complements the target sequence and features a characteristic hairpin motif [197,263]. They are chemically modified to prevent ribonuclease degradation. These gRNAs are therefore stable in the cells several days after transfection and efforts are being made to increase the stability to several weeks. This will be an important milestone in the therapeutic process that reduces the frequency of "drug" delivery to the patients.

During this study, the ASOs with varying amounts of chemical modifications were used to correct the *PEX1-G843D* mutation. The correction efficiency of these ASOs ranged from 9% to almost 50%. In both types of cells used (M2H and HEK Flp-In), the highest correction efficiency was seen when transfected with the most chemically modified ASO (TMR205). Although these are only preliminary data, the results look assuring and further optimizations in the preparation of ASOs and the delivery process into the cells might help to develop this method. The goal here is not just to increase the correction of the mutation sites in the mRNA but to get the protein in its natural state. Therefore, the method should be developed to achieve longer and stable complementation of the peroxisomal import.

While RNA editing holds immense potential for therapeutic applications, achieving optimal editing rates remains a challenge. One hurdle lies in delivering the antisense oligonucleotides (ASOs) used for editing into the nucleus, where the process likely occurs before mRNA export to the cytoplasm. This additional barrier can significantly impact editing efficiency if the ASOs struggle to reach their target location. Interestingly, recent research suggests that increasing cellular stress might be a promising avenue for optimization. The use of interferon might as well increase the editing efficiency of the ASOs as demonstrated by Merkle *et al.* 2019 [164]. In another experiment by the Stafforst group, pre-transfecting wildtype cells with a mutated PEX1 gene followed by ASO delivery resulted in higher editing rates compared to direct ASO transfection in mutant cells (unpublished data). This two-step process, introducing stress through an additional transfection, seems to mimic the effect of interferon, known to enhance editing rates. This finding suggests that exploring the impact of controlled stress on editing efficiency could be a valuable optimization strategy.

4.2.3 Further optimizations can improve mRNA editing strategy

Next step in the project after having successfully shown that PEX1 mRNA is corrected and that import is functioning again, is to show that key biochemical features of the peroxisomes are restored as well. Biochemical assays, examining the degradation of long-chain fatty acids, should be conducted to show fully restored peroxisomes after ASO-treatment.

More research is needed to investigate the optimal level and type of stress for different editing targets and cell types. A controlled increase of the stress induced on the cells should be tested to examine whether the stress level the cells are in has an impact on the editing. Potentially a second transfection with our gRNAs 24 h before the ASO transfection might be a starting point to figure out the stress impact. Increasing stress by splitting the cells more often might also be a feasible approach. A second or even third transfection of the ASOs can be done to see the possible effects as they tend to degrade. Irrespective of the first transfection, these successive transfections can be done via lipofection to the already adhering cells without the need of detaching them.

Additionally, improving the nuclear delivery of ASOs, potentially through targeted modifications or carrier systems, remains crucial for maximizing editing yields. By

addressing these challenges, we can unlock the full potential of RNA editing for therapeutic interventions.

4.2.4 Choice of PEX1-G843D mutant cell lines

During this study, two types of cells with the PEX1-G843D mutation were used: (i) M2H, a patient fibroblast cell line additionally engineered to code for the PTS1-EGFP protein [141], and (ii) HEK293(T) PEX1-G843D, generated via CRISPR gene editing [217]. Both cell types contain one mutated and one null allele of the *PEX1* gene.

While both cell types offered insights, they also presented limitations. M2H cells showed occasional correction in negative controls, making quantitative analysis unreliable. Conversely, the presence of PTS1-EGFP facilitated rapid microscopic examination for evaluating the effects on peroxisomal export-import mechanisms. The disadvantage lies in the overexpression of the PTS1-EGFP compared to other PTS1-tagged proteins. Even if the import mechanism is fully restored, the probability of other peroxisomal matrix proteins, like catalase, being imported into the peroxisome decreases with the high amount of PTS1-EGFP competing for peroxisomal import. PTS1-EGFP also behaves differently in cells than regular peroxisomal proteins like thiolase as indicated by Klouwer *et al.* [217]. This shows that the M2H cell line in general and especially using the PTS1-EGFP for detection is a poor choice for showing repaired peroxisomal functions. Besides influencing the biochemical properties, the PTS1-EGFP has a negative impact on immunofluorescence microscopy. The overexpressed GFP superposes the signals from other proteins, hindering clean IF results. The use of HEK cells overcame this problem, but a 20 bp deletion near the mutation site led to overlapping PCR products during sequencing. Promising results were obtained using a new primer pair targeting the mutation site specifically, enhancing sequencing accuracy.

Another issue in handling the PEX1-G843D cells lies in their temperature sensitivity. It has been reported that the PEX1-G843D missense mutation causes misfolding of the protein but is stable at lower temperatures [138–140]. Therefore, the change in temperature during gRNA transfection could lead to artificially higher import rates not resulting from editing. Such effects were occasionally seen in the M2H cells where the EGFP protein is localized in the peroxisomes. Cells with high expression of EGFP also tend to die and detach from the surface faster. Although there is no presence of such highly

expressing proteins targeted to the peroxisomes in the HEK PEX1-G843D cells, care should be taken not to expose these cells longer at room temperature. Having said that, the temperature sensitivity had little to no effect on the mRNA levels and the correction efficiency obtained from the gRNA transfection should be reliable.

4.2.5 Development of RNA-based treatments

Oligonucleotide-directed RNA targeting methods appear to be emerging as a significant platform in drug discovery and are approaching their position alongside other major approaches. The development of RNA-based treatments continues in parallel with DNA-based therapies due to several key advantages. RNA-based approaches offer a unique opportunity to target diseases with the potential for rapid development and modification, making them particularly suitable for addressing emerging health challenges. Their precise targeting capabilities and transient effects enable personalized medical strategies while minimizing off-target effects and enhancing therapeutic efficacy. Therapeutic RNA degrades after a period of time, which may be beneficial in cases where long-term expression of a therapeutic gene may not be necessary or may be detrimental. Furthermore, the clinical effects can be lowered by adjusting the dosage and frequency of administered gRNAs [199].

RNA-based therapies are versatile in their mechanisms and can modulate gene expression in various ways, opening new avenues for therapeutic interventions and complementing existing treatment modalities to achieve better patient outcomes. Some RNA targeted therapies have already been approved that can be administered via subcutaneous, intravitreal, intravitreal and intrathecal routes [reviewed in 83] and the absorption rate is also rapid (within few hours) [265]. While progress has been made more gradually, advancements in medicinal chemistry have increased the effectiveness, minimized pro-inflammatory effects, and improved the pharmacokinetics of ASOs [266]. RNA base editing by harnessing the endogenous enzyme is simpler, precise, and reversible. Therefore, this technology may be used not just for rare genetic diseases but also for other common diseases.

Nearly all patients with a peroxisomal disorder, regardless of the degree of severity, exhibit visual impairment, often involving retinopathy. This underscores the crucial functions that peroxisomes have in vision, with a specific emphasis on maintaining the

integrity of the retina [267]. Injecting wildtype PEX1-encoding AAVs into the retina of the PEX1-G844D mouse model has been shown to improve ocular symptoms associated with peroxisomal dysfunction. This restoration of peroxisome function solely in retinal cells has potential as a therapy to alleviate visual symptoms in individuals with mild ZSD [268]. Owing to these results, similar therapies could be developed by delivering ASOs specific to the PEX1 mRNA. Targeting organs like eyes and liver could significantly improve the quality of life for the patients. The approval time for mRNA therapy might even be faster than for gene therapy. Historically, gene therapy has faced significant regulatory hurdles, leading to longer approval timelines while mRNA-based therapies have gained attention for their rapid development and potential for quick regulatory approval. Therefore, the continuation of the studies for the optimization and possible delivery systems of the ASOs seems very plausible.

5 References

1. Islinger M, Voelkl A, Fahimi HD, Schrader M. The peroxisome: an update on mysteries 2.0. *Histochem Cell Biol*. Published online September 15, 2018. doi:10.1007/s00418-018-1722-5

2. Rhodin JAG. *Correlation of Ultrastructural Organization: And Function in Normal and Experimentally Changed Proximal Convoluted Tubule Cells of the Mouse Kidney: An Electron Microscopic Study*. Dept. of Anatomy, Karolinska Institutet; 1954.

3. De Duve C, Baudhuin P. Peroxisomes (microbodies and related particles). *Physiol Rev*. 1966;46(2):323-357. doi:10.1152/physrev.1966.46.2.323

4. de Boer R, van der Klei IJ. Correlative Light- and Electron Microscopy in Peroxisome Research. *Methods Mol Biol Clifton NJ*. 2023;2643:93-104. doi:10.1007/978-1-0716-3048-8_7

5. Lazarow PB, Fujiki Y. Biogenesis of peroxisomes. *Annu Rev Cell Biol*. 1985;1:489-530. doi:10.1146/annurev.cb.01.110185.002421

6. Galiani S, Eggeling C, Reglinski K. Super-resolution microscopy and studies of peroxisomes. *Biol Chem*. 2023;404(2-3):87-106. doi:10.1515/hsz-2022-0314

7. de Lange EMF, Vlijm R. Super-Resolution Imaging of Peroxisomal Proteins Using STED Nanoscopy. In: Schrader M, ed. *Peroxisomes: Methods and Protocols*. Methods in Molecular Biology. Springer US; 2023:65-84. doi:10.1007/978-1-0716-3048-8_5

8. Gabaldón T. Peroxisome diversity and evolution. *Philos Trans R Soc B Biol Sci*. 2010;365(1541):765-773. doi:10.1098/rstb.2009.0240

9. Jansen RLM, Santana-Molina C, van den Noort M, Devos DP, van der Klei IJ. Comparative Genomics of Peroxisome Biogenesis Proteins: Making Sense of the PEX Proteins. *Front Cell Dev Biol*. 2021;9:1229. doi:10.3389/fcell.2021.654163

10. Nordgren M, Fransen M. Peroxisomal metabolism and oxidative stress. *Biochimie*. 2014;98:56-62. doi:10.1016/j.biochi.2013.07.026

11. Argyriou C, D'Agostino MD, Braverman N. Peroxisome biogenesis disorders. *Transl Sci Rare Dis*. 2016;1(2):111-144. doi:10.3233/TRD-160003

12. Yifrach E, Holbrook-Smith D, Bürgi J, et al. Systematic multi-level analysis of an organelle proteome reveals new peroxisomal functions. *Mol Syst Biol*. 2022;18(9):e11186. doi:10.15252/msb.202211186

13. Islinger M, Grille S, Fahimi HD, Schrader M. The peroxisome: an update on mysteries. *Histochem Cell Biol*. 2012;137(5):547-574. doi:10.1007/s00418-012-0941-4

14. Silva BSC, DiGiovanni L, Kumar R, Carmichael RE, Kim PK, Schrader M. Maintaining social contacts: The physiological relevance of organelle interactions. *Biochim*

Biophys Acta BBA - Mol Cell Res. 2020;1867(11):118800. doi:10.1016/j.bbamcr.2020.118800

15. Wanders RJA, Baes M, Ribeiro D, Ferdinandusse S, Waterham HR. The physiological functions of human peroxisomes. *Physiol Rev*. 2023;103(1):957-1024. doi:10.1152/physrev.00051.2021

16. Waterham HR, Ferdinandusse S, Wanders RJA. Human disorders of peroxisome metabolism and biogenesis. *Biochim Biophys Acta BBA - Mol Cell Res*. 2016;1863(5):922-933. doi:10.1016/j.bbamcr.2015.11.015

17. Poirier Y, Antonenkov VD, Glumoff T, Hiltunen JK. Peroxisomal β-oxidation—A metabolic pathway with multiple functions. *Biochim Biophys Acta BBA - Mol Cell Res*. 2006;1763(12):1413-1426. doi:10.1016/j.bbamcr.2006.08.034

18. Wanders RJA, Waterham HR. Biochemistry of mammalian peroxisomes revisited. *Annu Rev Biochem*. 2006;75:295-332. doi:10.1146/annurev.biochem.74.082803.133329

19. Wanders RJA. Metabolic functions of peroxisomes in health and disease. *Biochimie*. 2014;98:36-44. doi:10.1016/j.biochi.2013.08.022

20. Hu J, Baker A, Bartel B, et al. Plant Peroxisomes: Biogenesis and Function. *Plant Cell*. 2012;24(6):2279-2303. doi:10.1105/tpc.112.096586

21. Russell DW. The Enzymes, Regulation, and Genetics of Bile Acid Synthesis. *Annu Rev Biochem*. 2003;72(1):137-174. doi:10.1146/annurev.biochem.72.121801.161712

22. Ferdinandusse S, Denis S, Mooijer PAW, et al. Identification of the peroxisomal β-oxidation enzymes involved in the biosynthesis of docosahexaenoic acid. *J Lipid Res*. 2001;42(12):1987-1995. doi:10.1016/S0022-2275(20)31527-3

23. Nagan N, Zoeller RA. Plasmalogens: biosynthesis and functions. *Prog Lipid Res*. 2001;40(3):199-229. doi:10.1016/S0163-7827(01)00003-0

24. Buchert R, Tawamie H, Smith C, et al. A Peroxisomal Disorder of Severe Intellectual Disability, Epilepsy, and Cataracts Due to Fatty Acyl-CoA Reductase 1 Deficiency. *Am J Hum Genet*. 2014;95(5):602-610. doi:10.1016/j.ajhg.2014.10.003

25. Lismont C, Nordgren M, Van Veldhoven PP, Fransen M. Redox interplay between mitochondria and peroxisomes. *Front Cell Dev Biol*. 2015;3. Accessed February 23, 2024. https://www.frontiersin.org/articles/10.3389/fcell.2015.00035

26. Walker CL, Pomatto LCD, Tripathi DN, Davies KJA. Redox Regulation of Homeostasis and Proteostasis in Peroxisomes. *Physiol Rev*. 2018;98(1):89-115. doi:10.1152/physrev.00033.2016

27. Bonekamp NA, Völkl A, Fahimi HD, Schrader M. Reactive oxygen species and peroxisomes: Struggling for balance. *BioFactors*. 2009;35(4):346-355. doi:10.1002/biof.48

28. Salido E, Pey AL, Rodriguez R, Lorenzo V. Primary hyperoxalurias: Disorders of glyoxylate detoxification. *Biochim Biophys Acta BBA - Mol Basis Dis*. 2012;1822(9):1453-1464. doi:10.1016/j.bbadis.2012.03.004

29. Momoi K, Fukui K, Watanabe F, Miyake Y. Molecular cloning and sequence analysis of cDNA encoding human kidney D-amino acid oxidase. *FEBS Lett*. 1988;238(1):180-184. doi:10.1016/0014-5793(88)80252-7

30. Dodt G, Gould SJ. Multiple PEX genes are required for proper subcellular distribution and stability of Pex5p, the PTS1 receptor: evidence that PTS1 protein import is mediated by a cycling receptor. *J Cell Biol*. 1996;135(6):1763-1774. doi:10.1083/jcb.135.6.1763

31. Lazarow PB. Chapter 3.1.7. The import receptor Pex7p and the PTS2 targeting sequence. *Biochim Biophys Acta BBA - Mol Cell Res*. 2006;1763(12):1599-1604. doi:10.1016/j.bbamcr.2006.08.011

32. Marzioch M, Erdmann R, Veenhuis M, Kunau WH. PAS7 encodes a novel yeast member of the WD-40 protein family essential for import of 3-oxoacyl-CoA thiolase, a PTS2-containing protein, into peroxisomes. *EMBO J*. 1994;13(20):4908-4918. Accessed May 15, 2017. http://www.ncbi.nlm.nih.gov/pmc/articles/PMC395431/

33. Brocard C, Hartig A. Peroxisome targeting signal 1: is it really a simple tripeptide? *Biochim Biophys Acta*. 2006;1763(12):1565-1573. doi:10.1016/j.bbamcr.2006.08.022

34. Braverman N, Dodt G, Gould SJ, Valle D. An Isoform of Pex5p, the Human PTS1 Receptor, is Required for the Import of PTS2 Proteins Into Peroxisomes. *Hum Mol Genet*. 1998;7(8):1195-1205. doi:10.1093/hmg/7.8.1195

35. Emmanouilidis L, Gopalswamy M, Passon DM, Wilmanns M, Sattler M. Structural biology of the import pathways of peroxisomal matrix proteins. *Biochim Biophys Acta BBA - Mol Cell Res*. 2016;1863(5):804-813. doi:10.1016/j.bbamcr.2015.09.034

36. Kunze M. The type-2 peroxisomal targeting signal. *Biochim Biophys Acta BBA - Mol Cell Res*. 2020;1867(2):118609. doi:10.1016/j.bbamcr.2019.118609

37. Dodt G, Warren D, Becker E, Rehling P, Gould SJ. Domain Mapping of Human PEX5 Reveals Functional and Structural Similarities to Saccharomyces cerevisiae Pex18p and Pex21p. *J Biol Chem*. 2001;276(45):41769-41781. doi:10.1074/jbc.M106932200

38. Einwächter H, Sowinski S, Kunau WH, Schliebs W. Yarrowia lipolytica Pex20p, Saccharomyces cerevisiae Pex18p/Pex21p and mammalian Pex5pL fulfil a common function in the early steps of the peroxisomal PTS2 import pathway. *EMBO Rep*. 2001;2(11):1035-1039. doi:10.1093/embo-reports/kve228

39. Francisco T, Rodrigues TA, Dias AF, Barros-Barbosa A, Bicho D, Azevedo JE. Protein transport into peroxisomes: Knowns and unknowns. *BioEssays*. 2017;39(10):1700047. doi:10.1002/bies.201700047

40. Gatto GJ, Geisbrecht BV, Gould SJ, Berg JM. Peroxisomal targeting signal-1 recognition by the TPR domains of human PEX5. *Nat Struct Mol Biol*. 2000;7(12):1091-1095. doi:10.1038/81930

41. Skowyra ML, Feng P, Rapoport TA. Towards solving the mystery of peroxisomal matrix protein import. *Trends Cell Biol*. Published online September 22, 2023. doi:10.1016/j.tcb.2023.08.005

42. Freitas MO, Francisco T, Rodrigues TA, et al. PEX5 Protein Binds Monomeric Catalase Blocking Its Tetramerization and Releases It upon Binding the N-terminal Domain of PEX14. *J Biol Chem*. 2011;286(47):40509-40519. doi:10.1074/jbc.M111.287201

43. Klein ATJ, van den Berg M, Bottger G, Tabak HF, Distel B. *Saccharomyces cerevisiae* Acyl-CoA Oxidase Follows a Novel, Non-PTS1, Import Pathway into Peroxisomes That Is Dependent on Pex5p*. *J Biol Chem*. 2002;277(28):25011-25019. doi:10.1074/jbc.M203254200

44. Gunkel K, van Dijk R, Veenhuis M, van der Klei IJ. Routing of Hansenula polymorpha Alcohol Oxidase: An Alternative Peroxisomal Protein-sorting Machinery. *Mol Biol Cell*. 2004;15(3):1347-1355. doi:10.1091/mbc.e03-04-0258

45. Reguenga C, Oliveira MEM, Gouveia AMM, Sá-Miranda C, Azevedo JE. Characterization of the Mammalian Peroxisomal Import Machinery: Pex2p, Pex5p, Pex12p, AND Pex14p ARE SUBUNITS OF THE SAME PROTEIN ASSEMBLY *. *J Biol Chem*. 2001;276(32):29935-29942. doi:10.1074/jbc.M104114200

46. Agne B, Meindl NM, Niederhoff K, et al. Pex8p: An Intraperoxisomal Organizer of the Peroxisomal Import Machinery. *Mol Cell*. 2003;11(3):635-646. doi:10.1016/S1097-2765(03)00062-5

47. Fransen M, Terlecky SR, Subramani S. Identification of a human PTS1 receptor docking protein directly required for peroxisomal protein import. *Proc Natl Acad Sci*. 1998;95(14):8087-8092. doi:10.1073/pnas.95.14.8087

48. Bottger G, Barnett P, Klein ATJ, Kragt A, Tabak HF, Distel B. Saccharomyces cerevisiae PTS1 Receptor Pex5p Interacts with the SH3 Domain of the Peroxisomal Membrane Protein Pex13p in an Unconventional, Non-PXXP–related Manner. *Mol Biol Cell*. 2000;11(11):3963. Accessed February 5, 2018. /pmcc/articles/PMC15050/?report=abstract

49. Neuhaus A, Kooshapur H, Wolf J, et al. A Novel Pex14 Protein-interacting Site of Human Pex5 Is Critical for Matrix Protein Import into Peroxisomes. *J Biol Chem*. 2014;289(1):437-448. doi:10.1074/jbc.M113.499707

50. Oliveira ME, Gouveia AM, Pinto RA, Sá-Miranda C, Azevedo JE. The Energetics of Pex5p-mediated Peroxisomal Protein Import *. *J Biol Chem*. 2003;278(41):39483-39488. doi:10.1074/jbc.M305089200

51. Francisco T, Rodrigues TA, Freitas MO, et al. A Cargo-centered Perspective on the PEX5 Receptor-mediated Peroxisomal Protein Import Pathway*. *J Biol Chem*. 2013;288(40):29151-29159. doi:10.1074/jbc.M113.487140

52. Gouveia AM, Guimaraes CP, Oliveira ME, Reguenga C, Sa-Miranda C, Azevedo JE. Characterization of the peroxisomal cycling receptor, Pex5p, using a cell-free in vitro import system. *J Biol Chem*. 2003;278(1):226-232. doi:10.1074/jbc.M209498200

53. Gao Y, Skowyra ML, Feng P, Rapoport TA. Protein import into peroxisomes occurs through a nuclear pore–like phase. *Science*. 2022;378(6625):eadf3971. doi:10.1126/science.adf3971

54. Ravindran R, Bacellar IOL, Castellanos-Girouard X, et al. Peroxisome biogenesis initiated by protein phase separation. *Nature*. 2023;617(7961):608-615. doi:10.1038/s41586-023-06044-1

55. Saidowsky J, Dodt G, Kirchberg K, et al. The di-aromatic pentapeptide repeats of the human peroxisome import receptor PEX5 are separate high affinity binding sites for the peroxisomal membrane protein PEX14. *J Biol Chem*. 2001;276(37):34524-34529. doi:10.1074/jbc.M104647200

56. Neufeld C, Filipp FV, Simon B, et al. Structural basis for competitive interactions of Pex14 with the import receptors Pex5 and Pex19. *EMBO J*. 2009;28(6):745-754. doi:10.1038/emboj.2009.7

57. Gopalswamy M, Zheng C, Gaussmann S, et al. Distinct conformational and energetic features define the specific recognition of (di)aromatic peptide motifs by PEX14. *Biol Chem*. 2023;404(2-3):179-194. doi:10.1515/hsz-2022-0177

58. Nair DM, Purdue PE, Lazarow PB. Pex7p translocates in and out of peroxisomes in Saccharomyces cerevisiae. *J Cell Biol*. 2004;167(4):599-604. doi:10.1083/jcb.200407119

59. Mukai S, Ghaedi K, Fujiki Y. Intracellular Localization, Function, and Dysfunction of the Peroxisome-targeting Signal Type 2 Receptor, Pex7p, in Mammalian Cells*. *J Biol Chem*. 2002;277(11):9548-9561. doi:10.1074/jbc.M108635200

60. Rodrigues TA, Alencastre IS, Francisco T, et al. A PEX7-Centered Perspective on the Peroxisomal Targeting Signal Type 2-Mediated Protein Import Pathway. *Mol Cell Biol*. 2014;34(15):2917-2928. doi:10.1128/MCB.01727-13

61. Gould SJ, Kalish JE, Morrell JC, Bjorkman J, Urquhart AJ, Crane DI. Pex13p is an SH3 protein of the peroxisome membrane and a docking factor for the predominantly cytoplasmic PTs1 receptor. *J Cell Biol*. 1996;135(1):85-95. doi:10.1083/jcb.135.1.85

62. Elgersma Y, Kwast L, Klein A, et al. The SH3 domain of the Saccharomyces cerevisiae peroxisomal membrane protein Pex13p functions as a docking site for Pex5p, a mobile receptor for the import PTS1-containing proteins. *J Cell Biol*. 1996;135(1):97-109. doi:10.1083/jcb.135.1.97

63. Toyama R, Mukai S, Itagaki A, et al. Isolation, Characterization and Mutation Analysis of PEX13-Defective Chinese Hamster Ovary Cell Mutants. *Hum Mol Genet*. 1999;8(9):1673-1681. doi:10.1093/hmg/8.9.1673

64. Barros-Barbosa A, Ferreira MJ, Rodrigues TA, et al. Membrane topologies of PEX13 and PEX14 provide new insights on the mechanism of protein import into peroxisomes. *FEBS J*. 2018;0(0). doi:10.1111/febs.14697

65. Erdmann R, Schliebs W. Peroxisomal matrix protein import: the transient pore model. *Nat Rev Mol Cell Biol*. 2005;6(9):738-742. doi:10.1038/nrm1710

66. Meinecke M, Bartsch P, Wagner R. Peroxisomal protein import pores. *Biochim Biophys Acta BBA - Mol Cell Res*. 2016;1863(5):821-827. doi:10.1016/j.bbamcr.2015.10.013

67. Alencastre IS, Rodrigues TA, Grou CP, Fransen M, Sá-Miranda C, Azevedo JE. Mapping the Cargo Protein Membrane Translocation Step into the PEX5 Cycling Pathway. *J Biol Chem*. 2009;284(40):27243-27251. doi:10.1074/jbc.M109.032565

68. Williams C, van den Berg M, Sprenger RR, Distel B. A conserved cysteine is essential for Pex4p-dependent ubiquitination of the peroxisomal import receptor Pex5p. *J Biol Chem*. 2007;282(31):22534-22543. doi:10.1074/jbc.M702038200

69. Carvalho AF, Pinto MP, Grou CP, et al. Ubiquitination of Mammalian Pex5p, the Peroxisomal Import Receptor. *J Biol Chem*. 2007;282(43):31267-31272. doi:10.1074/jbc.M706325200

70. Miyata N, Fujiki Y. Shuttling Mechanism of Peroxisome Targeting Signal Type 1 Receptor Pex5: ATP-Independent Import and ATP-Dependent Export. *Mol Cell Biol*. 2005;25(24):10822-10832. doi:10.1128/MCB.25.24.10822-10832.2005

71. Platta HW, Grunau S, Rosenkranz K, Girzalsky W, Erdmann R. Functional role of the AAA peroxins in dislocation of the cycling PTS1 receptor back to the cytosol. *Nat Cell Biol*. 2005;7(8):817-822. doi:10.1038/ncb1281

72. Grou CP, Carvalho AF, Pinto MP, et al. Members of the E2D (UbcH5) Family Mediate the Ubiquitination of the Conserved Cysteine of Pex5p, the Peroxisomal Import Receptor. *J Biol Chem*. 2008;283(21):14190-14197. doi:10.1074/jbc.M800402200

73. Koller A, Snyder WB, Faber KN, et al. Pex22p of Pichia pastoris, Essential for Peroxisomal Matrix Protein Import, Anchors the Ubiquitin-Conjugating Enzyme, Pex4p, on the Peroxisomal Membrane. *J Cell Biol*. 1999;146(1):99-112. doi:10.1083/jcb.146.1.99

74. Traver MS, Bradford SE, Olmos JLJ, et al. The Structure of the Arabidopsis PEX4-PEX22 Peroxin Complex—Insights Into Ubiquitination at the Peroxisomal Membrane. *Front Cell Dev Biol*. 2022;10. doi:10.3389/fcell.2022.838923

75. Miyata N, Okumoto K, Mukai S, Noguchi M, Fujiki Y. AWP1/ZFAND6 Functions in Pex5 Export by Interacting with Cys-Monoubiquitinated Pex5 and Pex6 AAA ATPase. *Traffic*. 2012;13(1):168-183. doi:10.1111/j.1600-0854.2011.01298.x

76. Grou CP, Francisco T, Rodrigues TA, et al. Identification of Ubiquitin-specific Protease 9X (USP9X) as a Deubiquitinase Acting on Ubiquitin-Peroxin 5 (PEX5) Thioester Conjugate *. *J Biol Chem*. 2012;287(16):12815-12827. doi:10.1074/jbc.M112.340158

77. Debelyy MO, Platta HW, Saffian D, et al. Ubp15p, a Ubiquitin Hydrolase Associated with the Peroxisomal Export Machinery *. *J Biol Chem*. 2011;286(32):28223-28234. doi:10.1074/jbc.M111.238600

78. Fransen M, Nordgren M, Wang B, Apanasets O, Van Veldhoven PP. Aging, Age-Related Diseases and Peroxisomes. In: del Río LA, ed. *Peroxisomes and Their Key Role in Cellular Signaling and Metabolism*. Subcellular Biochemistry. Springer Netherlands; 2013:45-65. doi:10.1007/978-94-007-6889-5_3

79. Di Cara F, Andreoletti P, Trompier D, et al. Peroxisomes in Immune Response and Inflammation. *Int J Mol Sci*. 2019;20(16):3877. doi:10.3390/ijms20163877

80. Kunze M, Berger J. Single Peroxisomal Enzyme and Transporter Deficiencies in Human Diseases and Mouse Models. In: Brocard C, Hartig A, eds. *Molecular Machines Involved in Peroxisome Biogenesis and Maintenance*. Springer; 2014:153-184. doi:10.1007/978-3-7091-1788-0_8

81. Wanders RJA, Waterham HR. Peroxisomal disorders: The single peroxisomal enzyme deficiencies. *Biochim Biophys Acta BBA - Mol Cell Res*. 2006;1763(12):1707-1720. doi:10.1016/j.bbamcr.2006.08.010

82. Chang CC, South S, Warren D, et al. Metabolic control of peroxisome abundance. *J Cell Sci*. 1999;112(10):1579-1590. doi:10.1242/jcs.112.10.1579

83. Kemp S, Berger J, Aubourg P. X-linked adrenoleukodystrophy: Clinical, metabolic, genetic and pathophysiological aspects. *Biochim Biophys Acta BBA - Mol Basis Dis*. 2012;1822(9):1465-1474. doi:10.1016/j.bbadis.2012.03.012

84. Wanders RJA, Visser WF, van Roermund CWT, Kemp S, Waterham HR. The peroxisomal ABC transporter family. *Pflüg Arch - Eur J Physiol*. 2007;453(5):719-734. doi:10.1007/s00424-006-0142-x

85. Morita M, Shimozawa N, Kashiwayama Y, Suzuki Y, Imanaka T. ABC Subfamily D Proteins and Very Long Chain Fatty Acid Metabolism as Novel Targets in Adrenoleukodystrophy. *Curr Drug Targets*. 12(5):694-706. Accessed March 12, 2024. https://www.eurekaselect.com/article/18635

86. Miller WP, Rothman SM, Nascene D, et al. Outcomes after allogeneic hematopoietic cell transplantation for childhood cerebral adrenoleukodystrophy: the largest single-institution cohort report. *Blood*. 2011;118(7):1971-1978. doi:10.1182/blood-2011-01-329235

87. Ferdinandusse S, Denis S, Hogenhout EM, et al. Clinical, biochemical, and mutational spectrum of peroxisomal acyl–coenzyme A oxidase deficiency. *Hum Mutat*. 2007;28(9):904-912. doi:10.1002/humu.20535

88. J.A.Wanders R, W.Denis S, Dacremont G. Studies on the Substrate Specificity of the Inducible and Non-Inducible Acyl-CoA Oxidases from Rat Kidney Perxiosomes1. *J Biochem (Tokyo)*. 1993;113(5):577-582. doi:10.1093/oxfordjournals.jbchem.a124086

89. Ebberink MS, Mooijer PAW, Gootjes J, Koster J, Wanders RJA, Waterham HR. Genetic classification and mutational spectrum of more than 600 patients with a Zellweger syndrome spectrum disorder. *Hum Mutat*. 2011;32(1):59-69. doi:10.1002/humu.21388

90. Matsumoto N, Tamura S, Fujiki Y. The pathogenic peroxin Pex26p recruits the Pex1p–Pex6p AAA ATPase complexes to peroxisomes. *Nat Cell Biol*. 2003;5(5):454-460. doi:10.1038/ncb982

91. Fujiki Y, Okumoto K. Peroxisome biogenesis in mammalian cells. *Front Physiol*. 2014;5. doi:10.3389/fphys.2014.00307

92. Braverman N, Steel G, Obie C, et al. Human PEX7 encodes the peroxisomal PTS2 receptor and is responsible for rhizomelic chondrodysplasia punctata. *Nat Genet*. 1997;15(4):369-376. doi:10.1038/ng0497-369

93. Fujiki Y, Okumoto K, Honsho M, Abe Y. Molecular insights into peroxisome homeostasis and peroxisome biogenesis disorders. *Biochim Biophys Acta BBA - Mol Cell Res*. 2022;1869(11):119330. doi:10.1016/j.bbamcr.2022.119330

94. Goldfischer S, Moore CL, Johnson AB, et al. Peroxisomal and Mitochondrial Defects in the Cerebro-Hepato-Renal Syndrome. *Science*. 1973;182(4107):62-64. doi:10.1126/science.182.4107.62

95. Ratbi I, Falkenberg KD, Sommen M, et al. Heimler Syndrome Is Caused by Hypomorphic Mutations in the Peroxisome-Biogenesis Genes *PEX1* and *PEX6*. *Am J Hum Genet*. 2015;97(4):535-545. doi:10.1016/j.ajhg.2015.08.011

96. Weller S, Gould SJ, Valle D. Peroxisome Biogenesis Disorders. *Annu Rev Genomics Hum Genet*. 2003;4(1):165-211. doi:10.1146/annurev.genom.4.070802.110424

97. Santos MJ, Imanaka T, Shio H, Lazarow PB. Peroxisomal integral membrane proteins in control and Zellweger fibroblasts. *J Biol Chem*. 1988;263(21):10502-10509. doi:10.1016/S0021-9258(19)81544-2

98. Berendse K, Engelen M, Ferdinandusse S, et al. Zellweger spectrum disorders: clinical manifestations in patients surviving into adulthood. *J Inherit Metab Dis*. 2016;39(1):93-106. doi:10.1007/s10545-015-9880-2

99. Barøy T, Koster J, Strømme P, et al. A novel type of rhizomelic chondrodysplasia punctata, RCDP5, is caused by loss of the PEX5 long isoform. *Hum Mol Genet*. 2015;24(20):5845-5854. doi:10.1093/hmg/ddv305

100. Spranger JW, Opitz JM, Bidder U. Heterogeneity of Chondrodysplasia punctata. *Humangenetik*. 1971;11(3):190-212. doi:10.1007/BF00274739

101. Gilbert EF, Opitz JM, Spranger JW, Langer LO, Wolfson JJ, Viseskul C. Chondrodysplasia punctata — Rhizomelic form. *Eur J Pediatr*. 1976;123(2):89-109. doi:10.1007/BF00442639

102. Briggs JN, Emery JL, Illingworth RS. Congenital Stippled Epiphyses. *Arch Dis Child*. 1953;28(139):209-212. doi:10.1136/adc.28.139.209

103. White AL, Modaff P, Holland-Morris F, Pauli RM. Natural history of rhizomelic chondrodysplasia punctata. *Am J Med Genet A*. 2003;118A(4):332-342. doi:10.1002/ajmg.a.20009

104. Waterham HR, Koster J, van Roermund CWT, Mooyer PAW, Wanders RJA, Leonard JV. A Lethal Defect of Mitochondrial and Peroxisomal Fission. *N Engl J Med*. 2007;356(17):1736-1741. doi:10.1056/NEJMoa064436

105. Shamseldin HE, Alshammari M, Al-Sheddi T, et al. Genomic analysis of mitochondrial diseases in a consanguineous population reveals novel candidate disease genes. *J Med Genet*. 2012;49(4):234-241. doi:10.1136/jmedgenet-2012-100836

106. Huber N, Guimaraes S, Schrader M, Suter U, Niemann A. Charcot-Marie-Tooth disease-associated mutants of GDAP1 dissociate its roles in peroxisomal and mitochondrial fission. *EMBO Rep*. 2013;14(6):545-552. doi:10.1038/embor.2013.56

107. Ebberink MS, Koster J, Visser G, et al. A novel defect of peroxisome division due to a homozygous non-sense mutation in the PEX11β gene. *J Med Genet*. 2012;49(5):307-313. doi:10.1136/jmedgenet-2012-100778

108. Ogura T, Wilkinson AJ. AAA+ superfamily ATPases: common structure–diverse function. *Genes Cells*. 2001;6(7):575-597. doi:10.1046/j.1365-2443.2001.00447.x

109. Sysoeva TA. Assessing heterogeneity in oligomeric AAA+ machines. *Cell Mol Life Sci*. 2017;74(6):1001-1018. doi:10.1007/s00018-016-2374-z

110. Saffert P, Enenkel C, Wendler P. Structure and Function of p97 and Pex1/6 Type II AAA+ Complexes. *Front Mol Biosci*. 2017;4. doi:10.3389/fmolb.2017.00033

111. Sakata E, Eisele MR, Baumeister W. Molecular and cellular dynamics of the 26S proteasome. *Biochim Biophys Acta BBA - Proteins Proteomics*. 2021;1869(3):140583. doi:10.1016/j.bbapap.2020.140583

112. Eustermann S, Schall K, Kostrewa D, et al. Structural basis for ATP-dependent chromatin remodelling by the INO80 complex. *Nature*. 2018;556(7701):386-390. doi:10.1038/s41586-018-0029-y

113. Ryu JK, Jahn R, Yoon TY. Review: Progresses in understanding N-ethylmaleimide sensitive factor (NSF) mediated disassembly of SNARE complexes. *Biopolymers*. 2016;105(8):518-531. doi:10.1002/bip.22854

114. White SR, Lauring B. AAA+ ATPases: Achieving Diversity of Function with Conserved Machinery. *Traffic*. 2007;8(12):1657-1667. doi:10.1111/j.1600-0854.2007.00642.x

115. Miller JM, Enemark EJ. Fundamental Characteristics of AAA+ Protein Family Structure and Function. *Archaea Vanc BC*. 2016;2016:9294307. doi:10.1155/2016/9294307

116. Wendler P, Ciniawsky S, Kock M, Kube S. Structure and function of the AAA+ nucleotide binding pocket. *Biochim Biophys Acta BBA - Mol Cell Res*. 2012;1823(1):2-14. doi:10.1016/j.bbamcr.2011.06.014

117. Prattes M, Grishkovskaya I, Hodirnau VV, et al. Structural basis for inhibition of the AAA-ATPase Drg1 by diazaborine. *Nat Commun*. 2021;12(1):3483. doi:10.1038/s41467-021-23854-x

118. Dougan DA, Mogk A, Zeth K, Turgay K, Bukau B. AAA+ proteins and substrate recognition, it all depends on their partner in crime. *FEBS Lett*. 2002;529(1):6-10. doi:10.1016/S0014-5793(02)03179-4

119. Matsumoto N, Tamura S, Furuki S, et al. Mutations in Novel Peroxin Gene PEX26 That Cause Peroxisome-Biogenesis Disorders of Complementation Group 8 Provide a Genotype-Phenotype Correlation. *Am J Hum Genet*. 2003;73(2):233-246. doi:10.1086/377004

120. Blok NB, Tan D, Wang RYR, et al. Unique double-ring structure of the peroxisomal Pex1/Pex6 ATPase complex revealed by cryo-electron microscopy. *Proc Natl Acad Sci*. 2015;112(30):E4017-E4025. doi:10.1073/pnas.1500257112

121. Reuber BE, Germain-Lee E, Collins CS, et al. Mutations in PEX1 are the most common cause of peroxisome biogenesis disorders. *Nat Genet*. 1997;17(4):445-448. doi:10.1038/ng1297-445

122. Geisbrecht BV, Collins CS, Reuber BE, Gould SJ. Disruption of a PEX1–PEX6 interaction is the most common cause of the neurologic disorders Zellweger syndrome, neonatal adrenoleukodystrophy, and infantile Refsum disease. *Proc Natl Acad Sci*. 1998;95(15):8630-8635. doi:10.1073/pnas.95.15.8630

123. Judy RM, Sheedy CJ, Gardner BM. Insights into the Structure and Function of the Pex1/Pex6 AAA-ATPase in Peroxisome Homeostasis. *Cells*. 2022;11(13):2067. doi:10.3390/cells11132067

124. Zhao C, Slevin JT, Whiteheart SW. Cellular functions of NSF: Not just SNAPs and SNAREs. *FEBS Lett*. 2007;581(11):2140-2149. doi:10.1016/j.febslet.2007.03.032

125. Latterich M, Fröhlich KU, Schekman R. Membrane fusion and the cell cycle: Cdc48p participates in the fusion of ER membranes. *Cell*. 1995;82(6):885-893. doi:10.1016/0092-8674(95)90268-6

126. Meyer H, Bug M, Bremer S. Emerging functions of the VCP/p97 AAA-ATPase in the ubiquitin system. *Nat Cell Biol*. 2012;14(2):117-123. doi:10.1038/ncb2407

127. Latterich M, Patel S. The AAA team: related ATPases with diverse functions. *Trends Cell Biol*. 1998;8(2):65-71. doi:10.1016/S0962-8924(98)80014-7

128. Neuwald AF, Aravind L, Spouge JL, Koonin EV. AAA+: A Class of Chaperone-Like ATPases Associated with the Assembly, Operation, and Disassembly of Protein Complexes. *Genome Res*. 1999;9(1):27-43. doi:10.1101/gr.9.1.27

129. Portsteffen H, Beyer A, Becker E, et al. Human PEX1 is mutated in complementation group 1 of the peroxisome biogenesis disorders. *Nat Genet*. 1997;17(4):449-452. doi:10.1038/ng1297-449

130. Ciniawsky S, Grimm I, Saffian D, Girzalsky W, Erdmann R, Wendler P. Molecular snapshots of the Pex1/6 AAA+ complex in action. *Nat Commun*. 2015;6. doi:10.1038/ncomms8331

131. Gardner BM, Chowdhury S, Lander GC, Martin A. The Pex1/Pex6 Complex Is a Heterohexameric AAA + Motor with Alternating and Highly Coordinated Subunits. *J Mol Biol*. 2015;427(6, Part B):1375-1388. doi:10.1016/j.jmb.2015.01.019

132. Tamura S, Shimozawa N, Suzuki Y, Tsukamoto T, Osumi T, Fujiki Y. A Cytoplasmic AAA Family Peroxin, Pex1p, Interacts with Pex6p. *Biochem Biophys Res Commun*. 1998;245(3):883-886. doi:10.1006/bbrc.1998.8522

133. Hänzelmann P, Schindelin H. Structural Basis of ATP Hydrolysis and Intersubunit Signaling in the AAA+ ATPase p97. *Structure*. 2016;24(1):127-139. doi:10.1016/j.str.2015.10.026

134. Pedrosa AG, Francisco T, Ferreira MJ, Rodrigues TA, Barros-Barbosa A, Azevedo JE. A Mechanistic Perspective on PEX1 and PEX6, Two AAA+ Proteins of the Peroxisomal Protein Import Machinery. *Int J Mol Sci*. 2019;20(21):5246. doi:10.3390/ijms20215246

135. Rüttermann M, Koci M, Lill P, et al. Structure of the peroxisomal Pex1/Pex6 ATPase complex bound to a substrate. *Nat Commun*. 2023;14(1):5942. doi:10.1038/s41467-023-41640-9

136. Ali BA, Judy RM, Chowdhury S, et al. The N1 domain of the peroxisomal AAA-ATPase Pex6 is required for Pex15 binding and proper assembly with Pex1. *J Biol Chem*. 2024;300(1):105504. doi:10.1016/j.jbc.2023.105504

137. Gardner BM, Castanzo DT, Chowdhury S, et al. The peroxisomal AAA-ATPase Pex1/Pex6 unfolds substrates by processive threading. *Nat Commun*. 2018;9(1):135. doi:10.1038/s41467-017-02474-4

138. Imamura A, Tamura S, Shimozawa N, et al. Temperature-Sensitive Mutation in PEX1 Moderates the Phenotypes of Peroxisome Deficiency Disorders. *Hum Mol Genet*. 1998;7(13):2089-2094. doi:10.1093/hmg/7.13.2089

139. Maxwell MA, Allen T, Solly PB, Svingen T, Paton BC, Crane DI. Novel PEX1 mutations and genotype–phenotype correlations in Australasian peroxisome

biogenesis disorder patients. *Hum Mutat*. 2002;20(5):342-351. doi:10.1002/humu.10128

140. Walter C, Gootjes J, Mooijer PA, et al. Disorders of Peroxisome Biogenesis Due to Mutations in PEX1: Phenotypes and PEX1 Protein Levels. *Am J Hum Genet*. 2001;69(1):35-48. doi:10.1086/321265

141. Zhang R, Chen L, Jiralerspong S, Snowden A, Steinberg S, Braverman N. Recovery of PEX1-Gly843Asp peroxisome dysfunction by small-molecule compounds. *Proc Natl Acad Sci*. 2010;107(12):5569-5574. doi:10.1073/pnas.0914960107

142. Argyriou C, Polosa A, Cecyre B, et al. A longitudinal study of retinopathy in the PEX1-Gly844Asp mouse model for mild Zellweger Spectrum Disorder. *Exp Eye Res*. 2019;186:107713. doi:10.1016/j.exer.2019.107713

143. Twomey EC, Ji Z, Wales TE, et al. Substrate processing by the Cdc48 ATPase complex is initiated by ubiquitin unfolding. *Science*. 2019;365(6452):eaax1033. doi:10.1126/science.aax1033

144. Nashiro C, Kashiwagi A, Matsuzaki T, Tamura S, Fujiki Y. Recruiting Mechanism of the AAA Peroxins, Pex1p and Pex6p, to Pex26p on the Peroxisomal Membrane. *Traffic*. 2011;12(6):774-788. doi:10.1111/j.1600-0854.2011.01182.x

145. Pan M, Yu Y, Ai H, et al. Mechanistic insight into substrate processing and allosteric inhibition of human p97. *Nat Struct Mol Biol*. 2021;28(7):614-625. doi:10.1038/s41594-021-00617-2

146. Hamdane D, Velours C, Cornu D, Nicaise M, Lombard M, Fontecave M. A chemical chaperone induces inhomogeneous conformational changes in flexible proteins. *Phys Chem Chem Phys*. 2016;18(30):20410-20421. doi:10.1039/C6CP03635J

147. Shin MH, Lim HS. Screening methods for identifying pharmacological chaperones. *Mol Biosyst*. 2017;13(4):638-647. doi:10.1039/C6MB00866F

148. MacLean GE, Argyriou C, Pietro ED, et al. Zellweger spectrum disorder patient–derived fibroblasts with the PEX1-Gly843Asp allele recover peroxisome functions in response to flavonoids. *J Cell Biochem*. 2018;0(0). doi:10.1002/jcb.27591

149. Varadi M, Anyango S, Deshpande M, et al. AlphaFold Protein Structure Database: massively expanding the structural coverage of protein-sequence space with high-accuracy models. *Nucleic Acids Res*. 2022;50(D1):D439-D444. doi:10.1093/nar/gkab1061

150. Jumper J, Evans R, Pritzel A, et al. Highly accurate protein structure prediction with AlphaFold. *Nature*. 2021;596(7873):583-589. doi:10.1038/s41586-021-03819-2

151. Dephoure N, Zhou C, Villén J, et al. A quantitative atlas of mitotic phosphorylation. *Proc Natl Acad Sci*. 2008;105(31):10762-10767. doi:10.1073/pnas.0805139105

152. Dinkel H, Chica C, Via A, et al. Phospho.ELM: a database of phosphorylation sites—update 2011. *Nucleic Acids Res*. 2011;39(suppl_1):D261-D267. doi:10.1093/nar/gkq1104

153. Landrum MJ, Lee JM, Benson M, et al. ClinVar: public archive of interpretations of clinically relevant variants. *Nucleic Acids Res*. 2016;44(D1):D862-D868. doi:10.1093/nar/gkv1222

154. Ginn SL, Alexander IE, Edelstein ML, Abedi MR, Wixon J. Gene therapy clinical trials worldwide to 2012 – an update. *J Gene Med*. 2013;15(2):65-77. doi:10.1002/jgm.2698

155. Van Alstyne M, Tattoli I, Delestrée N, et al. Gain of toxic function by long-term AAV9-mediated SMN overexpression in the sensorimotor circuit. *Nat Neurosci*. 2021;24(7):930-940. doi:10.1038/s41593-021-00827-3

156. Komor AC, Kim YB, Packer MS, Zuris JA, Liu DR. Programmable editing of a target base in genomic DNA without double-stranded DNA cleavage. *Nature*. 2016;533(7603):420-424. doi:10.1038/nature17946

157. Gaudelli NM, Komor AC, Rees HA, et al. Programmable base editing of A•T to G•C in genomic DNA without DNA cleavage. *Nature*. 2017;551(7681):464-471. doi:10.1038/nature24644

158. Doudna JA. The promise and challenge of therapeutic genome editing. *Nature*. 2020;578(7794):229-236. doi:10.1038/s41586-020-1978-5

159. Cox DBT, Platt RJ, Zhang F. Therapeutic genome editing: prospects and challenges. *Nat Med*. 2015;21(2):121-131. doi:10.1038/nm.3793

160. Ran FA, Hsu PD, Wright J, Agarwala V, Scott DA, Zhang F. Genome engineering using the CRISPR-Cas9 system. *Nat Protoc*. 2013;8(11):2281-2308. doi:10.1038/nprot.2013.143

161. Vogel P, Stafforst T. Critical review on engineering deaminases for site-directed RNA editing. *Curr Opin Biotechnol*. 2019;55:74-80. doi:10.1016/j.copbio.2018.08.006

162. Fry LE, Peddle CF, Barnard AR, McClements ME, MacLaren RE. RNA Editing as a Therapeutic Approach for Retinal Gene Therapy Requiring Long Coding Sequences. *Int J Mol Sci*. 2020;21(3):777. doi:10.3390/ijms21030777

163. Vogel P, Moschref M, Li Q, et al. Efficient and precise editing of endogenous transcripts with SNAP-tagged ADARs. *Nat Methods*. 2018;15(7):535-538. doi:10.1038/s41592-018-0017-z

164. Merkle T, Merz S, Reautschnig P, et al. Precise RNA editing by recruiting endogenous ADARs with antisense oligonucleotides. *Nat Biotechnol*. 2019;37(2):133-138. doi:10.1038/s41587-019-0013-6

165. Gulei D, Raduly L, Berindan-Neagoe I, Calin GA. CRISPR-based RNA editing: diagnostic applications and therapeutic options. *Expert Rev Mol Diagn*. 2019;19(2):83-88. doi:10.1080/14737159.2019.1568242

166. Song J, Zhuang Y, Yi C. Programmable RNA base editing via targeted modifications. *Nat Chem Biol*. 2024;20(3):277-290. doi:10.1038/s41589-023-01531-y

167. Booth BJ, Nourreddine S, Katrekar D, et al. RNA editing: Expanding the potential of RNA therapeutics. *Mol Ther*. 2023;31(6):1533-1549. doi:10.1016/j.ymthe.2023.01.005

168. Zinshteyn B, Nishikura K. Adenosine-to-inosine RNA editing. *WIREs Syst Biol Med*. 2009;1(2):202-209. doi:10.1002/wsbm.10

169. Smith HC, Bennett RP, Kizilyer A, McDougall WM, Prohaska KM. Functions and regulation of the APOBEC family of proteins. *Semin Cell Dev Biol*. 2012;23(3):258-268. doi:10.1016/j.semcdb.2011.10.004

170. Huang X, Lv J, Li Y, et al. Programmable C-to-U RNA editing using the human APOBEC3A deaminase. *EMBO J*. 2020;39(22):e104741. doi:10.15252/embj.2020104741

171. Auxilien S, Crain PF, Trewyn RW, Grosjean H. Mechanism, Specificity and General Properties of the Yeast Enzyme Catalysing the Formation of Inosine 34 in the Anticodon of Transfer RNA. *J Mol Biol*. 1996;262(4):437-458. doi:10.1006/jmbi.1996.0527

172. Nishikura K. A-to-I editing of coding and non-coding RNAs by ADARs. *Nat Rev Mol Cell Biol*. 2016;17(2):83-96. doi:10.1038/nrm.2015.4

173. Bass BL, Weintraub H. A developmentally regulated activity that unwinds RNA duplexes. *Cell*. 1987;48(4):607-613. doi:10.1016/0092-8674(87)90239-X

174. Rebagliati MR, Melton DA. Antisense RNA injections in fertilized frog eggs reveal an RNA duplex unwinding activity. *Cell*. 1987;48(4):599-605. doi:10.1016/0092-8674(87)90238-8

175. Wagner RW, Smith JE, Cooperman BS, Nishikura K. A double-stranded RNA unwinding activity introduces structural alterations by means of adenosine to inosine conversions in mammalian cells and Xenopus eggs. *Proc Natl Acad Sci*. 1989;86(8):2647-2651. doi:10.1073/pnas.86.8.2647

176. Kim U, Garner TL, Sanford T, Speicher D, Murray JM, Nishikura K. Purification and characterization of double-stranded RNA adenosine deaminase from bovine nuclear extracts. *J Biol Chem*. 1994;269(18):13480-13489. doi:10.1016/S0021-9258(17)36857-6

177. O'Connell MA, Keller W. Purification and properties of double-stranded RNA-specific adenosine deaminase from calf thymus. *Proc Natl Acad Sci*. 1994;91(22):10596-10600. doi:10.1073/pnas.91.22.10596

178. Gerber A, O'Connell MA, Keller W. Two forms of human double-stranded RNA-specific editase 1 (hRED1) generated by the insertion of an Alu cassette. *RNA N Y N*. 1997;3(5):453-463. Accessed March 21, 2024. https://europepmc.org/articles/PMC1369496

179. Chen CX, Cho DSC, Wang Q, Lai F, Carter KC, Nishikura K. A third member of the RNA-specific adenosine deaminase gene family, ADAR3, contains both single- and double-stranded RNA binding domains. *RNA*. 2000;6(5):755-767. doi:10.1017/S1355838200000170

180. Patterson JB, Samuel CE. Expression and Regulation by Interferon of a Double-Stranded-RNA-Specific Adenosine Deaminase from Human Cells: Evidence for Two Forms of the Deaminase. *Mol Cell Biol*. Published online October 1, 1995. doi:10.1128/MCB.15.10.5376

181. Lykke-Andersen S, Piñol-Roma S, Kjems J. Alternative splicing of the ADAR1 transcript in a region that functions either as a 5′-UTR or an ORF. *RNA*. 2007;13(10):1732-1744. doi:10.1261/rna.567807

182. Herbert A, Alfken J, Kim YG, Mian IS, Nishikura K, Rich A. A Z-DNA binding domain present in the human editing enzyme, double-stranded RNA adenosine deaminase. *Proc Natl Acad Sci*. 1997;94(16):8421-8426. doi:10.1073/pnas.94.16.8421

183. Baker AR, Slack FJ. ADAR1 and its implications in cancer development and treatment. *Trends Genet*. 2022;38(8):821-830. doi:10.1016/j.tig.2022.03.013

184. Strehblow A, Hallegger M, Jantsch MF. Nucleocytoplasmic Distribution of Human RNA-editing Enzyme ADAR1 Is Modulated by Double-stranded RNA-binding Domains, a Leucine-rich Export Signal, and a Putative Dimerization Domain. *Mol Biol Cell*. 2002;13(11):3822-3835. doi:10.1091/mbc.e02-03-0161

185. Tan MH, Li Q, Shanmugam R, et al. Dynamic landscape and regulation of RNA editing in mammals. *Nature*. 2017;550(7675):249-254. doi:10.1038/nature24041

186. Datta R, Adamska JZ, Bhate A, Li JB. A-to-I RNA editing by ADAR and its therapeutic applications: From viral infections to cancer immunotherapy. *WIREs RNA*. 2024;15(1):e1817. doi:10.1002/wrna.1817

187. Nishikura K. Functions and Regulation of RNA Editing by ADAR Deaminases. *Annu Rev Biochem*. 2010;79(Volume 79, 2010):321-349. doi:10.1146/annurev-biochem-060208-105251

188. Stephens OM, Yi-Brunozzi HY, Beal PA. Analysis of the RNA-Editing Reaction of ADAR2 with Structural and Fluorescent Analogues of the GluR-B R/G Editing Site. *Biochemistry*. 2000;39(40):12243-12251. doi:10.1021/bi0011577

189. Keegan LP, Gallo A, O'Connell MA. The many roles of an RNA editor. *Nat Rev Genet*. 2001;2(11):869-878. doi:10.1038/35098584

190. Gallo A, Locatelli F. ADARs: allies or enemies? The importance of A-to-I RNA editing in human disease: from cancer to HIV-1. *Biol Rev*. 2012;87(1):95-110. doi:10.1111/j.1469-185X.2011.00186.x

191. Bass BL. RNA Editing by Adenosine Deaminases That Act on RNA. *Annu Rev Biochem*. 2002;71(Volume 71, 2002):817-846. doi:10.1146/annurev.biochem.71.110601.135501

192. Nishikura K. Editor meets silencer: crosstalk between RNA editing and RNA interference. *Nat Rev Mol Cell Biol*. 2006;7(12):919-931. doi:10.1038/nrm2061

193. Galeano F, Leroy A, Rossetti C, et al. Human BLCAP transcript: new editing events in normal and cancerous tissues. *Int J Cancer*. 2010;127(1):127-137. doi:10.1002/ijc.25022

194. Wahlstedt H, Daniel C, Ensterö M, Öhman M. Large-scale mRNA sequencing determines global regulation of RNA editing during brain development. *Genome Res*. 2009;19(6):978-986. doi:10.1101/gr.089409.108

195. Qu L, Yi Z, Zhu S, et al. Programmable RNA editing by recruiting endogenous ADAR using engineered RNAs. *Nat Biotechnol*. 2019;37(9):1059-1069. doi:10.1038/s41587-019-0178-z

196. Merkle T, Stafforst T. New Frontiers for Site-Directed RNA Editing: Harnessing Endogenous ADARs. In: Picardi E, Pesole G, eds. *RNA Editing: Methods and Protocols*. Methods in Molecular Biology. Springer US; 2021:331-349. doi:10.1007/978-1-0716-0787-9_19

197. Wettengel J, Reautschnig P, Geisler S, Kahle PJ, Stafforst T. Harnessing human ADAR2 for RNA repair – Recoding a PINK1 mutation rescues mitophagy. *Nucleic Acids Res*. 2017;45(5):2797-2808. doi:10.1093/nar/gkw911

198. Khosravi HM, Jantsch MF. Site-directed RNA editing: recent advances and open challenges. *RNA Biol*. 2021;18(sup1):41-50. doi:10.1080/15476286.2021.1983288

199. Pfeiffer LS, Stafforst T. Precision RNA base editing with engineered and endogenous effectors. *Nat Biotechnol*. Published online September 21, 2023:1-17. doi:10.1038/s41587-023-01927-0

200. Stafforst T, Schneider MF. An RNA–Deaminase Conjugate Selectively Repairs Point Mutations. *Angew Chem Int Ed*. 2012;51(44):11166-11169. doi:10.1002/anie.201206489

201. Vogel P, Schneider MF, Wettengel J, Stafforst T. Improving Site-Directed RNA Editing In Vitro and in Cell Culture by Chemical Modification of the GuideRNA. *Angew Chem Int Ed*. 2014;53(24):6267-6271. doi:10.1002/anie.201402634

202. Vogel P, Hanswillemenke A, Stafforst T. Switching Protein Localization by Site-Directed RNA Editing under Control of Light. *ACS Synth Biol*. 2017;6(9):1642-1649. doi:10.1021/acssynbio.7b00113

203. Hanswillemenke A, Kuzdere T, Vogel P, Jékely G, Stafforst T. Site-Directed RNA Editing in Vivo Can Be Triggered by the Light-Driven Assembly of an Artificial Riboprotein. *J Am Chem Soc*. 2015;137(50):15875-15881. doi:10.1021/jacs.5b10216

204. Bennett CF, Baker BF, Pham N, Swayze E, Geary RS. Pharmacology of Antisense Drugs. *Annu Rev Pharmacol Toxicol*. 2017;57(Volume 57, 2017):81-105. doi:10.1146/annurev-pharmtox-010716-104846

205. Shen X, Corey DR. Chemistry, mechanism and clinical status of antisense oligonucleotides and duplex RNAs. *Nucleic Acids Res*. 2018;46(4):1584-1600. doi:10.1093/nar/gkx1239

206. Crooke ST, Baker BF, Crooke RM, Liang X hai. Antisense technology: an overview and prospectus. *Nat Rev Drug Discov*. 2021;20(6):427-453. doi:10.1038/s41573-021-00162-z

207. Dowdy SF. Overcoming cellular barriers for RNA therapeutics. *Nat Biotechnol*. 2017;35(3):222-229. doi:10.1038/nbt.3802

208. Doherty EE, Karki A, Wilcox XE, et al. ADAR activation by inducing a syn conformation at guanosine adjacent to an editing site. *Nucleic Acids Res*. 2022;50(19):10857-10868. doi:10.1093/nar/gkac897

209. Pastrana DV, Tolstov YL, Becker JC, Moore PS, Chang Y, Buck CB. Quantitation of Human Seroresponsiveness to Merkel Cell Polyomavirus. *PLOS Pathog*. 2009;5(9):e1000578. doi:10.1371/journal.ppat.1000578

210. Hartley JL, Temple GF, Brasch MA. DNA Cloning Using In Vitro Site-Specific Recombination. *Genome Res*. 2000;10(11):1788-1795. doi:10.1101/gr.143000

211. Bushman W, Thompson JF, Vargas L, Landy A. Control of Directionality in Lambda Site Specific Recombination. *Science*. 1985;230(4728):906-911. doi:10.1126/science.2932798

212. Škalamera D, Dahmer M, Purdon AS, et al. Generation of a Genome Scale Lentiviral Vector Library for EF1α Promoter-Driven Expression of Human ORFs and Identification of Human Genes Affecting Viral Titer. *PLOS ONE*. 2012;7(12):e51733. doi:10.1371/journal.pone.0051733

213. Teschendorf C, Warrington KH, Siemann DW, Muzyczka N. Comparison of the EF-1 alpha and the CMV promoter for engineering stable tumor cell lines using recombinant adeno-associated virus. *Anticancer Res*. 2002;22(6A):3325-3330.

214. Wang X, Xu Z, Tian Z, et al. The EF-1α promoter maintains high-level transgene expression from episomal vectors in transfected CHO-K1 cells. *J Cell Mol Med*. 2017;21(11):3044-3054. doi:10.1111/jcmm.13216

215. Buck CB, Pastrana DV, Lowy DR, Schiller JT. Efficient Intracellular Assembly of Papillomaviral Vectors. *J Virol*. 2004;78(2):751-757. doi:10.1128/jvi.78.2.751-757.2004

216. Collins CS, Gould SJ. Identification of a common PEX1 mutation in Zellweger syndrome. *Hum Mutat*. 1999;14(1):45-53. doi:10.1002/(SICI)1098-1004(1999)14:1<45::AID-HUMU6>3.0.CO;2-J

217. Klouwer FCC, Falkenberg KD, Ofman R, et al. Autophagy Inhibitors Do Not Restore Peroxisomal Functions in Cells With the Most Common Peroxisome Biogenesis Defect. *Front Cell Dev Biol*. 2021;0. doi:10.3389/fcell.2021.661298

218. Givan AL. Flow Cytometry: An Introduction. In: Hawley TS, Hawley RG, eds. *Flow Cytometry Protocols*. Methods in Molecular Biology. Humana Press; 2011:1-29. doi:10.1007/978-1-61737-950-5_1

219. Picot J, Guerin CL, Le Van Kim C, Boulanger CM. Flow cytometry: retrospective, fundamentals and recent instrumentation. *Cytotechnology*. 2012;64(2):109-130. doi:10.1007/s10616-011-9415-0

220. McKinnon KM. Flow Cytometry: An Overview. *Curr Protoc Immunol*. 2018;120(1):5.1.1-5.1.11. doi:10.1002/cpim.40

221. Pandey S, Dodt G. Purification of a Recombinant Human PEX1/PEX6 AAA+ ATPase Complex from HEK293TT Cells. In: Schrader M, ed. *Peroxisomes: Methods and Protocols*. Methods in Molecular Biology. Springer US; 2023:359-372. doi:10.1007/978-1-0716-3048-8_25

222. Smith PK, Krohn RI, Hermanson GT, et al. Measurement of protein using bicinchoninic acid. *Anal Biochem*. 1985;150(1):76-85. doi:10.1016/0003-2697(85)90442-7

223. Laemmli UK. Cleavage of Structural Proteins during the Assembly of the Head of Bacteriophage T4. *Nature*. 1970;227(5259):680-685. doi:10.1038/227680a0

224. Blum H, Beier H, Gross HJ. Improved silver staining of plant proteins, RNA and DNA in polyacrylamide gels. *ELECTROPHORESIS*. 1987;8(2):93-99. doi:10.1002/elps.1150080203

225. Merril CR, Pratt ME. A silver stain for the rapid quantitative detection of proteins or nucleic acids on membranes or thin layer plates. *Anal Biochem*. 1986;156(1):96-110. doi:10.1016/0003-2697(86)90160-0

226. Burnette WN. "Western Blotting": Electrophoretic transfer of proteins from sodium dodecyl sulfate-polyacrylamide gels to unmodified nitrocellulose and radiographic detection with antibody and radioiodinated protein A. *Anal Biochem*. 1981;112(2):195-203. doi:10.1016/0003-2697(81)90281-5

227. Towbin H, Staehelin T, Gordon J. Electrophoretic transfer of proteins from polyacrylamide gels to nitrocellulose sheets: procedure and some applications. *Proc Natl Acad Sci*. 1979;76(9):4350-4354. doi:10.1073/pnas.76.9.4350

228. Renart J, Reiser J, Stark GR. Transfer of proteins from gels to diazobenzyloxymethyl-paper and detection with antisera: a method for studying

antibody specificity and antigen structure. *Proc Natl Acad Sci*. 1979;76(7):3116-3120. doi:10.1073/pnas.76.7.3116

229. Wozniak-Knopp G, Bartl S, Bauer A, et al. Introducing antigen-binding sites in structural loops of immunoglobulin constant domains: Fc fragments with engineered HER2/neu-binding sites and antibody properties. *Protein Eng Des Sel*. 2010;23(4):289-297. doi:10.1093/protein/gzq005

230. Wiegand S. Thermal diffusion in liquid mixtures and polymer solutions. *J Phys Condens Matter*. 2004;16(10):R357. doi:10.1088/0953-8984/16/10/R02

231. Duhr S, Braun D. Why molecules move along a temperature gradient. *Proc Natl Acad Sci U S A*. 2006;103(52):19678-19682. doi:10.1073/pnas.0603873103

232. Jerabek-Willemsen M, André T, Wanner R, et al. MicroScale Thermophoresis: Interaction analysis and beyond. *J Mol Struct*. 2014;1077:101-113. doi:10.1016/j.molstruc.2014.03.009

233. Tschammer N, Höfer S, Weigert S, et al. Protein Labeling One-step, purification-free and site-specific labeling of polyhistidine-tagged proteins for MST. Published online August 1, 2016.

234. Monolith NT.115 User Manual. Published May 15, 2019. Accessed October 31, 2023. https://nanotemper.my.site.com/explore/s/article/Monolith-NT-115-User-Manual

235. MO-L018 Monolith His-Tag Labeling Kit RED-tris-NTA 2nd Generation. Published December 2, 2019. Accessed October 31, 2023. https://nanotemper.my.site.com/explore/s/article/MO-L018-Monolith-His-Tag-Labeling-Kit-RED-tris-NTA-2nd-Generation

236. Matsumoto N, Tamura S, Moser A, et al. The peroxin Pex6p gene is impaired in peroxisomal biogenesis disorders of complementation group 6. *J Hum Genet*. 2001;46(5):273-277. doi:10.1007/s100380170078

237. Zhang Z, Suzuki Y, Shimozawa N, et al. Genomic structure and identification of 11 novel mutations of the PEX6 (peroxisome assembly factor-2) gene in patients with peroxisome biogenesis disorders. *Hum Mutat*. 1999;13(6):487-496. doi:10.1002/(SICI)1098-1004(1999)13:6<487::AID-HUMU9>3.0.CO;2-T

238. Saffian D, Grimm I, Girzalsky W, Erdmann R. ATP-dependent assembly of the heteromeric Pex1p–Pex6p-complex of the peroxisomal matrix protein import machinery. *J Struct Biol*. 2012;179(2):126-132. doi:10.1016/j.jsb.2012.06.002

239. Pedrosa AG, Francisco T, Bicho D, et al. Peroxisomal monoubiquitinated PEX5 interacts with the AAA ATPases PEX1 and PEX6 and is unfolded during its dislocation into the cytosol. *J Biol Chem*. Published online June 8, 2018:jbc.RA118.003669. doi:10.1074/jbc.RA118.003669

240. Tamura S, Yasutake S, Matsumoto N, Fujiki Y. Dynamic and Functional Assembly of the AAA Peroxins, Pex1p and Pex6p, and Their Membrane Receptor Pex26p. *J Biol Chem*. 2006;281(38):27693-27704. doi:10.1074/jbc.M605159200

241. Falkenberg KD, Braverman NE, Moser AB, et al. Allelic Expression Imbalance Promoting a Mutant PEX6 Allele Causes Zellweger Spectrum Disorder. *Am J Hum Genet*. 2017;101(6):965-976. doi:10.1016/j.ajhg.2017.11.007

242. Yik WY, Steinberg SJ, Moser AB, Moser HW, Hacia JG. Identification of novel mutations and sequence variation in the Zellweger syndrome spectrum of peroxisome biogenesis disorders. *Hum Mutat*. 2009;30(3):E467-E480. doi:10.1002/humu.20932

243. Preuss N, Brosius U, Biermanns M, Muntau AC, Conzelmann E, Gärtner J. PEX1 Mutations in Complementation Group 1 of Zellweger Spectrum Patients Correlate with Severity of Disease. *Pediatr Res*. 2002;51(6):706-714. doi:10.1203/00006450-200206000-00008

244. Keppler A, Gendreizig S, Gronemeyer T, Pick H, Vogel H, Johnsson K. A general method for the covalent labeling of fusion proteins with small molecules in vivo. *Nat Biotechnol*. 2003;21(1):86-89. doi:10.1038/nbt765

245. Gronemeyer T, Chidley C, Juillerat A, Heinis C, Johnsson K. Directed evolution of O6-alkylguanine-DNA alkyltransferase for applications in protein labeling. *Protein Eng Des Sel*. 2006;19(7):309-316. doi:10.1093/protein/gzl014

246. Poole B, Leighton F, De Duve C. THE SYNTHESIS AND TURNOVER OF RAT LIVER PEROXISOMES : II. Turnover of Peroxisome Proteins. *J Cell Biol*. 1969;41(2):536-546. doi:10.1083/jcb.41.2.536

247. Huybrechts SJ, Van Veldhoven PP, Brees C, Mannaerts GP, Los GV, Fransen M. Peroxisome Dynamics in Cultured Mammalian Cells. *Traffic*. 2009;10(11):1722-1733. doi:10.1111/j.1600-0854.2009.00970.x

248. Grimm I, Saffian D, Girzalsky W, Erdmann R. Nucleotide-dependent assembly of the peroxisomal receptor export complex. *Sci Rep*. 2016;6:srep19838. doi:10.1038/srep19838

249. Birschmann I, Stroobants AK, van den Berg M, et al. Pex15p of Saccharomyces cerevisiae Provides a Molecular Basis for Recruitment of the AAA Peroxin Pex6p to Peroxisomal Membranes. *Mol Biol Cell*. 2003;14(6):2226-2236. doi:10.1091/mbc.e02-11-0752

250. Nuttall JM, Motley AM, Hettema EH. Deficiency of the exportomer components Pex1, Pex6, and Pex15 causes enhanced pexophagy in Saccharomyces cerevisiae. *Autophagy*. 2014;10(5):835-845. doi:10.4161/auto.28259

251. Sargent G, van Zutphen T, Shatseva T, et al. PEX2 is the E3 ubiquitin ligase required for pexophagy during starvation. *J Cell Biol*. 2016;214(6):677-690. doi:10.1083/jcb.201511034

252. Law KB, Bronte-Tinkew D, Pietro ED, et al. The peroxisomal AAA ATPase complex prevents pexophagy and development of peroxisome biogenesis disorders. *Autophagy*. 2017;13(5):868-884. doi:10.1080/15548627.2017.1291470

253. Yu H, Kamber RA, Denic V. The peroxisomal exportomer directly inhibits phosphoactivation of the pexophagy receptor Atg36 to suppress pexophagy in yeast. Nakatogawa H, Ron D, Subramani S, eds. *eLife*. 2022;11:e74531. doi:10.7554/eLife.74531

254. Schieferdecker A, Wendler P. Structural Mapping of Missense Mutations in the Pex1/Pex6 Complex. *Int J Mol Sci*. 2019;20(15):3756. doi:10.3390/ijms20153756

255. Osumi T, Tsukamoto T, Hata S, et al. Amino-terminal presequence of the precursor of peroxisomal 3-ketoacyl-CoA thiolase is a cleavable signal peptide for peroxisomal targeting. *Biochem Biophys Res Commun*. 1991;181(3):947-954. doi:10.1016/0006-291X(91)92028-I

256. Wanders RJA, Romeijn GJ. Cholesterol biosynthesis, peroxisomes and peroxisomal disorders: Mevalonate kinase is not only deficient in Zellweger syndrome but also in rhizomelic chondrodysplasia punctata. *J Inherit Metab Dis*. 1998;21(3):309-312. doi:10.1023/A:1005353129761

257. Jansen GA, Oftnan R, Ferdinandusse S, et al. Refsum disease is caused by mutations in the phytanoyl–CoA hydroxylase gene. *Nat Genet*. 1997;17(2):190-193. doi:10.1038/ng1097-190

258. Glynn SE, Martin A, Nager AR, Baker TA, Sauer RT. Structures of Asymmetric ClpX Hexamers Reveal Nucleotide-Dependent Motions in a AAA+ Protein-Unfolding Machine. *Cell*. 2009;139(4):744-756. doi:10.1016/j.cell.2009.09.034

259. Miron A, Aprotosoaie AC, Trifan A, Xiao J. Flavonoids as modulators of metabolic enzymes and drug transporters. *Ann N Y Acad Sci*. 2017;1398(1):152-167. doi:10.1111/nyas.13384

260. Berendse K, Ebberink MS, IJlst L, Poll-The BT, Wanders RA, Waterham HR. Arginine improves peroxisome functioning in cells from patients with a mild peroxisome biogenesis disorder. *Orphanet J Rare Dis*. 2013;8(1):138. doi:10.1186/1750-1172-8-138

261. Liu Y, Weaver CM, Sen Y, et al. The Nitric Oxide Donor, S-Nitrosoglutathione, Rescues Peroxisome Number and Activity Defects in PEX1G843D Mild Zellweger Syndrome Fibroblasts. *Front Cell Dev Biol*. 2021;9. Accessed December 12, 2022. https://www.frontiersin.org/articles/10.3389/fcell.2021.714710

262. Bajad P, Jantsch MF, Keegan L, O'Connell M. A to I editing in disease is not fake news. *RNA Biol*. 2017;14(9):1223-1231. doi:10.1080/15476286.2017.1306173

263. Fukuda M, Umeno H, Nose K, Nishitarumizu A, Noguchi R, Nakagawa H. Construction of a guide-RNA for site-directed RNA mutagenesis utilising intracellular A-to-I RNA editing. *Sci Rep*. 2017;7(1):41478. doi:10.1038/srep41478

264. Crooke ST, Witztum JL, Bennett CF, Baker BF. RNA-Targeted Therapeutics. *Cell Metab*. 2018;27(4):714-739. doi:10.1016/j.cmet.2018.03.004

265. Geary RS, Norris D, Yu R, Bennett CF. Pharmacokinetics, biodistribution and cell uptake of antisense oligonucleotides. *Adv Drug Deliv Rev*. 2015;87:46-51. doi:10.1016/j.addr.2015.01.008

266. Bennett CF, Swayze EE. RNA Targeting Therapeutics: Molecular Mechanisms of Antisense Oligonucleotides as a Therapeutic Platform. *Annu Rev Pharmacol Toxicol*. 2010;50(1):259-293. doi:10.1146/annurev.pharmtox.010909.105654

267. Das Y, Swinkels D, Baes M. Peroxisomal Disorders and Their Mouse Models Point to Essential Roles of Peroxisomes for Retinal Integrity. *Int J Mol Sci*. 2021;22(8):4101. doi:10.3390/ijms22084101

268. Argyriou C, Polosa A, Song JY, et al. AAV-mediated PEX1 gene augmentation improves visual function in the PEX1-Gly844Asp mouse model for mild Zellweger spectrum disorder. *Mol Ther - Methods Clin Dev*. 2021;23:225-240. doi:10.1016/j.omtm.2021.09.002

6 Appendix

6.1 Plasmid maps and protein sequence

6.1.1 pGwf_PEX1.TEV.HIS6

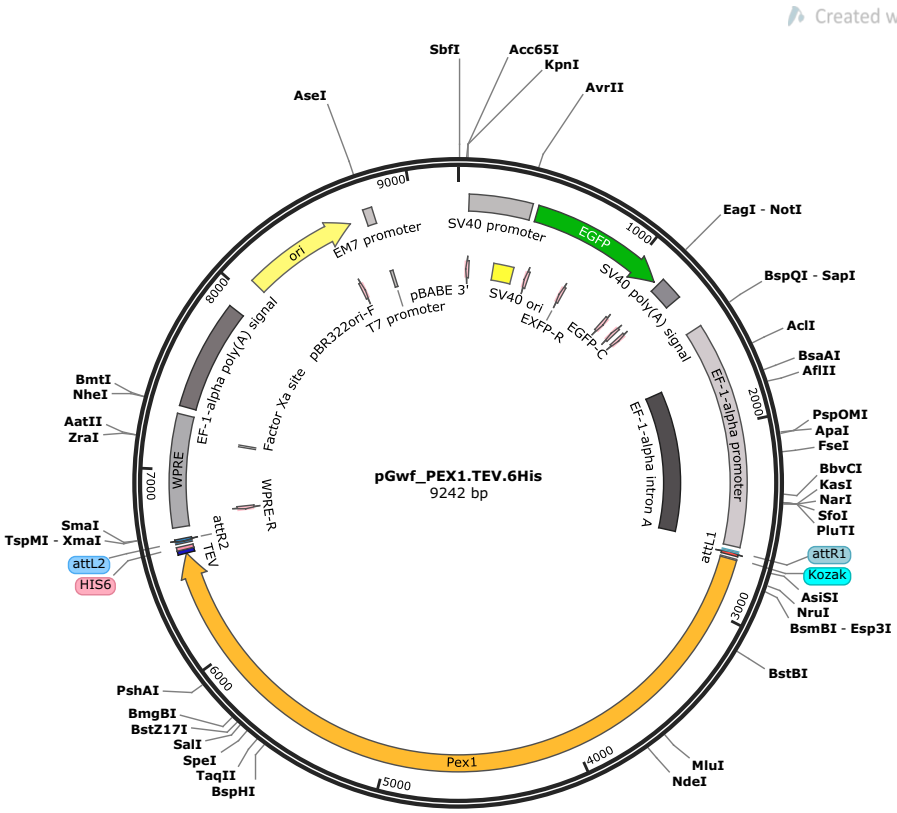

MWGSDRLAGAGGGGAAVTVAFTNARDCFLHLPRRLVAQLHLLQNQAIEVVWSHQPAFLSWVEGRHFSDQG
ENVAEINRQVGQKLGLSNGGQVFLKPCSHVVSCQQVEVEPLSADDWEILELHAVSLEQHLLDQIRIVFPKAIF
PVWVDQQTYIFIQIVALIPAASYGRLETDTKLLIQPKTRRAKENTFSKADAEYKKLHSYGRDQKGMMKELQT
KQLQSNTVGITESNENESEIPVDSSSVASLWTMIGSIFSFQSEKKQETSWGLTEINAFKNMQSKVVPLDNIFRV
CKSQPPSIYNASATSVFHKHCAIHVFPWDQEYFDVEPSFTVTYGKLVKLLSPKQQQSKTKQNVLSPEKEKQM
SEPLDQKKIRSDHNEEDEKACVLQVVWNGLEELNNAIKYTKNVEVLHLGKVWIPDDLRKRLNIEMHAVVRI
TPVEVTPKIPRSLKLQPRENLPKDISEEDIKTVFYSWLQQSTTTMLPLVISEEEFIKLETKDGLKEFSLSIVHSW
EKEKDKNIFLLSPNLLQKTTIQVLLDPMVKEENSEEIDFILPFLKLSSLGGVNSLGVSSLEHITHSLLGRPLSRQ
LMSLVAGLRNGALLLTGGKGSGKSTLAKAICKEAFDKLDAHVERVDCKALRGKRLENIQKTLEVAFSEAVW
MQPSVVLLDDLDLIAGLPAVPEHEHSPDAVQSQRLAHALNDMIKEFISMGSLVALIATSQSQQSLHPLLVSAQ
GVHIFQCVQHIQPPNQEQRCEILCNVIKNKLDCDINKFTDLDLQHVAKETGGFVARDFTVLVDRAIHSRLSRQ
SISTREKLVLTTLDFQKALRGFLPASLRSVNLHKPRDLGWDKIGGLHEVRQILMDTIQLPAKYPELFANLPIR
QRTGILLYGPPGTGKTLLAGVIARESRMNFISVKGPELLSKYIGASEQAVRDIFIRAQAAKPCILFFDEFESIAPR
RGHDNTGVTDRVVNQLLTQLDGVEGLQGVYVLAATSRPDLIDPALLRPGRLDKCVYCPPPDQVSRLEILNVL
SDSLPLADDVDLQHVASVTDSFTGADLKALLYNAQLEALHGMLLSSGLQDGSSSSDSDLSLSSMVFLNHSSGS
DDSAGDGECGLDQSLVSLEMSEILPDESKFNMYRLYFGSSYESELGNGTSSDLSSQCLSAPSSMTQDLPGVPG
KDQLFSQPPVLRTASQEGCQELTQEQRDQLRADISIIKGRYRSQSGEDESMNQPGPIKTRLAISQSHLMTALG
HTRPSISEDDWKNFAELYESFQNPKRRKNQSGTMFRPGQKVTLAENLYFQGHHHHHH*

6.1.2 pGwf_PEX1(G843D).TEV.HIS6

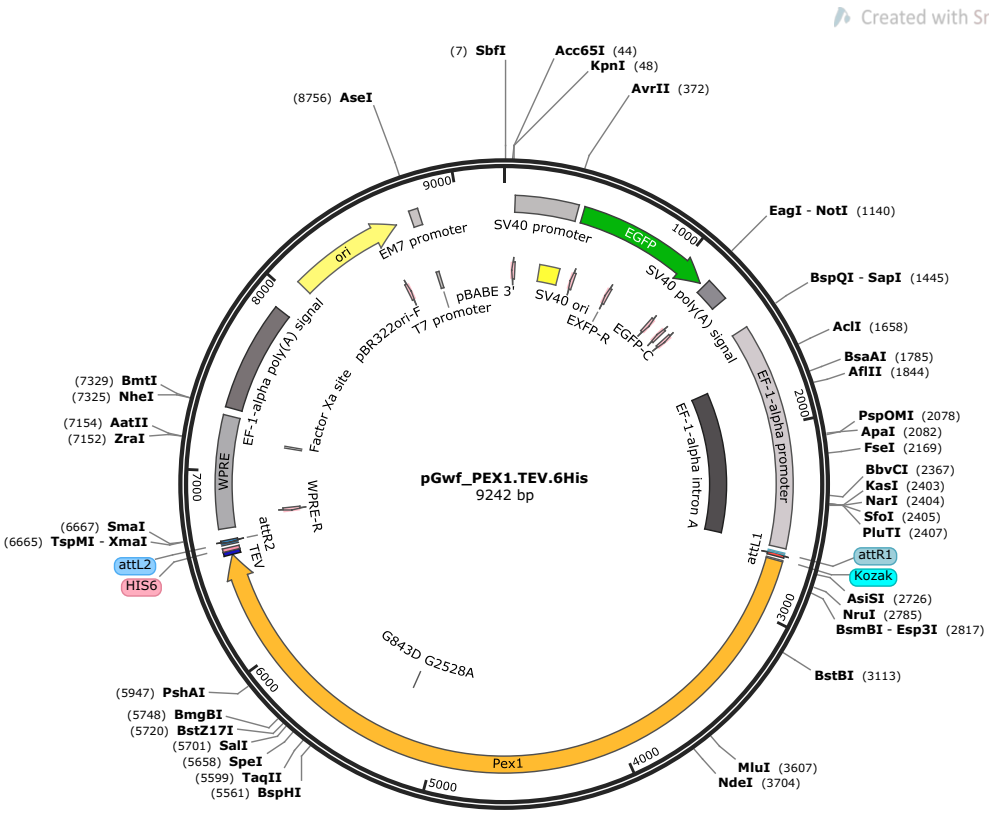

MWGSDRLAGAGGGGAAVTVAFTNARDCFLHLPRRLVAQLHLLQNQAIEVVWSHQPAFLSWVEGRHFSDQG
ENVAEINRQVGQKLGLSNGGQVFLKPCSHVVSCQQVEVEPLSADDWEILELHAVSLEQHLLDQIRIVFPKAIF
PVWVDQQTYIFIQIVALIPAASYGRLETDTKLLIQPKTRRAKENTFSKADAEYKKLHSYGRDQKGMMKELQT
KQLQSNTVGITESNENESEIPVDSSSVASLWTMIGSIFSFQSEKKQETSWGLTEINAFKNMQSKVVPLDNIFRV
CKSQPPSIYNASATSVFHKHCAIHVFPWDQEYFDVEPSFTVTYGKLVKLLSPKQQQSKTKQNVLSPEKEKQM
SEPLDQKKIRSDHNEEDEKACVLQVVWNGLEELNNAIKYTKNVEVLHLGKVWIPDDLRKRLNIEMHAVVRI
TPVEVTPKIPRSLKLQPRENLPKDISEEDIKTVFYSWLQQSTTTMLPLVISEEEFIKLETKDGLKEFSLSIVHSW
EKEKDKNIFLLSPNLLQKTTIQVLLDPMVKEENSEEIDFILPFLKLSSLGGVNSLGVSSLEHITHSLLGRPLSRQ
LMSLVAGLRNGALLLTGGKGSGKSTLAKAICKEAFDKLDAHVERVDCKALRGKRLENIQKTLEVAFSEAVW
MQPSVVLLDDLDLIAGLPAVPEHEHSPDAVQSQRLAHALNDMIKEFISMGSLVALIATSQSQQSLHPLLVSAQ
GVHIFQCVQHIQPPNQEQRCEILCNVIKNKLDCDINKFTDLDLQHVAKETGGFVARDFTVLVDRAIHSRLSRQ
SISTREKLVLTTLDFQKALRGFLPASLRSVNLHKPRDLGWDKIDGLHEVRQILMDTIQLPAKYPELFANLPIR
QRTGILLYGPPGTGKTLLAGVIARESRMNFISVKGPELLSKYIGASEQAVRDIFIRAQAAKPCILFFDEFESIAPR
RGHDNTGVTDRVVNQLLTQLDGVEGLQGVYVLAATSRPDLIDPALLRPGRLDKCVYCPPPDQVSRLEILNVL
SDSLPLADDVDLQHVASVTDSFTGADLKALLYNAQLEALHGMLLSSGLQDGSSSSDSDLSLSSMVFLNHSSGS
DDSAGDGECGLDQSLVSLEMSEILPDESKFNMYRLYFGSSYESELGNGTSSDLSSQCLSAPSSMTQDLPGVPG
KDQLFSQPPVLRTASQEGCQELTQEQRDQLRADISIIKGRYRSQSGEDESMNQPGPIKTRLAISQSHLMTALG
HTRPSISEDDWKNFAELYESFQNPKRRKNQSGTMFRPGQKVTLAENLYFQGHHHHHH*

6.1.3 pGwf_PEX6.2xFLAG

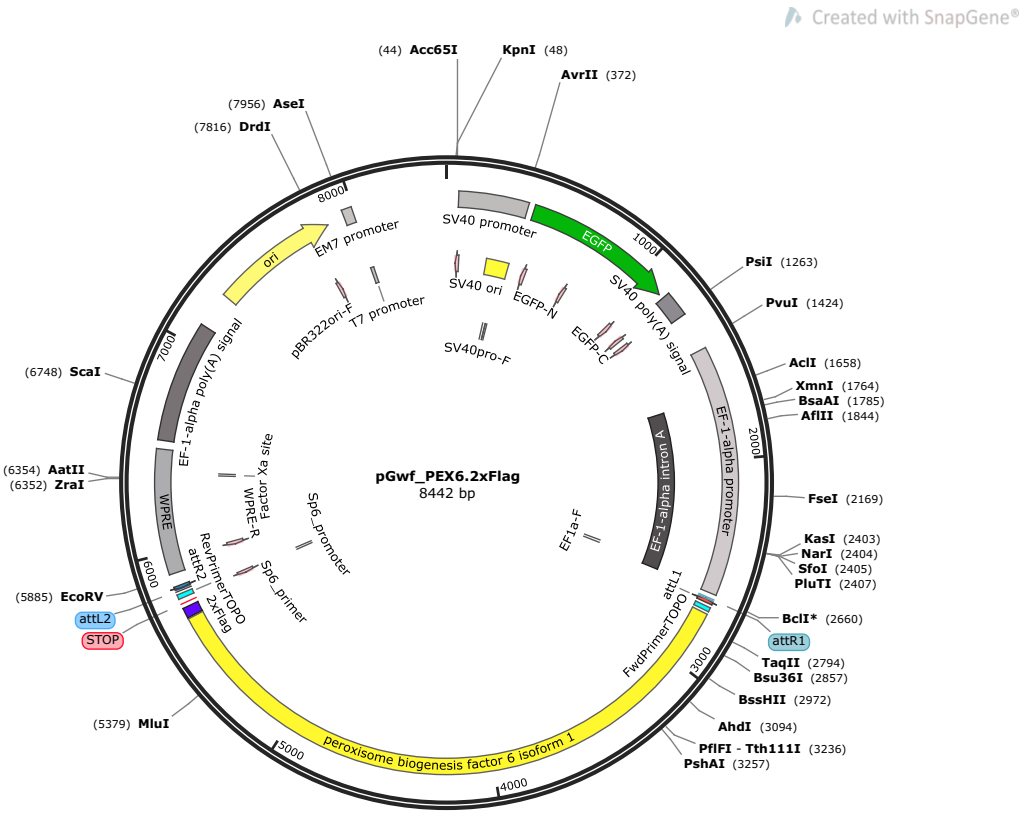

MALAVLRVLEPFPTETPPLAVLLPPGGPWPAAELGLVLALRPAGESPAGPALLVAALEGPDAGTEEQGPGPP
QLLVSRALLRLLALGSGAWVRARAVRRPPALGWALLGTSLGPGLGPRVGPLLVRRGETLPVPGPRVLETRPA
LQGLLGPGTRLAVTELRGRARLCPESGDSSRPPPPPVVSSFAVSGTVRRLQGVLGGTGDSLGVSRSCLRGLGLF
QGEWVWVAQARESSNTSQPHLARVQVLEPRWDLSDRLGPGSGPLGEPLADGLALVPATLAFNLGCDPLEM
GELRIQRYLEGSIAPEDKGSCSLLPGPPFARELHIEIVSSPHYSTNGNYDGVLYRHFQIPRVVQEGDVLCVPTIG
QVEILEGSPEKLPRWREMFFKVKKTVGEAPDGPASAYLADTTHTSLYMVGSTLSPVPWLPSEESTLWSSLSP
PGLEALVSELCAVLKPRLQPGGALLTGTSSVLLRGPPGCGKTTVVAAACSHLGLHLLKVPCSSLCAESSGAVET
KLQAIFSRARRCRPAVLLLTAVDLLGRDRDGLGEDARVMAVLRHLLLNEDPLNSCPPLMVVATTSRAQDLP
ADVQTAFPHELEVPALSEGQRLSILRALTAHLPLGQEVNLAQLARRCAGFVVGDLYALLTHSSRAACTRIKNS
GLAGGLTEEDEGELCAAGFPLLAEDFGQALEQLQTAHSQAVGAPKIPSVSWHDVGGLQEVKKEILETIQLPLE
HPELLSLGLRRSGLLLHGPPGTGKTLLAKAVATECSLTFLSVKGPELINMYVGQSEENVREVFARARAAAPCII
FFDELDSLAPSRGRSGDSGGVMDRVVSQLLAELDGLHSTQDVFVIGATNRPDLLDPALLRPGRFDKLVFVGA
NEDRASQLRVLSAITRKFKLEPSVSLVNVLDCCPPQLTGADLYSLCSDAMTAALKRRVHDLEEGLEPGSSALM
LTMEDLLQAAARLQPSVSEQELLRYKRIQRKFAACIDDYKDDDDKDYKDDDDKAAARACI*

6.1.4 pGwf_StrepII.TEV.PEX6

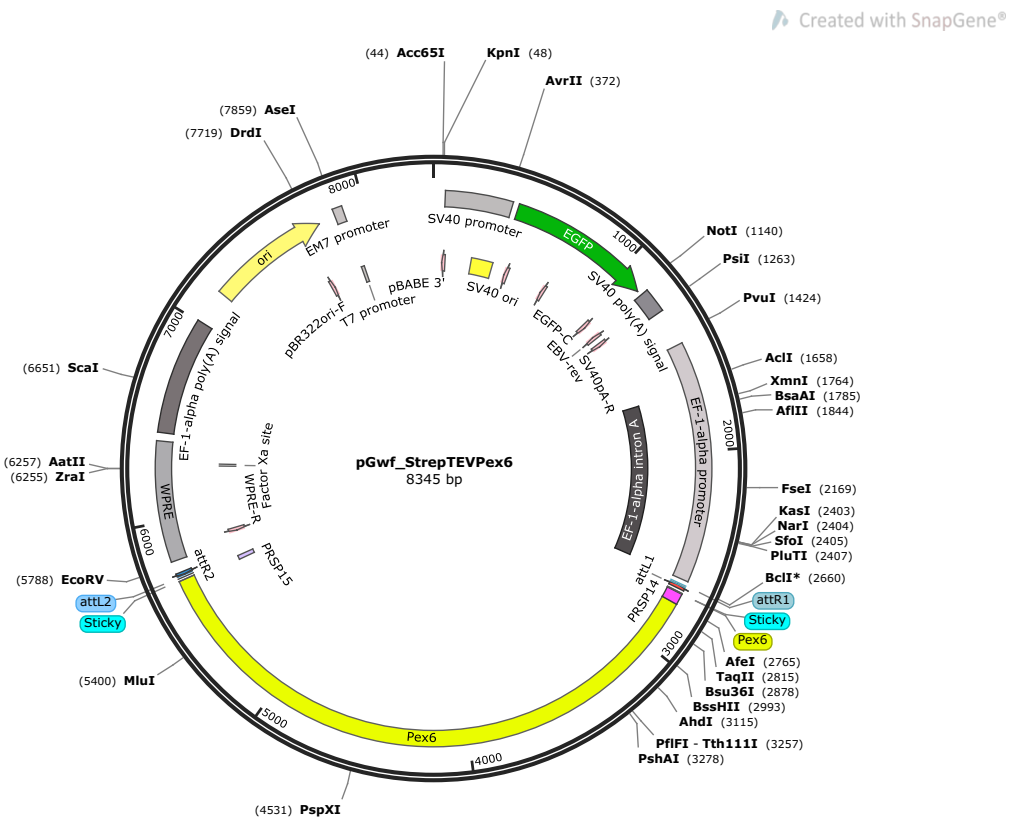

MATMWSHPQFEKENLYFQGALAVLRVLEPFPTETPPLAVLLPPGGPWPAAELGLVLALRPAGESPAGPALL
VAALEGPDAGTEEQGPGPPQLLVSRALLRLLALGSGAWVRARAVRRPPALGWALLGTSLGPGLGPRVGPLLV
RRGETLPVPGPRVLETRPALQGLLGPGTRLAVTELRGRARLCPESGDSSRPPPPPVVSSFAVSGTVRRLQGVL
GGTGDSLGVSRSCLRGLGLFQGEWVWVAQARESSNTSQPHLARVQVLEPRWDLSDRLGPGSGPLGEPLADG
LALVPATLAFNLGCDPLEMGELRIQRYLEGSIAPEDKGSCSLLPGPPFARELHIEIVSSPHYSTNGNYDGVLYR
HFQIPRVVQEGDVLCVPTIGQVEILEGSPEKLPRWREMFFKVKKTVGEAPDGPASAYLADTTHTSLYMVGST
LSPVPWLPSEESTLWSSLSPPGLEALVSELCAVLKPRLQPGGALLTGTSSVLLRGPPGCGKTTVVAAACSHLG
LHLLKVPCSSLCAESSGAVETKLQAIFSRARRCRPAVLLLTAVDLLGRDRDGLGEDARVMAVLRHLLLNEDPL
NSCPPLMVVATTSRAQDLPADVQTAFPHELEVPALSEGQRLSILRALTAHLPLGQEVNLAQLARRCAGFVVG
DLYALLTHSSRAACTRIKNSGLAGGLTEEDEGELCAAGFPLLAEDFGQALEQLQTAHSQAVGAPKIPSVSWH
DVGGLQEVKKEILETIQLPLEHPELLSLGLRRSGLLLHGPPGTGKTLLAKAVATECSLTFLSVKGPELINMYVG
QSEENVREVFARARAAAPCIIFFDELDSLAPSRGRSGDSGGVMDRVVSQLLAELDGLHSTQDVFVIGATNRPD
LLDPALLRPGRFDKLVFVGANEDRASQLRVLSAITRKFKLEPSVSLVNVLDCCPPQLTGADLYSLCSDAMTAA
LKRRVHDLEEGLEPGSSALMLTMEDLLQAAARLQPSVSEQELLRYKRIQRKFAAC*

6.1.5 pGwf_PEX6.Strep

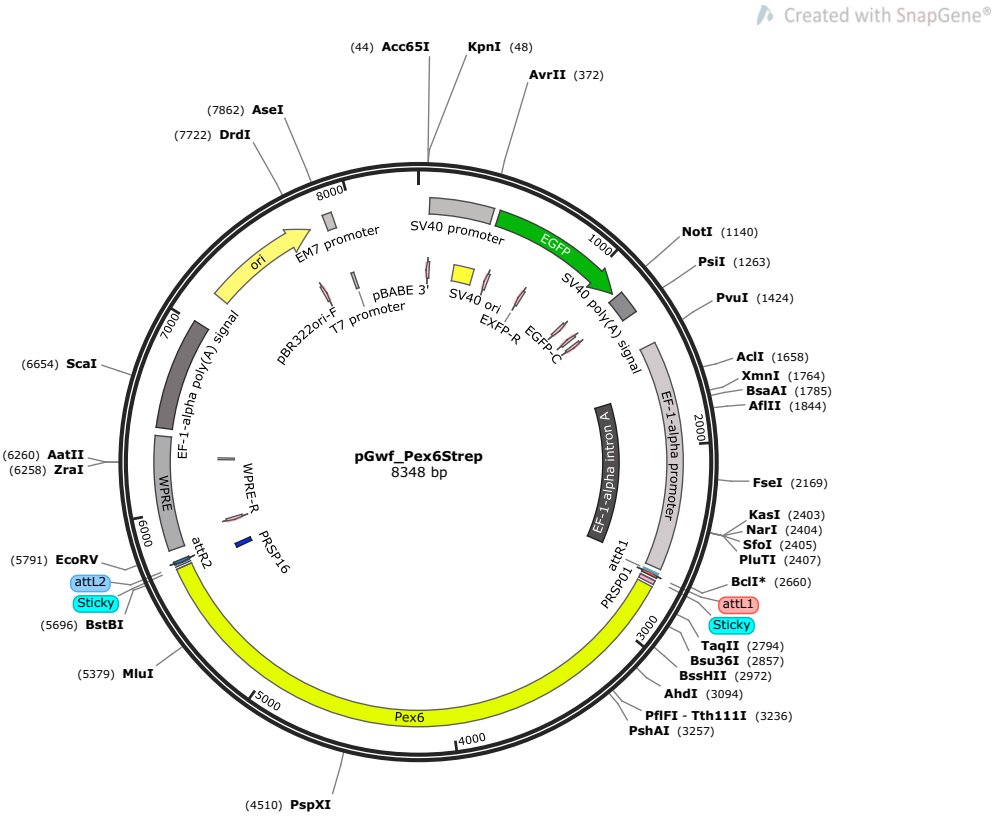

MALAVLRVLEPFPTETPPLAVLLPPGGPWPAAELGLVLALRPAGESPAGPALLVAALEGPDAGTEEQGPGPP
QLLVSRALLRLLALGSGAWVRARAVRRPPALGWALLGTSLGPGLGPRVGPLLVRRGETLPVPGPRVLETRPA
LQGLLGPGTRLAVTELRGRARLCPESGDSSRPPPPPVVSSFAVSGTVRRLQGVLGGTGDSLGVSRSCLRGLGLF
QGEWVWVAQARESSNTSQPHLARVQVLEPRWDLSDRLGPGSGPLGEPLADGLALVPATLAFNLGCDPLEM
GELRIQRYLEGSIAPEDKGSCSLLPGPPFARELHIEIVSSPHYSTNGNYDGVLYRHFQIPRVVQEGDVLCVPTIG
QVEILEGSPEKLPRWREMFFKVKKTVGEAPDGPASAYLADTTHTSLYMVGSTLSPVPWLPSEESTLWSSLSP
PGLEALVSELCAVLKPRLQPGGALLTGTSSVLLRGPPGCGKTTVVAAACSHLGLHLLKVPCSSLCAESSGAVET
KLQAIFSRARRCRPAVLLLTAVDLLGRDRDGLGEDARVMAVLRHLLLNEDPLNSCPPLMVVATTSRAQDLP
ADVQTAFPHELEVPALSEGQRLSILRALTAHLPLGQEVNLAQLARRCAGFVVGDLYALLTHSSRAACTRIKNS
GLAGGLTEEDEGELCAAGFPLLAEDFGQALEQLQTAHSQAVGAPKIPSVSWHDVGGLQEVKKEILETIQLPLE
HPELLSLGLRRSGLLLHGPPGTGKTLLAKAVATECSLTFLSVKGPELINMYVGQSEENVREVFARARAAAPCII
FFDELDSLAPSRGRSGDSGGVMDRVVSQLLAELDGLHSTQDVFVIGATNRPDLLDPALLRPGRFDKLVFVGA
NEDRASQLRVLSAITRKFKLEPSVSLVNVLDCCPPQLTGADLYSLCSDAMTAALKRRVHDLEEGLEPGSSALM
LTMEDLLQAAARLQPSVSEQELLRYKRIQRKFAACWSHPQFEK*

6.2 Publication

Pandey, Saroj, and Gabriele Dodt. 2023. "Purification of a Recombinant Human PEX1/PEX6 AAA+ ATPase Complex from HEK293TT Cells." In *Peroxisomes: Methods and Protocols*, edited by Michael Schrader, 359–72. Methods in Molecular Biology. New York, NY: Springer US. https://doi.org/10.1007/978-1-0716-3048-8_25.

6.3 Conferences and seminars attended

Oral presentation

- Peroxisomal disorders: an overview, IFIB Retreat, Hechingen, Germany, July 25-26, 2018.

Poster presentation

- Functional analysis of human PEX1/PEX6 complex and SNAP-tagged ADARs and ASO-mediated editing of PEX1 (G843D) mutation, 8th Open European Peroxisome Meeting, Aveiro, Portugal, September 22-24, 2022

Acknowledgement

This project could not have been accomplished without the contributions of the kind people around me. They, in various capacities, have extended valuable assistance in the preparation and finalization of this manuscript.

I am most grateful to my supervisor, Prof. Dr. Gabriele Dodt for her invaluable guidance and support throughout my research journey. Her wisdom, insights, and critiques have greatly enhanced the quality of my work. I would also like to extend my gratitude to my current and former colleagues: Karin Steiger, Erman Koçak, Vera Hagmann and Ashwin Mathew for their stimulating and enriching discussions, and for creating a positive and collaborative research environment.

I am deeply indebted to Prof. Dr. Thorsten Stafforst for providing me the opportunity for a collaboration with his lab. His colleagues, especially Karthika and Laura, deserve my sincere appreciation for providing all necessary materials as well as for their invaluable input.

I also wish to extend my sincere gratitude to Prof. Dr. Doron Rapaport and Prof. Dr. Dirk Schwarzer for their valuable time and effort, and for accepting to be the members of my doctoral examination committee.

All students who were involved in this project equally deserve my heartfelt gratitude for their valuable contributions and dedication. I would also like to thank the academic and technical support of the Interfaculty Institute of Biochemistry (IFIB) family and its staffs. I am equally thankful to Prof. Dr. Nancy Braverman, Dr. Catherine Argyriou, Prof. Dr. Hans R. Waterham and Janet Koster for providing cells lines and materials required for this project.

The steadfast support of my family back home has been a constant source of strength throughout this journey, as it always has been. Mere words of gratitude fall short in conveying the depth of my appreciation.

I am profoundly grateful to Subash dai, Sabine vauju, Gaurav dai, Madika, Pratik, Rajiv, Kailash, Raunak, Sushma, Bikash, Aditi and Niran, who have played a pivotal role in creating a close-knit family away from home. Their camaraderie and shared experiences have made this journey an unforgettable and enriching adventure. Their friendship has been a source of comfort and belonging, and I am very thankful to them for being part of this journey.

No words of gratitude can justify the unwavering support and encouragement of my beloved wife “dp” throughout this endeavor. Your friendship, laughter, and steadfast belief filled with warmth and belonging, have made this journey not just meaningful but truly enjoyable. Thank you for being my pillar of strength and for navigating challenges and celebrating successes together. Your companionship has been a constant source of joy and comfort, and I am thankful beyond words for your presence in my life.